Best
Available
Copy

AD A015872

ARPA-NRL X-Ray Laser Program
Semiannual Technical Report
to Defense Advanced Research Projects Agency
1 January 1975 - 30 June 1975
ARPA Order 2694

Interaction Physics Branch
Optical Sciences Division

September 1975

D D C

OCT 21 1975

B

NAVAL RESEARCH LABORATORY
Washington, D.C.

The Interaction Physics Branch of the Optical Sciences Division, Naval Research Laboratory, Washington, D.C., prepared this semiannual report on work sponsored jointly by the Defense Advanced Research Projects Agency, DARPA Order 2694, and the Naval Research Laboratory. Co-authors of the report were R. C. Elton, J. Reintjes, R. C. Eckardt, R. H. Dixon, R. Waynant, T. N. Lee, L. J. Palumbo, R. Lehmberg, J. DeRosa, and W. Jones.

REPORT DOCUMENTATION PAGE

READ INSTRUCTIONS
BEFORE COMPLETING FORM

1. REPORT NUMBER	2. GOVT ACCESSION NO.	3. RECIPIENT'S CATALOG NUMBER
NRL Memorandum Report 3130		

4. TITLE (and Subtitle)

ARPA/NRL X-RAY LASER PROGRAM — SEMIANNUAL TECHNICAL REPORT TO DEFENSE ADVANCED RESEARCH PROJECTS AGENCY — 1 January 1975 — 30 June 1975.

5. TYPE OF REPORT & PERIOD COVERED

Semiannual technical report; work continuing.

6. PERFORMING ORG. REPORT NUMBER

7. AUTHOR(s)

Interaction Physics Branch
Optical Sciences Division

8. CONTRACT OR GRANT NUMBER(s)

NRL-MR-3130

9. PERFORMING ORGANIZATION NAME AND ADDRESS

Naval Research Laboratory
Washington, D. C. 20375

10. PROGRAM ELEMENT, PROJECT, TASK AREA & WORK UNIT NUMBERS

NRL — NO1-43, NO1-33
ARPA Order 2694 Program
Code 4D10

11. CONTROLLING OFFICE NAME AND ADDRESS

Defense Advanced Research Projects Agency
Arlington, Va. 22209

12. REPORT DATE

Sep 75

13. NUMBER OF PAGES

170

14. MONITORING AGENCY NAME & ADDRESS(If different from Controlling Office)	15. SECURITY CLASS. (of this report)
	Unclassified
	15a. DECLASSIFICATION DOWNGRADING SCHEDULE

16. DISTRIBUTION STATEMENT (of this Report)

Approved for public release; distribution unlimited.

17. DISTRIBUTION STATEMENT (of the abstract entered in Block 20, If different from Report)

18. SUPPLEMENTARY NOTES

19. KEY WORDS (Continue on reverse side if necessary and identify by block number)

X-ray lasers
Lasers
Ultraviolet lasers
Laser-plasma interactions

20. ABSTRACT (Continue on reverse side if necessary and identify by block number)

The ARPA/NRL x-ray laser program is concerned with demonstrating gain in the soft x-ray region. The program is jointly supported by ARPA and NRL. The approaches include electron-collisional pumping in picosecond laser pumped plasmas, resonant charge transfer pumping, optical parametric mixing to short wavelengths, traveling wave e-beam pumping, and analysis and numerical modeling. This report covers the progress made during the second half of FY-75.
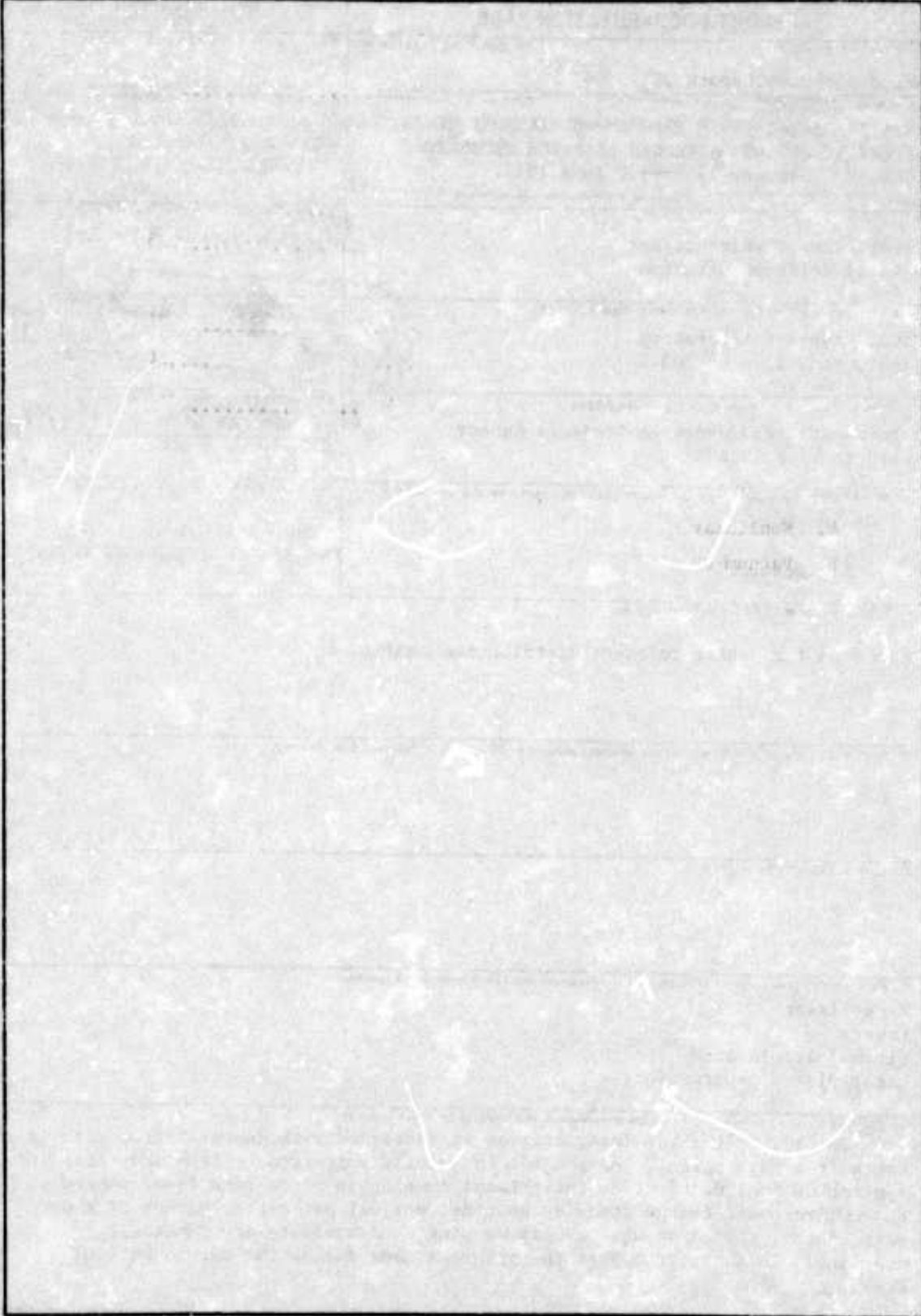
DD FORM 1473 EDITION OF 1 NOV 65 IS OBSOLETE
1 JAN 73
S/N 0102-014-6601

1

251950

CONTENTS

SEMIANNUAL TECHNICAL REPORT

Reporting Period

1 January 1975 - 30 June 1975

1.	DARPA Order	2694
2.	Program Code No.	4D10
3.	Name of Contractor	Naval Research Laboratory Optical Sciences Division
4.	Effective Date of Contract	1 January 1974
5.	Contract Expiration Date	Continuing
6.	Amount of Contract	$250K (FY 75)
7.	Contract No.	N/A
8.	Principal Investigator	Dr. R. C. Elton (Acting)
9.	Telephone No.	202-767-3528
10.	Scientific Officer	Dr. C. M. Stickley, ARPA
11.	Title of Work	X-Ray Lasers

Sponsored by

Defense Advance Research Projects Agency

ARPA ORDER 2694

ARPA/NRL X-RAY LASER PROGRAM
Semiannual Technical Report to Defense Advanced Research Projects Agency
1 January 1975 - 30 June 1975

I. INTRODUCTION

This is the third semiannual technical progress report for the
ARPA/NRL X-Ray Laser Program. There is no intention to duplicate
background material from previous reports*, since the format is
similar and copies are available upon request. Rather, the intent here
is to provide an update on program progress during this reporting
period with brief statements of motivation and goals.

The basic individual activities in the program have remained the
same, i.e.,

o Nonlinear optical mixing for producing coherent radiation in
   the vacuum-UV region,

o Amplification of such coherent radiation, beginning in the
   1600 Å region in preparation for further frequency upconversion,

o Electron collisional pumping of ions in a plasma with enhanced
   heating by picosecond laser irradiation,

o Investigation of resonant charge transfer pumping at a high
   rate into preferential levels as an advanced soft x-ray
   amplifier, and

o Theory, analysis and numerical modeling in support of these
   approaches and continual investigation of new concepts.

The overall theme in this program is to generate a coherent, collimated
laser beam at as short a wavelength as possible. The general approach
is to transfer a high degree of coherence from long wavelengths, with
amplification through molecular and ionic devices in an eventual
chain system.

---

*Previous semiannual reports on this project are referred to liberally
in the present report. These are published as NRL Memorandum Reports
No. 2910 (October 1974) and No. 3057 (March 1975). Copies are
available on request.

NOTE: Manuscript submitted September 5, 1975.

It is appropriate here to reproduce one figure (Fig. 1) from a recent presentation[1] (copy included in the Appendix) which resulted from a somewhat bold projection of currently popular approaches to amplification at short wavelengths. Plotted is the mean density between amplifiers (N_0) and pumpers (N_p) for a realistically useful gain factor of $\alpha=5$. There are a number of reasons to seek lower density operation, e.g., reduced line widths, less collisional effects, approach to solid densities at short wavelengths, decreased pumping requirements, and flexibility for increased gain or compensation for unforeseen-losses. The bold lines indicate the regions of current interest at NRL in developing suitable amplifiers consistent with this aim towards decreased density. This analysis was done as part of our continuing evaluation of the entire field and indicates that, with current knowledge, we are indeed on the right track with a reasonable program.

Each component of our overall program is in a different phase of development, as detailed in the following sections. The nonlinear mixing experiments are essentially assembled now, experimental activity has increased, and preliminary results are reported. The first stage of amplification at 1600 A is undergoing a reevaluation at present due to unexpected complexities in the traveling wave electron beam device and soaring time and cost requirements. We may revert back to the proven discharge mode of operation or switch to a noble gas approach. The final decision will be influenced by our current tests on ability to synchronize the various devices to the driving coherent beam. Amplification on ions by picosecond pumping of preformed plasmas has definitely moved now into the target irradiation phase, as synchronization between the two laser beams improves. Further development towards higher laser power are being postponed until vacuum-UV x-ray and interferometric (density) measurements can be completed at the current plateau. Numerical modeling of atomic schemes here is also progressing smoothly with the development of very versatile laser codes. The search for direct experimental evidence of enhanced population of specific energy levels by resonance charge transfer is progressing with a very simple experiment designed for rapid proof-of-concept. An unexpected delay due to collection of debris in the spectrograph slit appears solved by a simple flushing technique and rapid progress can now be expected. A major physics question here is whether a sufficiently dense interaction region can be generated, and we are looking to computational assistance from other portions of the ARPA program in support of this experiment during the next six months.

The following sections of this report describe the details of progress made in each of these areas during the last six months. A summary of the important points is included in the last section. In some instances the work has been prepared for publication or has been published. In these cases the reprint has been included as an appendix and only brief mention of the work is made in the main body of the report. Each section also contains a few sentences about where the
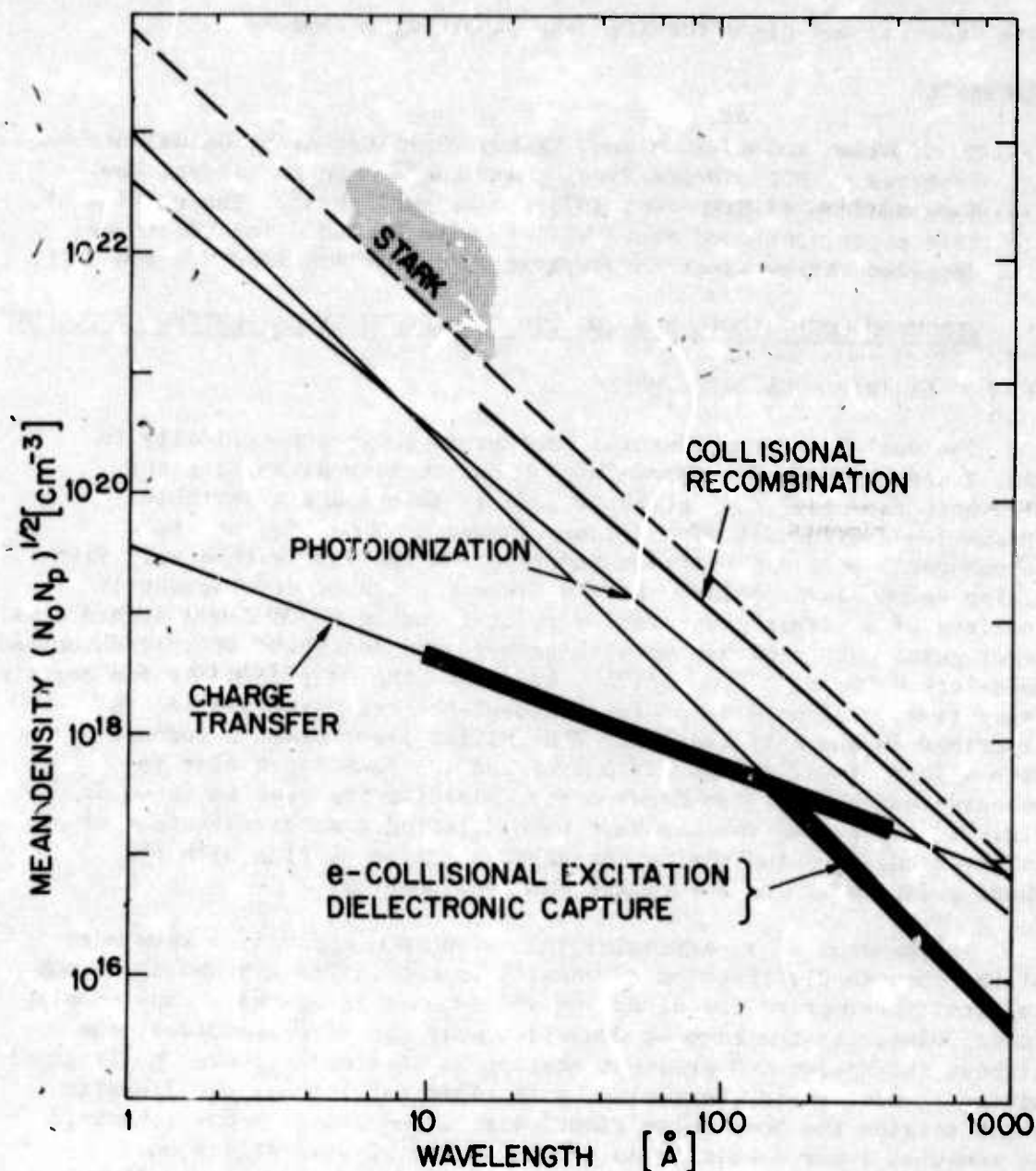
2

Fig. 1. Mean particle densities (solid lines) versus wavelength for a
gain factor of $\alpha=5$ and for selected pumping mechanisms. Stark broadening
becomes important for large charged particle densities (same scale) in
the region above the dashed line, also a region of approaching collisional
equilibrium. Collisional recombination is plotted for fixed $N_e=10^{21}$ cm^{-3}
and terminates at ~ 15 Å due to dominance of radiative recombination to
lower levels. Heavy lines indicate regions considered promising for
present experiments at NRL.

work is going and plans for the next reporting period.

REFERENCE

1.   R. C. Elton and R. H. Dixon, "X-Ray Laser Research: Guidelines and
     Progress at NRL", Proceedings Third Conference on Lasers, New
     York Academy of Sciences, 1975 (to be published). The portion of
     this paper mentioned above will be also included in a forthcoming
     detailed review paper in preparation for publication for the IEEE.

II.   ELECTRON COLLISIONAL PUMPING VIA PICOSECOND LASER PUMPING OF PLASMAS.

II. A.   LASER/PLASMA EXPERIMENT

   The dual-laser experimental concept is shown schematically in
Fig. 2 and has been discussed in previous semiannual reports and
elsewhere recently[1,2]. The basic idea is to prepare a suitable
plasma ion environment with a laser-target combination, and to
subsequently pump a population inversion on the ions with a very fast
rising second laser pulse. At its present stage of development it
consists of a plasma generated by point focusing a 2.0 J Q-switched glass
laser pulse onto a magnesium slab target, and injection of a synchronized
mode-locked 25 ps, 150 mJ Nd:YAG laser into the Mg-plasma after a certain
delay time. The details of the state-of-the-art laser system are
described in the next section. The initial laser beam is focused
with a 30 cm focal length, f/15 lens and the focal spot size is
measured using a silicon diode array, yielding the results shown in
Fig. 3. First observations have been directed towards detection of
enhanced emission indicating increased electron heating with the
short pulse laser and associated enhanced pumping.

   Independent of a particular inversion atomic model, a knowledge
of the spatial distribution of density in the initial expanding plasma
is vital information for directing and synchronizing the second pumping
laser pulse. At the highest densities near the target surface, the
highest absorption and greatest heating is obtained; however collisional
mixing is most rapid there also, with rapid collisional equilibration
which strains the pump pulse risetime requirements for many schemes.
At somewhat lower densities in the expanding plasma, collisional
rates are lower and plausible inversion schemes are more identifiable[3],
particularly for low-Z targets. Multiple passes or extended lengths
then become a possible requirement for sufficient absorption. The
determination of the density distribution can be accomplished
relatively simply in-situ using an interferometric technique which
utilizes the existing synchronized 25 ps Nd:YAG laser as a probing
light source, frequency doubled. This is presently being set up.

   Meanwhile, the ionic composition of the expanding plasma as well
as the temperature can be appreciated using x-ray photography and
spectroscopy. Figs. 4a and 4b illustrate images of the x-ray emitting

4

LASER
BEAM#2
0.15 J
25ps
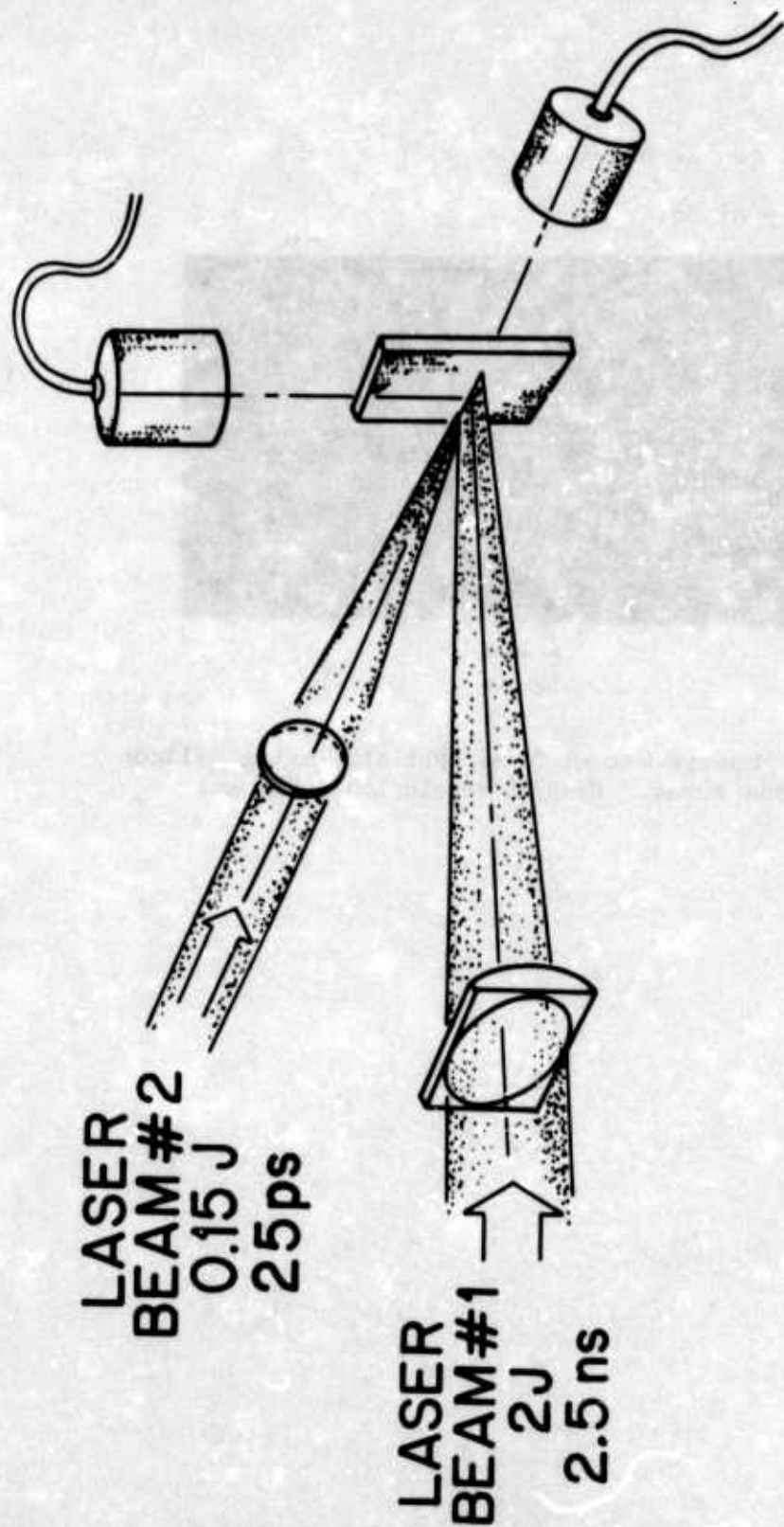
LASER
BEAM#1
2J
2.5 ns

Fig. 2 Schematic of experiment designed to verify gain on transitions pumped
by electron collisions in a plasma.

5
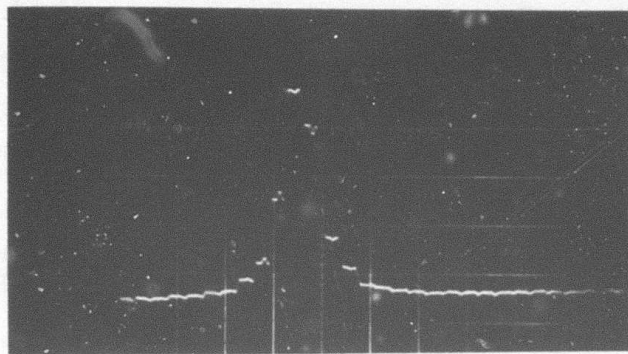
100 μm

Fig. 3 Measurement of focal spot size using silicon
diode array. Spatial resolution is 25 μm.

X—RAY (1—1.5 keV) PHOTOGRAPHS

a) PINHOLE (50 μm)

← LASER

1mm →| |←

Mg

E = 2 J
Δt = 2.5 ns
d = 100 μm (POINT)
p/a = 10^13 W/cm^2

b) TUBULAR
(5 cm × 400 μm)
COLLIMATOR

← LASER

1mm →| |←

Fig. 4   Time integrated X-ray image of expanding plasma

    (a)   using a 50 μm pinhole.

    (b)   using a bundle of 5 cm long metallic tubes of which inner
           diameter is 400 μm.

7

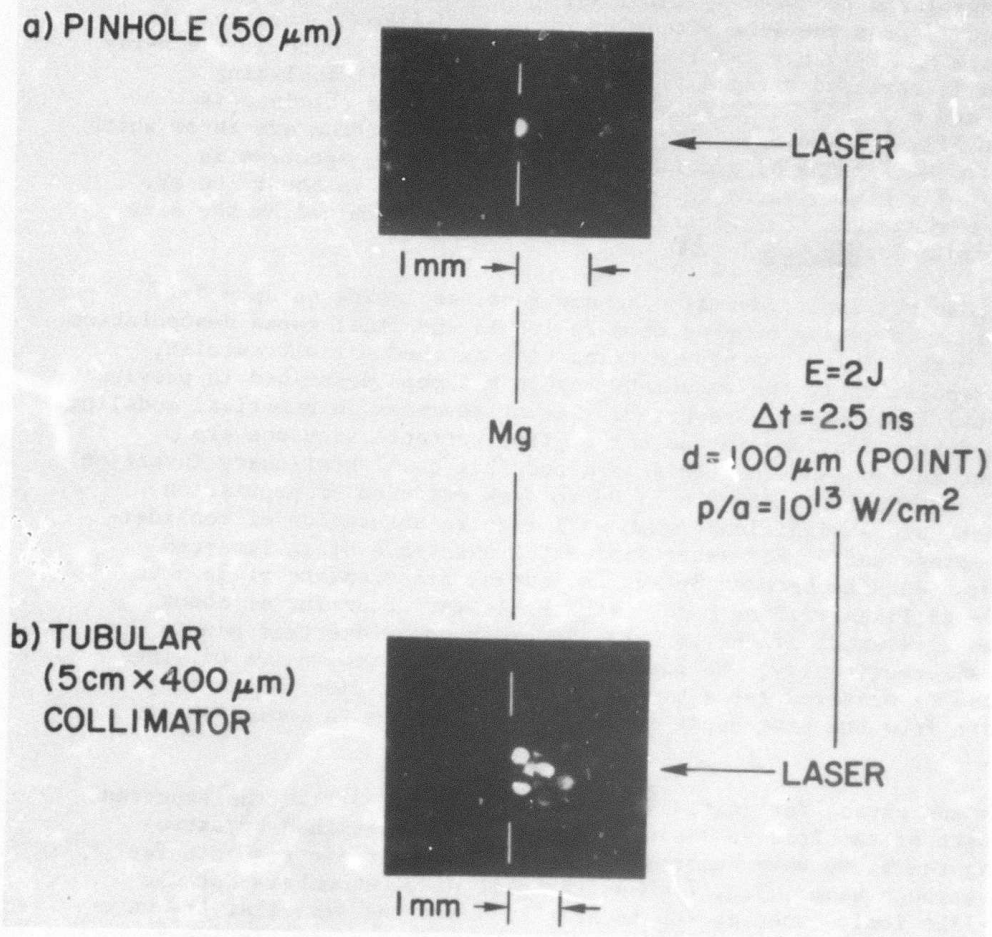initial plasma obtained, respectively, with a 50 μm pinhole and through a bundle of 5 cm long metallic tubes (i.d. = 400 μm), both of which recorded x-ray photons of 1 to 1.5 keV. While the former shows only the most intense x-ray emitting region (∼ 250 μm) in the vicinity of the target, the latter also records rather faint x-rays originating from tenuous expanding plasma which extends as far as 1 mm along the target and 1.8 mm away from the target. A peak electron temperature of the Mg-plasma produced by the Q-switched glass laser may be estimated[4,5] from the line intensity ratio of H-like Mg XII 2p → 1s to He-like Mg XI 1s2p → 1s^2 lines, assuming a coronal model. The x-ray spectrum is obtained using a flat RAP (2d = 26.121 Å) analyzing crystal and a microdensitometer scan of the spectrum obtained is shown in Fig. 5. The main line features in the spectrum are those which arise from He-like Mg XI and Li-like Mg X ions. The spectrum is typical[4] of a plasma where the electron temperature is about 100 eV. In this arrangement the spectral line width is determined by the size of the radiating source (∼ 250 μm).

A possible ionic inversion scheme involves lasing on 3p → 3s transitions following pumping from 2p levels and final rapid depopulation from 3s → 2p. This is a proven transition in the near ultraviolet, and extrapolation to the vacuum-UV region has been described in previous semiannual reports and elsewhere[3]. Recent advances in numerical modeling of this scheme for ions in the carbon isoelectronic sequence are described in Section V.A. This is a possible quasi-stationary inversion scheme, and the first stage will be to seek evidence of population inversion, since significant gain will require absorption of considerable pumping energy. For ascertaining the existence of an inverted population density between 3p and 3s levels, measurements of 3p → 3s and 3s → 2p lines will be made, with the latter occurring at about 1/10 the wavelength of the former. In order to bridge this gap in instrument sensitivity, the 3d → 3p and 3d → 2p nearby pairs of lines will also be measured for a branching ratio calibration, since they originate from the same upper level. This approach is indicated in Fig. 6.

Th ion chosen for initial studies is Mg^{6+} (Mg VII). The expected wavelength of the 2p3s ^{3}P lasing line has been determined by extrapolating the known wave numbers in the CI isoelectronic sequence for carbon through neon. Fig. 7 shows the plot of wave numbers for the carbon-like ionic species (up to Ar XIII), and one sees that the wavelength for Mg VII falls at 1625 ± 10 Å. A 1-meter normal-incidence vacuum UV spectrometer with a 1,200 lines-per-millimeter ruled grating (blazed at 1200 Å) has been set up for the spectroscopic analysis, and the target chamber is mounted directly on the front of the entrance slit assembly. The distance between the target focal spot to the entrance slit is 11 cm. Fig. 8 shows a microdensitometer scan of a typical time-integrated spectrum in the region of 1400 to 1800 Å, taken with a 20 shot (Q-switched glass laser only) exposure. The Mg-target used in this particular exposure contained aluminum and carbon as impurities; the AℓII 3s3p ^{1}P - 3s^2 ^{1}S line at 1670.8 Å and

8
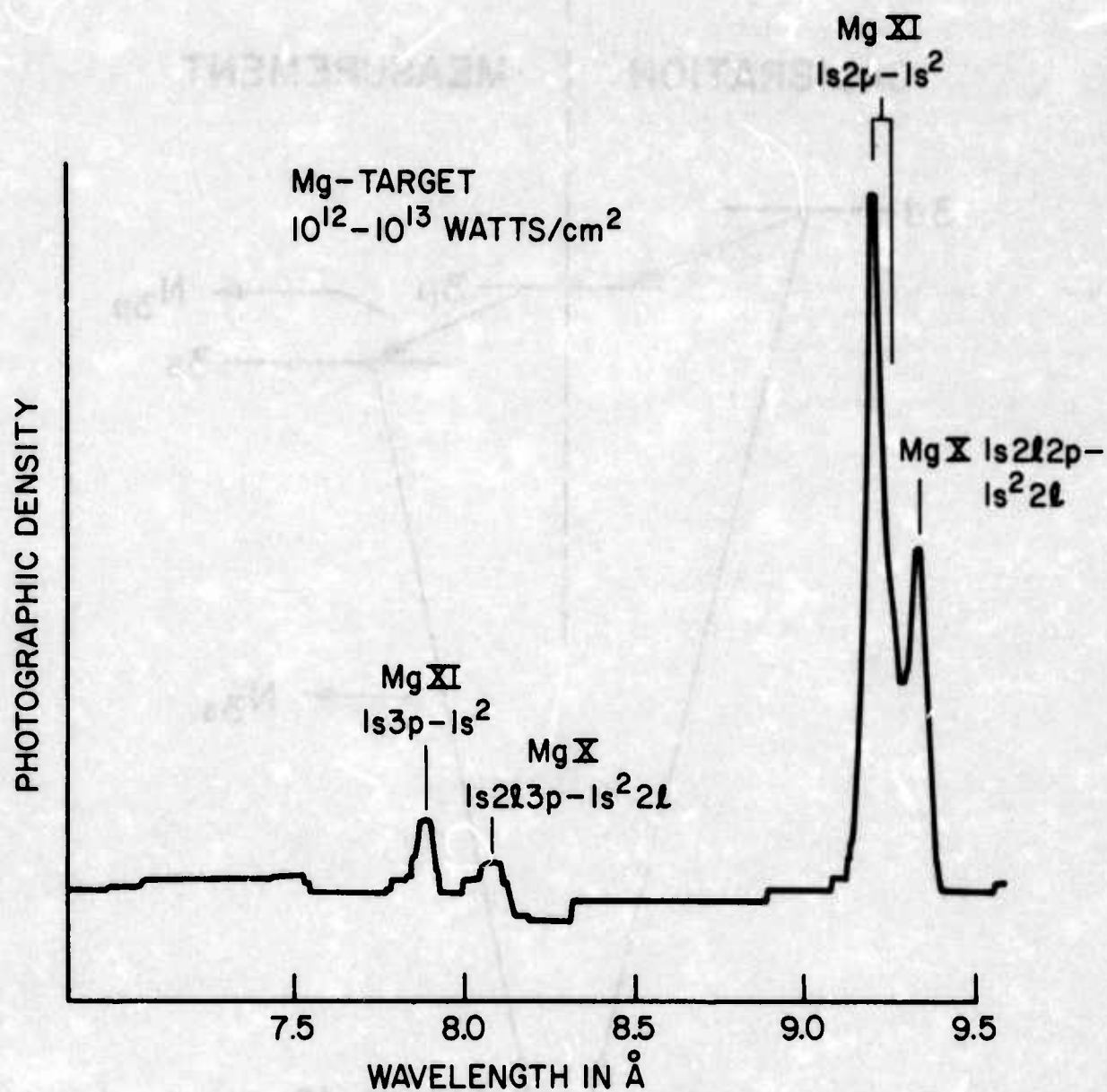
Fig. 5 K-x-ray spectrum of Mg-plasma obtained with RAP analyzing crystal. Q-switched glass laser is focus onto a Mg-target to form a 100 μm dia focal spot.

CALIBRATION | MEASUREMENT
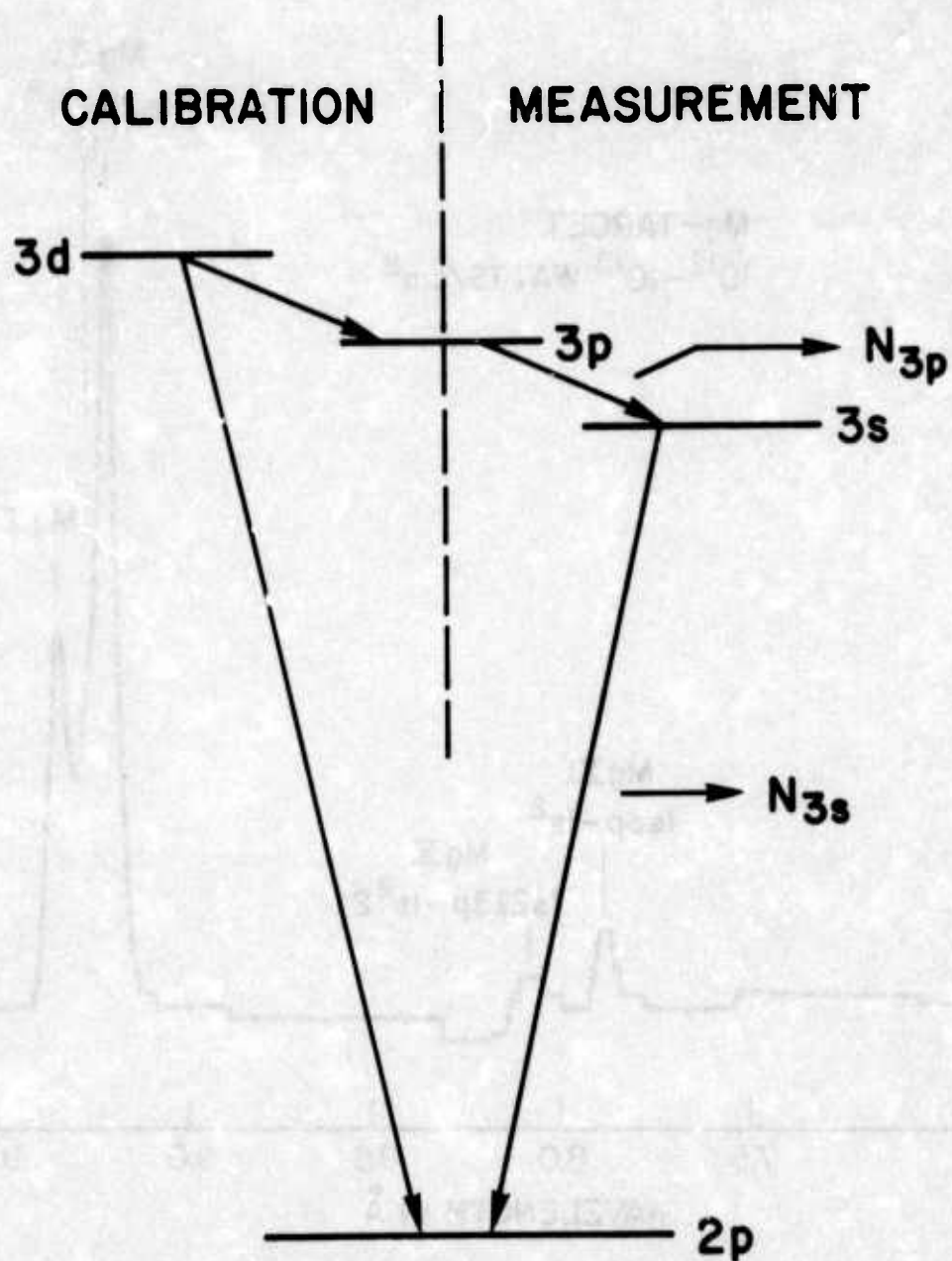
Fig. 6 Transitions involved in determining the population inversion
ratio N_{3p}/N_{3s} from relative line intensities, using branching transitions
shown from the 3d level for instrumental calibration.

Fig. 7 Extrapolation of 2p3p ^{3}D - 2p3s ^{3}P transition lines in carbon-like isoelectronic sequence.

11

Fig. 8 Vacuum UV spectrum of laser (Q-switched glass laser) produced Mg-plasma.

12

the CIV 2p ^{2}P - 2s^{2}S doublets at 1550.8 Å and 1548.2 Å providing
excellent references. Some of the lines identified so far are listed
in Table 1. The spectrum consists of mostly lines arising from Mg IV
and Mg III ions in this spectral range; however, it is conceivable
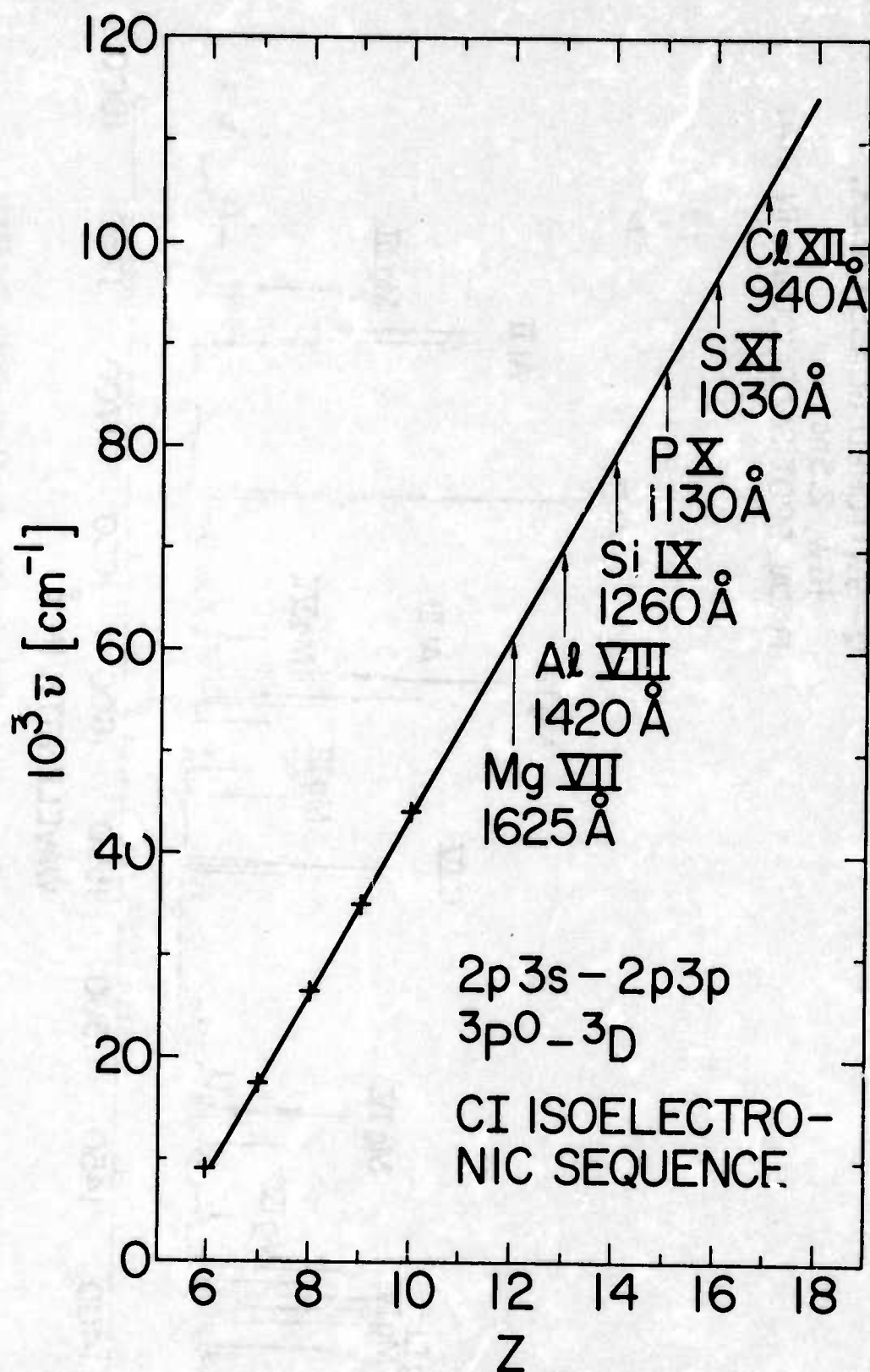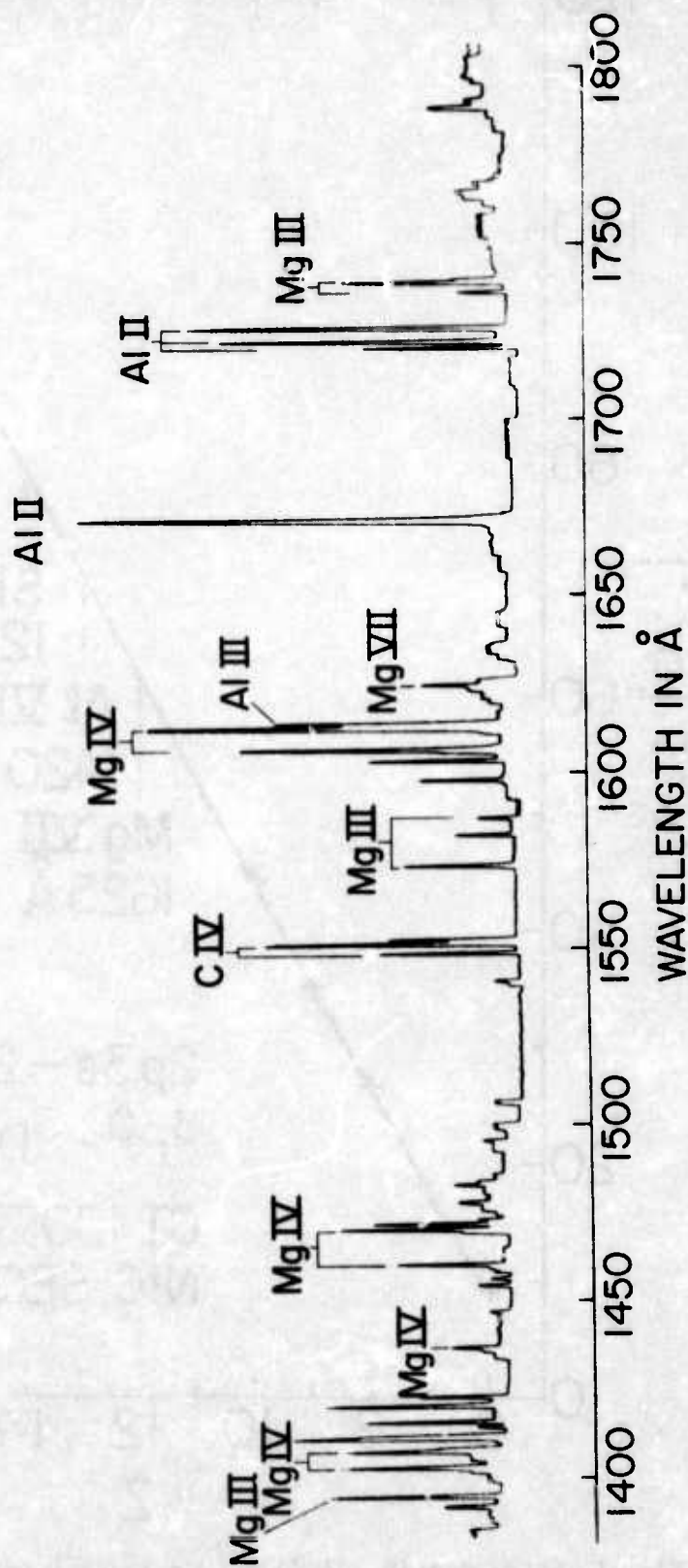that some of the unidentified lines are those which originate from
Mg ions of higher stages of ionization. For example, a weak line at
1625 Å may be the Mg VII (2p3p ^{3}D - 2p3s ^{3}P) transition as predicted.
The shorter wavelength 3s → 2p (and 3d - 2p) lines for Mg VII require
grazing incidence spectroscopy. Preliminary space resolved measure-
ments on a separate system (charge transfer experiment described in
Section III) indicate the presence and resolution of these lines in
magnesium as shown in Fig. 9.

It is planned to compare two space-resolved Mg-spectra, obtained
with and without the injection of the 25 ps Nd:YAG laser firing in conjunction
with the Q-switched glass laser pulse, as soon as the electron density
profile of the expanding plasma is known. Also, some experiments may be
conducted with a lower-Z material such as fluorine, so that both
long and short wavelength lines can be measured on the same instrument,
to prove the technique.

REFERENCES

1. R. C. Elton, in Progress in Lasers and Laser Fusion, p. 117
   (Plenum Press, New York, 1975).

2. R. A. Andrews in Progress in Lasers and Laser Fusion, p. 235
   (Plenum Press, New York, 1975).

3. R. C. Elton, Appl. Optics 14, 97 (1975).

4. D. Mosher, Phys. Rev. A 10, 2330 (1974).

5. T. N. Lee and D. J. Nagel, J. Appl. Phys.; Sept., 1975 .

II.B. SYNCHRONIZED DUAL LASER FACILITY

The experiments described above (Section II.A) require a high
power Q-switched laser to generate a plasma of proper ionic consistency;
and a second, synchronized, short pulsed mode locked laser to produce
population inversion during the pre-equilibrium period of high electron
temperature. This coupled mode-locked Q-switched laser system is
now nearing completion. The full synchronizing sequence is operational,
and the jitter between the mode locked and Q-switched pulses have
been reduced to ± 0.12 ns. The gain in each amplifier has been
measured independently. During this reporting period the Q-switched
laser was operated at full output power for the first time; and some
time was spent on longitudinal mode control in the oscillator.
Additional path delays were introduced into both the Q-switched and
mode locked lasers so that the shuttered portion of the Q-switched laser

TABLE 1: Extrapolation of Lasing Transitions on Carbon-Like Ions.

| ION SPECIES	λ in Å	CONFIGURATION
Mg III	1738.8	$2p^5 3p\ ^3D - 5p^5\ 3d\ ^3F$
Mg IV	1736.8	$2p^4 3s\ ^2P - 2p^4\ 3p\ ^2S$
Aℓ II	1725	
Aℓ II	1721.2 } 1721.3 }	$3S\ 3P\ ^3P - 3s\ 3d\ ^3D$
Aℓ II	1670.8	$3s^2\ ^1S - 3s\ 3p\ ^?$
Mg VII	1625 ?	$2p\ 3s\ ^3P - 2p\ 3p\ 3D$
Aℓ III	1611.9	$3p\ ^2P - 3d\ ^2D$
Mg IV	1611.2 }	
Mg IV	1607.1 }	$2p^4\ 3s\ ^2D - 2p^4\ 3p\ ^2D$
Mg III	1586.2 }	
Mg III	1572.7 }	$2p^5\ 3p\ ^3S - 2p^5\ 3d\ ^3P$
CIV	1550.8 }	
CIV	1548.2 }	$2s\ ^2S - 2p\ ^2P$
Mg IV	1470.8	$2p^4\ 3p\ ^2P - 2p^4\ 3d\ ^2D$
Mg IV	1459.6	$2p^4\ 3s\ ^4P - 2p^4\ 3p\ ^4S$
Mg IV	1437.5	$2p^4\ 3p\ ^2D - 2p^4\ 3d\ ^2F$
Mg IV	1409 }	
Mg IV	1404.7 }	$2p^4\ 3p\ ^2F - 2p^4\ 3d\ ^2G$
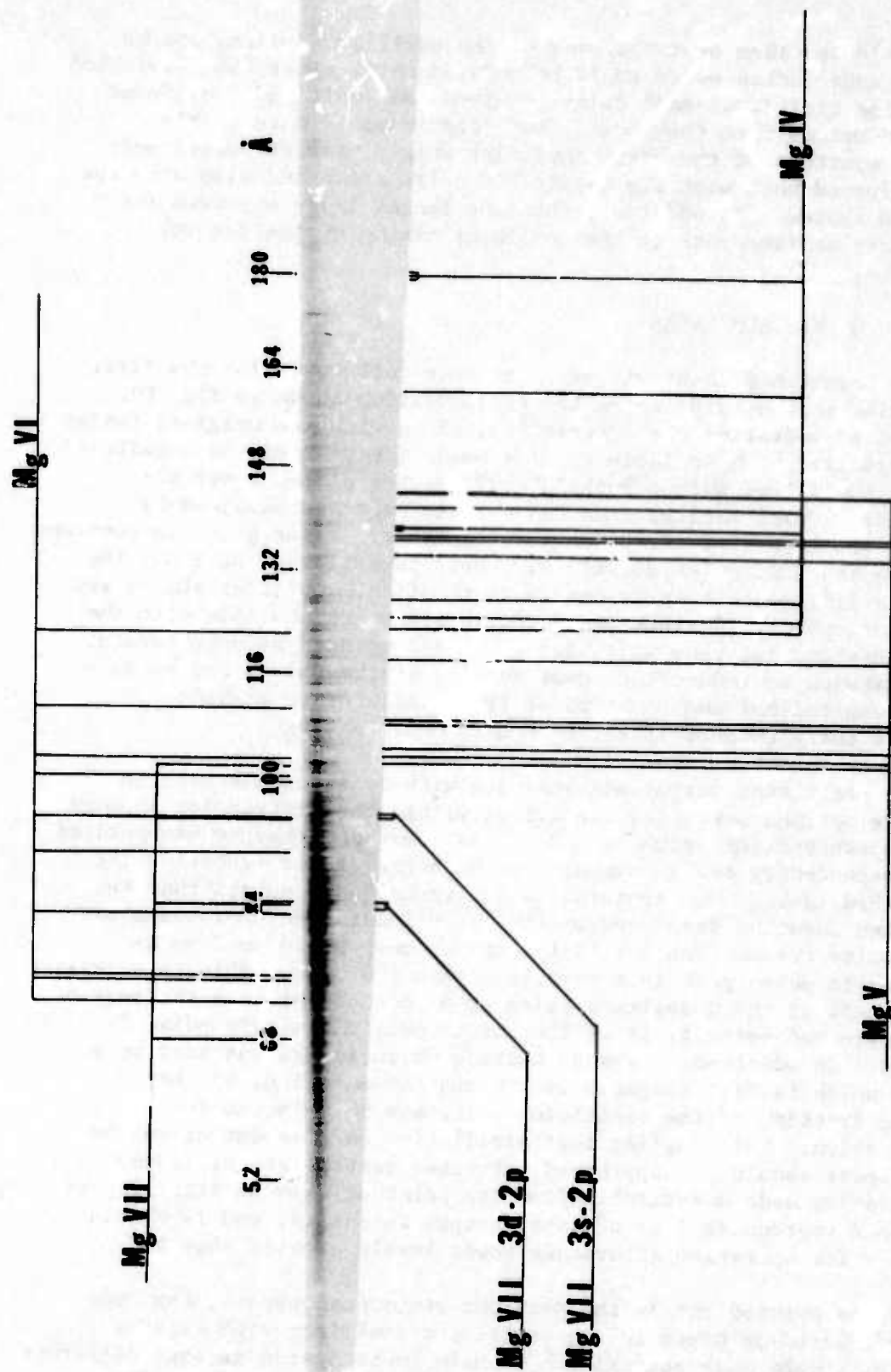
Fig. 9 Grazing incidence magnesium spectrum.

15

pulse could be taken near the peak of the oscillator pulse, and so that the mode locked pulse could be delayed until after the Q-switched pulse. The additional path delay required the addition of cylinder expansion optics into the mode locked laser beam to more nearly fill the aperture of the final amplifier stage. Target experiments were performed both with the Q-switched pulse alone and also with the two-pulse system. In addition, the mode locked laser was used for preliminary measurements of the nonlinear mixing system for VUV generation.

II. B.1. Q-SWITCHED LASER

The Q-switched laser was operated near full power for the first time during this period, using the configuration shown in Fig. 10. The measured operating characteristics, along with the original design parameters are shown in Table 2. The pulse duration of the Q-switched laser is controlled with a Pockels cell shutter placed after the oscillator. Pulse lengths from 0.5 to 10 nsec are obtained by changing the length of the pulse forming cable. Laser power is constant over this range of pulse durations. Above power levels of 1 GW, the output is limited chiefly by damage to the final amplifier stages and subsequent optics. Further increases in power are possible with the current system, but they will have to be accompanied by more careful beam expansion to reduce the power density at the output and by more stable longitudinal mode control of the oscillator to prevent excessive instantaneous intensity due to mode beating.

The oscillator output was analyzed with considerable care to determine optimum operating condition, within the restriction imposed by the synchronizing sequence. This laser was designed to be operated both independently and in synchronism with the single (short) pulse mode-locked laser. The synchronization technique requires that the Q-switched laser be triggered on the early leading edge of the mode-locked pulse train. The oscillator output must build up from Q-switching to pulse peak in a time less than 150 nsec. This is necessary for the peak of the Q-switched pulse to be coincident with the peak of the mode-locked pulse train at the point where the single pulse is selected. In addition, any mode beating which is present must be on a scale which is fast compared to the shutter duration, so that a reliable fraction of the oscillator pulse may be selected for amplification. This implies that oscillation on adjacent or nearby cavity modes should be suppressed. Further restriction of lasing to a single cavity mode is desirable from the point of view of stability of timing and reproducibility of laser output intensity, and is absolutely necessary for operation at average power levels greater than 1 GW.

As was pointed out in the previous semiannual report, the need for rapid build-up times in the oscillator conflicts with requirements for single mode operation.[1] We have investigated several different cavity configurations for longitudinal mode selection under conditions of rapid pulse build-up. Preliminary studies indicated that a three

16
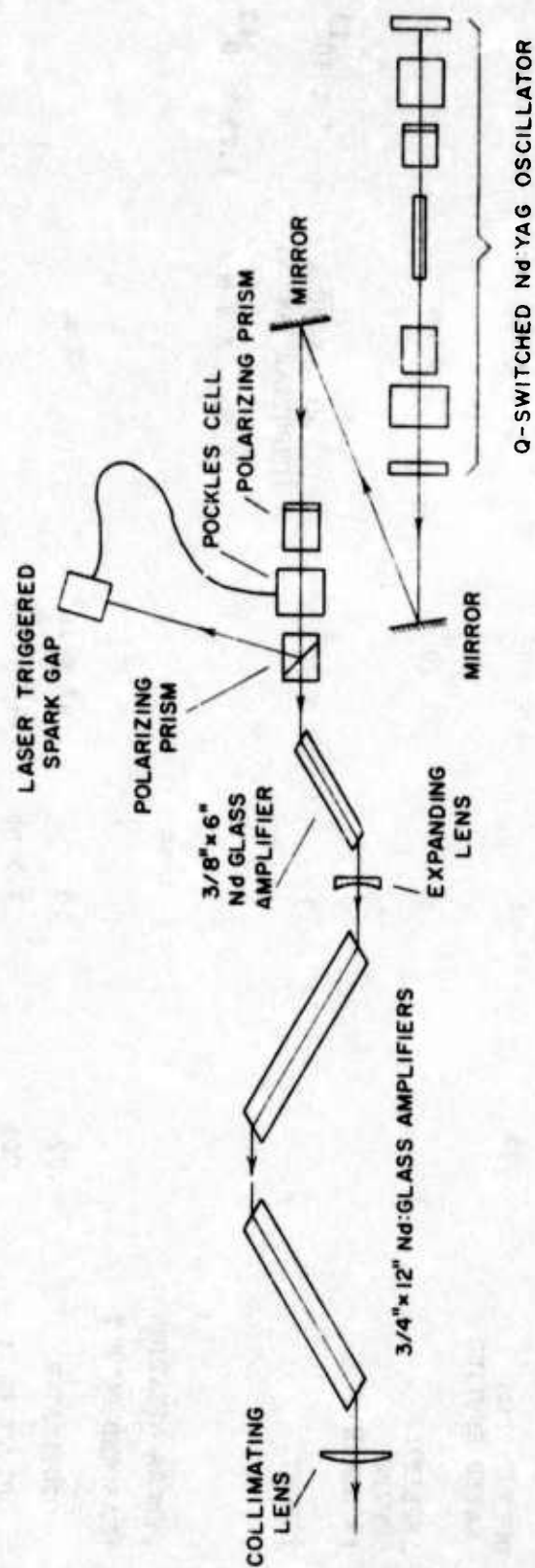
Fig. 10   Schematic of Q-switched laser system setup to be run independently of second laser.

17

TABLE 2:   LASER SYSTEM PARAMETERS

Q-SWITCHED LASER (SYNCHRONIZED)

● DESIGN GOALS

STAGE	PULSE ENERGY (J)	PULSE DURATION (ns)	POWER (W)	BEAM PROFILE	INTENSITY (W/CM)^2
OSCILLATOR OUTPUT	.05	50	1 X 10^6 (PEAK)	2 mm (CIRCULAR GAUSSIAN)	
OUTPUT FROM GATED SHUTTER	.003	3	1 X 10^6	2 mm	
AMPLIFIER OUTPUT (3 STAGE)	3	3	1 X 10^9	2 cm	
TARGET	3	3	1 X 10^9	50 μ X 50 μ (CIRCULAR FOCUS)	5 X 10^{13}
				50 μ X 2 mm	1.25 X 10^{12}

SYNCHRONIZATION   ≤ 1 ns

● MEASURED OUTPUT

STAGE	PULSE ENERGY (J)	PULSE DURATION (ns)	POWER (W)	BEAM PROFILE	INTENSITY (W/CM)^2
OSCILLATOR	.02	20	.67 X 10^6	2 mm	
OUTPUT FROM SHUTTER	.001	2.5 ns	.4 X 10^6		
AMPLIFIER OUTPUT	3	2.5	1.2 X 10^9	1 cm	
TARGET EXPERIMENTS	3	2.5	1.2 X 10^9	30μ (CIRCULAR FOCUS)	16 X 10^{13}
				50 μ X 2 mm (LINE FOCUS)	1.5 X 10^{12}

18

element resonant reflector, or a two element reflector combined with a birefringent filter[2], would be necessary to achieve sufficient discrimination. Calculations indicated that an acceptable performance could be obtained with a resonant reflector which consists of a combination of a 5 cm long quartz flat, and a flat mirror combined with a 5 cm long birefringent calcite plate (Fig. 11). Discrimination against adjacent and nearby cavity modes is obtained with the two element resonant reflector (Fig. 12) and discrimination against widely spaced modes is provided by the calcite plate (Fig. 13). Theoretical analysis of the combination indicates that the reflectivity of the second largest mode is 0.91 of the reflectivity of the mode of maximum feedback.

Experimental investigation of the combination was performed in steps. The output of the laser oscillator was measured on a planar-diode and 519 oscilloscope with response time of 0.5 ns, an image converter-streak camera with a resolution of 30 psec, and a Lummer-Gehrcke interferometer with a free spectral range of 1.14 cm^{-1} and a resolution of 0.08 cm^{-1}. These three devices provided detection of all mode spacings with good overlap in the ranges.

A study was first made of the laser output using the 2 inch SiO_2 plate and a 45% flat mirror. Typical measurements are shown in Fig. 14. Considerable variation could be observed in the output as the distance from the mirror to the quartz plate was varied and, at an optimum spacing, oscillations fluctuated between true single mode behavior on modes too widely spaced for the beating to be resolved on the 519 oscilloscope. Beating between nearby modes was effectively reduced, as is expected from the curve in Fig. 12; and the resulting pulse is sufficient for use in the current set of experiments.

Attempts were made to reduce the remaining mode beating with the use of additional frequency selection. A Laser Optics "Ekalon" resonant reflector was substituted for the 45% mirror. With adjustment of reflector spacing, improved frequency selection was obtained; however, it was not stable. After approximately 10 shots, single mode operation deteriorated to multimode modulated output (Fig. 15).

The birefringent calcite plate was added next. As expected, the suppression of oscillations on widely spaced modes was improved. Oscillation on nearby modes, however, reappeared. This can be attributed to a number of factors. The thickness of the "Ekalon" device is fixed, therefore its reflection cannot be tuned to the transmission peak of the birefringent filter and to the peak of the Nd:YAG fluorescence. The combination of the 45% mirror, 2 inch fused silica flat, and birefringent filter should overcome this problem. Testing of this last combination had to be postponed to allow target experiments to continue. Additional effort shall be placed on further isolation of the laser oscillator using mechanical and acoustical isolation and a permanent shield. Methods of temperature stabilization are also being investigated. It

19
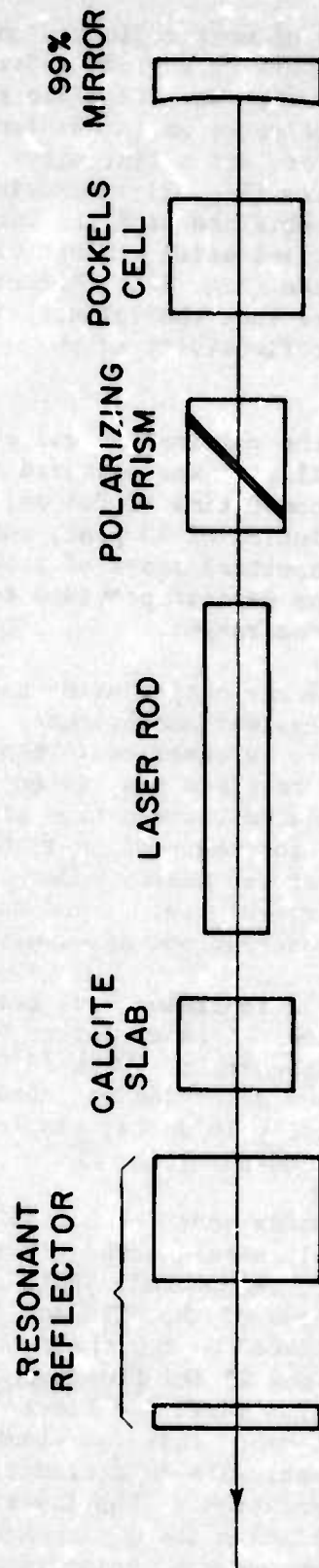
Fig. 11 Q-switched oscillator with frequency selection components.

99% MIRROR

POCKELS CELL

POLARIZING PRISM

LASER ROD

CALCITE SLAB

RESONANT REFLECTOR
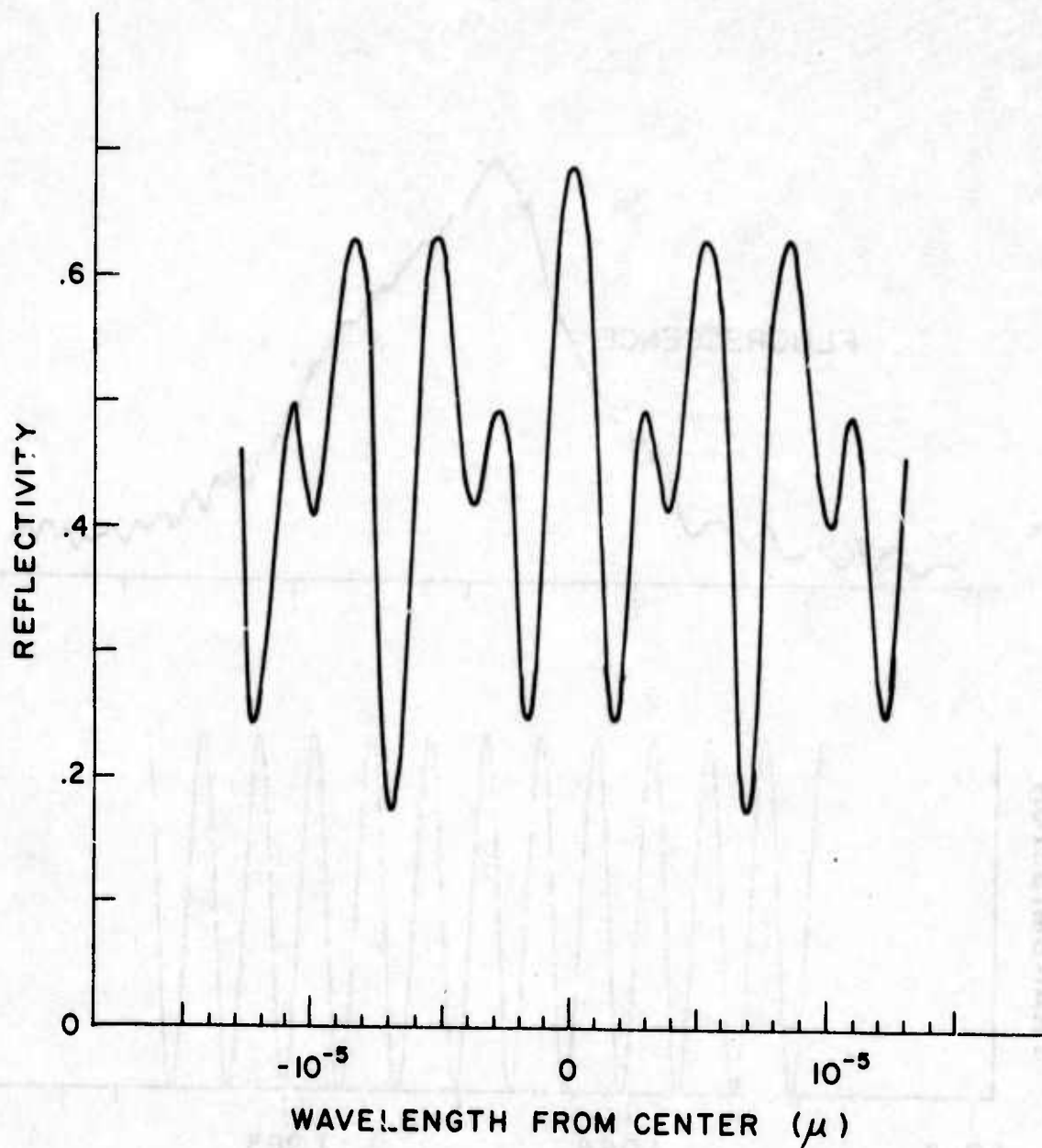
Fig. 12   Reflectivity of two element reflector consisting of 45% single
surface mirror and 2 inch thick flat-parallel fused quartz reflector
spaced 4.35 inches.

21
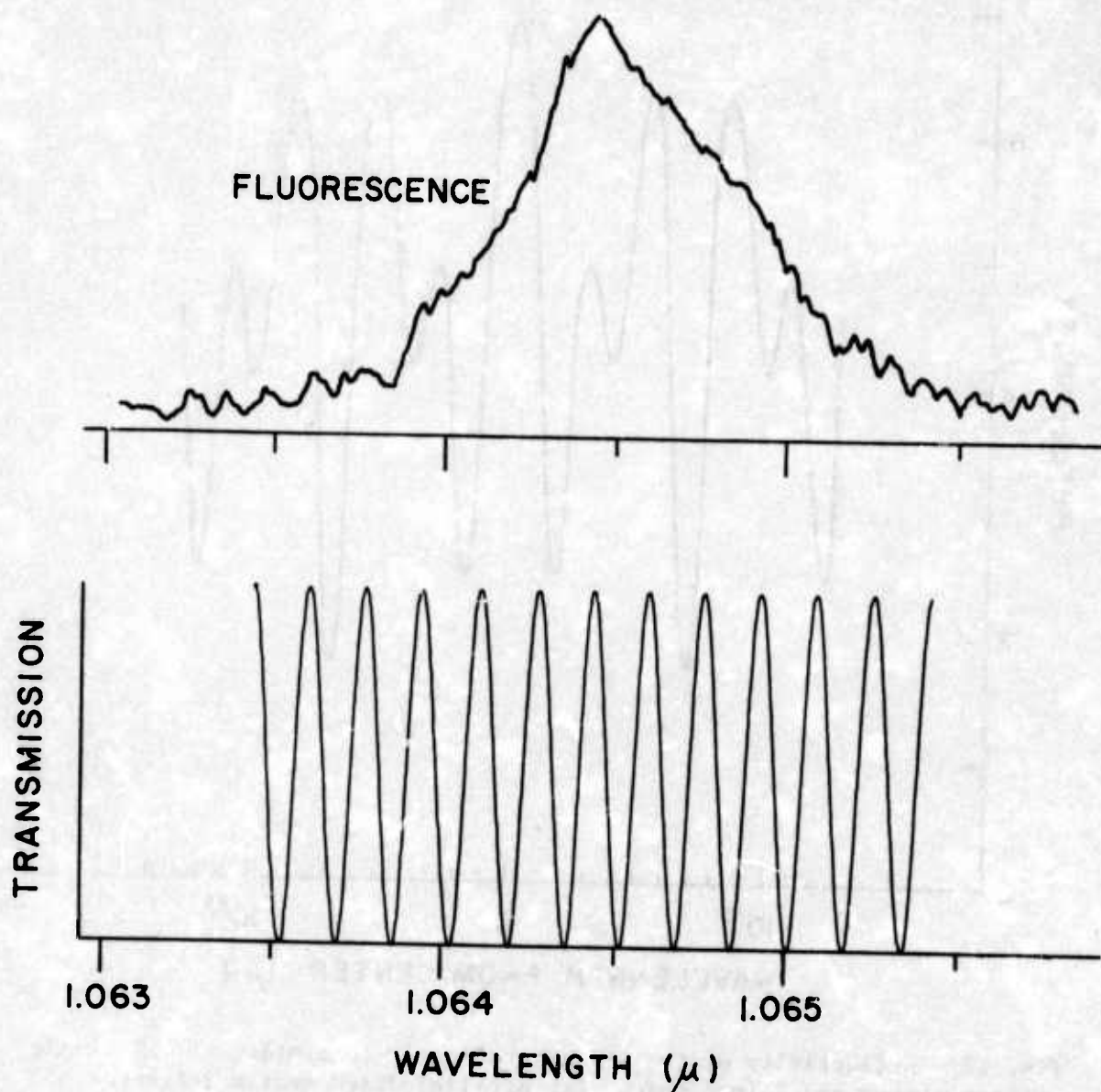
Fig. 13 Transmission of calcite plate and polarizer compared to Nd:YAG fluorescence.

22
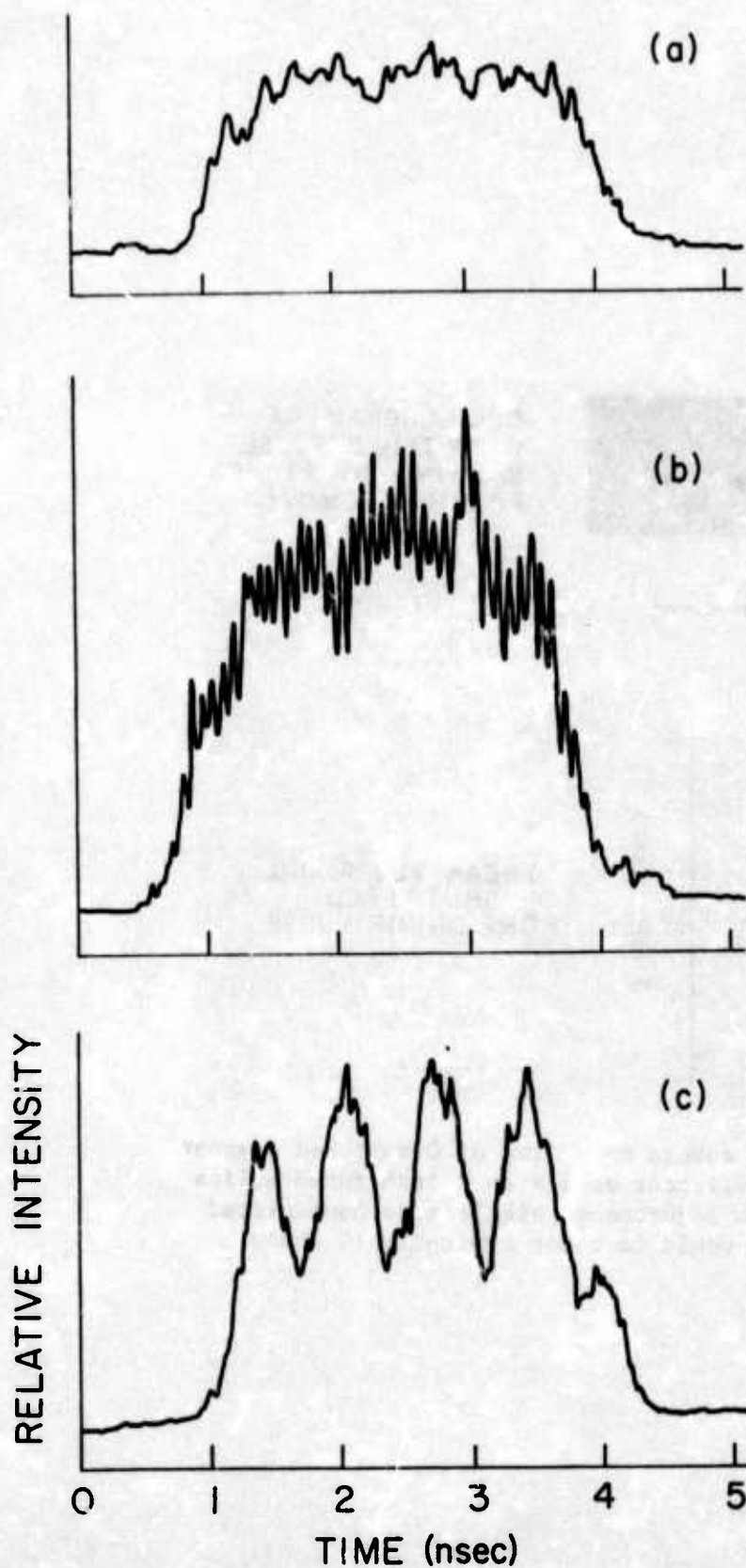
Fig. 14 Streak camera recordings of a 3 nsec segment of the Q-switched laser pulse. This performance is typical for operation with the 2 inch reflector and 45% mirror alone. Laser output would vary between single mode (a) and two widely spaced modes (b). Translating the 45% mirror a fraction of a wavelength produced the slower modulation of closely spaced modes (c).

23

OSCILLOGRAM OF
Q-SWITCHED PULSE
SHOWING SHUTTERED
PORTION REMOVED

|← 120 nsec →|

STREAK RECORDING
OF SHUTTERED
PORTION OF PULSE

Fig. 15 Streak camera recording of Q-switched segment
with "Ekalon" reflector used with 2 inch fused silica
reflector. With adjustment, signle mode unmodulated
output as shown would last for typically 10 shots.

24

is anticipated that with these improvements, stable operation on a single mode can be achieved with the system in Fig. 10.

II.B.2. MODE-LOCKED SHORT-PULSE LASER

The mode-locked laser is now fully operational, and routinely operates with output energies between 150 and 200 mJ. During the course of arranging components for the synchronizing sequence, it became necessary to add about 4 ns of delay to the mode-locked laser (Fig. 16). This added path resulted in astigmatic propagation of the mode-locked pulse because of its elliptical profile (see first semiannual report), and a reduction in pulse energy to the 80 - 90 mJ level was observed. Introduction of cylinder expansion i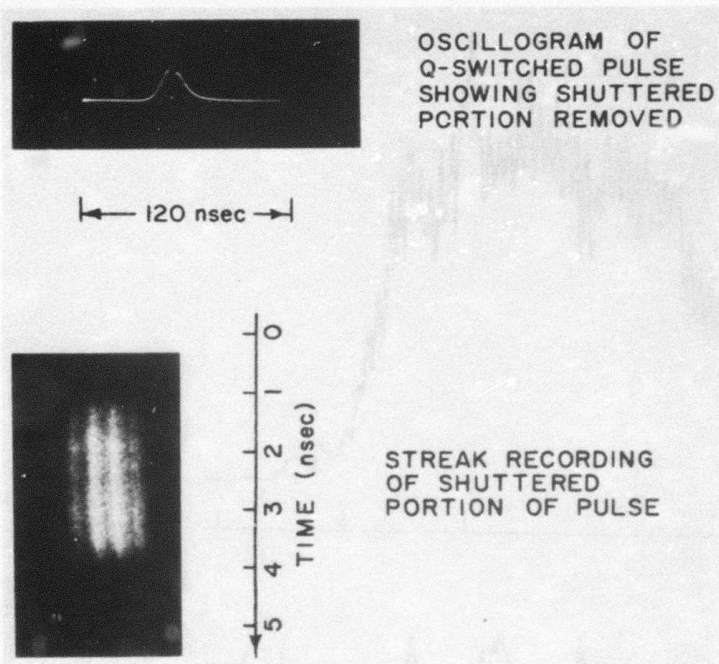nto each arm before the $\frac{1}{2}$ inch amplifier resulted in an overall beam size which more nearly fills the amplifier rods, and has restored the output energy to its original value near 200 mJ. Each beam was then collimated by an appropriate cylindrical lens at a position which gives a circular profile. The resulting beam can then be focused to a smaller spot than the elliptical one, giving greater intensity in the focal region, or can be expanded for amplification in a glass amplifier.

Further work on the mode locked laser will be in the areas of target isolation involving the addition of isolating Pockels cell (Fig. 16), and gradual improvement of its operation in the areas of efficiency and reliability. Equipment has also been assembled for the addition of a 32 mm glass amplifier which can raise the output power to 2 J.

REFERENCES

1. P. W. Smith, "Mode Selection in Lasers" Proc. IEEE 60, 422-440 (April 1972).

2. G. Holtom and O. Teschlse, "Design of a Birefringent Filter for High-Power Dye Lasers" IEEE J. Quantum Electron. QE-10, 577-579 (August 1974).

II.B.3. REDUCTION OF SELF FOCUSING

While no serious experiments have been performed in this area during this reporting period, some thoughts have continued since self-focusing is a potential problem as lasers of increased power become a necessity for short wavelength pumping sources. Thoughts are directed towards a method of compensating for self focusing (and self phase modulation) in high power lasers, and thereby extending their power capabilities.

BACKGROUND

The useful output power that can be generated in many pulsed solid state lasers is limited by the occurrence of self focusing and
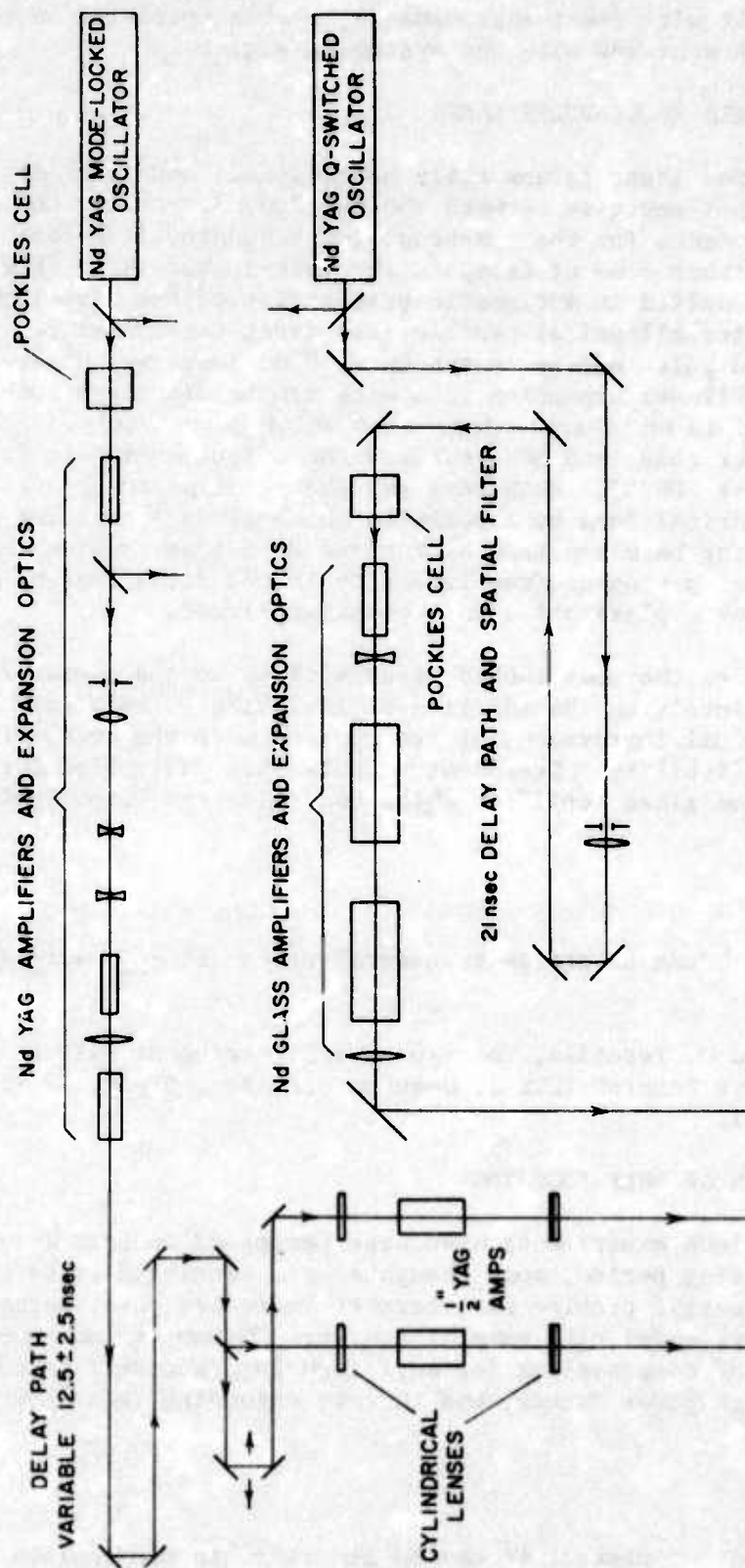
Fig. 16 Synchronized laser schematic showing additional delays and beam expansion optics.

self phase modulation due to the positive nonlinear refractive index n_2 of the amplifying medium. Self focusing need not involve the entire beam; in fact, it occurs most often in the form of filaments or "hot spots". These grow exponentially out of low amplitude spatial inhomogeneities in the input beam as the pulse propagates through the laser amplifier chain. In general, the growth rate of the hot spot intensity is proportional to the product of the nonlinear index n_2, the average beam intensity I_0, and the <u>total</u> propagation path length ℓ through all of the amplifying stages. At moderate power levels, self focusing degrades the pulse by distorting its wavefront and broadening is spectral width through self phase modulation. At high power levels, the hot spots can grow to catastrophic intensities and cause serious damage to the final amplifier stages.

Present techniques for minimizing self focusing include (i) minimizing spatial ripples (e.g., due to interference effects) in the input beams; (ii) use of large aperture amplifiers to keep the average intensity low; (iii) use of high gain, low n_2 amplifying materials to minimize $n_2\ell$; (iv) spatial filtering between amplifier stages to eliminate higher spatial frequency inhomogeneities, which tend to grow more rapidly; and (v) use of an aspheric diverging lens to counteract whole-beam self focusing and reduce the growth rate of the hot spots. Minimization of ripples on the input beam is a necessary first step; however, it is difficult to reduce the effects initiated by small random inhomogeneities in the amplifying material itself. Moreover, one cannot eliminate the spatial frequency components introduced by apodization of the beam. The use of large aperture amplifiers is limited by cost, and by such factors as parasitic oscillations. In practice, apertures are limited to about 20 cm. The recent development of high gain, low n_2 materials, such as phosphate glasses, may allow an increase in useful output power by a factor of two or three. The gain of an amplifier stage is limited by parasitic oscillation, and conventional methods for reducing n_2 are not likely to effect reductions significantly greater than 30%. Spatial filtering can eliminate only the higher spatial frequency components (e.g., spatial frequencies > 10 cm^{-1}). As the intensity increases, however, the lower spatial frequencies begin to grow rapidly, and whole-beam distortion becomes important. A diverging lens has the disadvantage that it can effectively counteract self focusing in only a narrow range of intensities. If it is effective at the peak of the pulse, then it offers little advantage elsewhere.

POSSIBLE SOLUTION

We propose to reduce or eliminate the self focusing by using a material with a negative n_2 to compensate for the positive n_2 of the laser amplifiers. Several materials exist with a negative n_2 in narrow frequency ranges accessible to the lasers most commonly used. For example, it has been noted that cesium should exhibit a negative value of n_2 at the Nd:YAG wavelength 1.064 μ.[1] A recent experimental and theoretical study of cesium vapor described in

27

previous semiannual reports and elsewhere[2] has confirmed that the n_2 is indeed negative at 1.064 μ, and that it can be made comparable in magnitude to the n_2 of typical laser glasses. With linearly polarized light, the effect arises mainly from a two-photon resonance between the pulse and the atomic levels 6s and 7s.[2] This means that the nonlinear refractive properties remain intensity-dependent, even for pulsewidths comparable to the inverse atomic linewidth - an advantage not shared by single-photon resonances[2,3,4] or thermally-induced nonlinear refractive effects.[5]

One practical embodiment of the compensation scheme would use a chain of amplifier-compensator units as illustrated in Fig. 17.
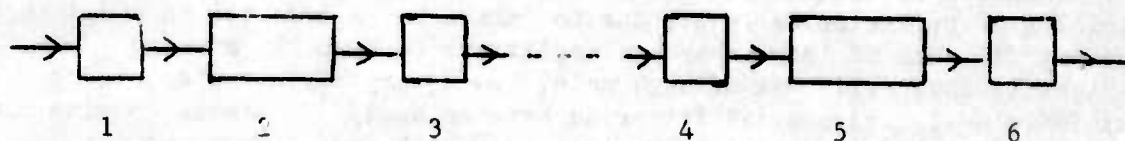

Figure 17

The fundamental unit of this chain is the symmetric combination (1) - (2) - (3). Here, (1) and (3) could be amplifier stages ($n_2 > 0$), while (2) is a negative n_2 compensator (e.g., a cesium vapor cell). Alternately, (1) and (3) could be compensators, and (2) would be the amplifier. The important point is that the magnitude of the product $I_0 n_2 \ell$ due to (2) should exactly cancel that due to the combination of (1) and (3). As long as individual amplifier stages contribute only a small amount to the nonlinear wavefront distortion, this unit allows that distortion to be corrected before it can propagate through additional amplifiers and thus grow into an appreciable change in beam size or develop into a hot spot. The symmetric configuration, in which (1) and (3) contribute equally to $I_0 n_2 \ell$, has the advantage that it eliminates any nonlinear change in beam size that could otherwise occur. A compensated laser amplifier chain can be built simply by combining two or more of these units, as indicated in the above illustration. If units (1) - (2) - (3) and (4) - (5) - (6) were adjacent, then, in practice, (3) and (4) could be combined to a single amplifier or compensator.

This negative n_2 compensation technique has the major advantage that it can virtually eliminate self focusing and self phase modulation in a multistage laser system, rather than merely containing it. It compensates at all intensity levels, and therefore, at all times during the pulse. With this type of compensation, intensity levels and power output can be raised appreciably. The only remaining limitations are (i) the intrinsic (breakdown) damage threshold of the laser materials,

and (ii) the requirement that individual amplifier stages contribute only a small amount to the nonlinear wavefront distortion. Intrinsic damage thresholds are typically larger than present allowable intensity levels by a factor of at least 10. In a multistage system, this technique - in combination with spatial filtering and the use of high gain, low n_2 amplifier materials - should allow intensities limited only by the intrinsic threshold.

The above compensation technique is currently under theoretical (and experimental) study. Two additional proposals also under study are:

(i) A negative n_2 cell which could be inserted into the cavity of a laser oscillator. This would eliminate the self focusing and self phase modulation that typically plague oscillators such as Nd:Glass. In this case, the product $I_0 n_2 \ell$ of the laser rod and compensator would be of equal magnitude, and the phase distortion would be cancelled each time the pulse traverses the cavity. The main problem here with Cs vapor would be dimer absorption at the low intensities.

(ii) Several other elements and ions may be suitable alternatives to cesium vapor; i.e., they have a pair of energy levels that provide a two-photon resonance around the predominant Nd laser lines $1.052\ \mu$ - $1.075\ \mu$, and these levels are strongly radiatively coupled to suitable intermediate states. Two examples are the 1s 2s ^1S - 1s 3s ^1S levels of parahelium, and the $3p^3\ ^4S^0$ - $3p^3\ ^2P^0$ levels of phosphorus. Other possible two-photon resonances exist in Ba, Zr^{+2}, and the trivalent rare earths Sm^{+3} and Ho^{+3}. The divalent and trivalent ions are especially interesting because of the possibility of doping them directly into the laser amplifier material. The effective n_2 of the material could then be lowered significantly, or even reduced to zero.

REFERENCES

1. R. B. Miles and S. E. Harris, "Optical Third Harmonic Generation in Alkali Metal Vapors", IEEE J. Quantum Electron. QE-9, 470 (1973).

2. R. H. Lehmberg, J. Reintjes, and R. C. Eckardt, "Two Photon Resonantly Enhanced Self-Defocusing in Cs Vapor at 1.06 μ", Appl. Phys. Lett. 25, 374 (1974); "Self Defocusing of Mode Locked Nd:YAG Pulses in Cesium Vapor", 1975 IEEE/OSA Conference on Laser Engineering and Applications (paper 17.11); "Two Photon Enhanced Negative Nonlinear Susceptibility of Cesium Vapor at 1.06 μ", submitted to Phys. Rev. (reprinted in the Appendix).

3. R. H. Lehmberg and J. Reintjes, "Generalized Adiabatic Following Approximation", submitted to Phys. Rev. (See Appendix).

4. D. Grischkowsky and J. A. Armstrong, "The Self-Defocusing of Light by Rubidium Vapor", Phys. Rev. A 6, 1566 (1972).

5.   S. A. Akhmanov, R. V. Khokhlov and A. P. Sukhorukov, "Self-Focusing, Self-Defocusing, and Self-Modulation of Laser Beams", Laser Handbook, Vol. 2, edited by F. T. Arecchi and E. O. Schulz-Dubois (North Holland, Amsterdam, 1972).

III.   RESONANT CHARGE TRANSFER PUMPING

The motivation for achieving preferential level population by a resonance charge transfer process (with a very large cross section), and a choice of particularly promising ion-atom combinations, was discussed in previous semiannual technical reports for this program and elsewhere[1,2]. Initial experiments are being conducted with highly-stripped carbon ions emitted from a laser-irradiated surface and expanding into a background gas. The program has been divided into two phases: the preliminary phase and the achievement phase. The first phase is concerned with obtaining   evidence of enhanced emission and associated level population and possibly inversion data and establishing methods which will determine the experimental arrangement and operation of the second phase. In this preliminary phase, the light pulse from a 20 ns, 6 Joule ruby laser is point-focused onto a carbon slab target. Soft x-ray spectra are obtained over multiple exposures with a grazing-incidence spectrogrpah, both with and without a surrounding neutral-atom background gas (helium). The second phase of the experiment will utilize the large NRL Glass Laser Facility tuned to produce a 30 ps, 10 Joule light pulse. This laser pulse will be line-focused onto a slab target producing a plasma that will expand into a background gas. The spectral line radiation from the expanding target plasma will be examined on a single-shot basis for further evidence of population inversion, enhanced x-ray emission, and evidence of significant lasing action.

The experimental program is well into the first phase. Several procedures are being examined and adapted into general use; also a few technical problems have been uncovered and are presently being resolved. The most persistant of these problems is the in-situ focusing of the spectrograph to obtain maximum resolution in first order where the light intensity is the highest--thus requiring fewer number of shots per exposure--and confusion with higher-order spectra is minimal. Focusing corrections are being made during this period of preliminary investigation and it is expected that the optimum focus will be achieved before the end of phase one.

Identification of the spectral lines obtained with a carbon target is continuing.[2] Besides the C^{4+} (CV) and C^{5+} (CVI) resonance series reported previously, several satellite lines and intercombination lines of carbon have been identified, as have higher series members at longer wavelengths. Recombination emission beginning at the series limits is also observed along with oxygen and sodium impurity lines.

Spatial resolution of the target plasma has been achieved by

installing a slot between the entrance slit and the grating, with the slot length orthogonal to the entrance slit (See Fig. 18). Initial spatially-resolved spectra (without helium) of limited resolution were obtained[2] with a 400 μm wide slot, and are reproduced in Fig. 19. The lines are seen to originate in the higher density region near the target surface where Stark broadening dominates and some self-reversal is observed, indicating a large optical depth. All of the spectral lines are observed to narrow at increasing distances from the target where the charged particle density is decreasing. The CVI lines and highly ionized impurity lines occur near the target surface along with the continuum emission at high densities, as shown in the densitometer tracings in Fig. 20. As the plasma expands away from the surface, the CVI lines fade first, with recombination supporting the CV line intensities as shown in Fig. 20 also.

The spectrum of Fig. 19 was obtained under vacuum conditions. A similar spectrum was obtained with the carbon target immersed in 10 Torr of He gas. A noticable difference between the two spectra was a spatial intensity variation of the CV resonance lines with the background gas present. Repeating the experiment with a narrower slot width (100 μm) suggested the presence of target debris between the jaws of the 25 μm wide entrance slit. Further investigation confirmed this suspicion. Rentention of target debris by the entrance slit could falsify intensity measurements on spatial resolution information obtained from spectra taken with multiple shot exposures. This becomes a major problem, because preliminary data indicate a necessity to go to even narrower entrance slits. The problem is being solved by installing a valve behind the entrance slit (to isolate it from the spectrograph chamber) so that the slit can be back-flushed with a puff of gas to clear the debris from the slit. The valve-gas-flush system is presently being installed in the spectrograph.

With the addition of this gas flushing system, it will be possible to compare relative line intensities with and without a neutral background gas in an appropriate region of high initial ion density (e.g., C^{5+} as in Fig. 20). From these comparisons it should be possible to ascertain whether any significant enhanced population is produced as expected. Other ions and gases will be tried at various pressures also. This would essentially complete the preliminary phase of the experiment.

Plans are underway and equipment is now being obtained for directing the large glass laser into the charge transfer chamber a s a first step in initiating the second phase of the experimental program.

REFERENCES

1.   R. C. Elton, "Three Quansi-CW Approaches to Short Wavelength Lasers" in <u>Progress in Lasers and Laser Fusion</u>, p. 117 (Plenum

31
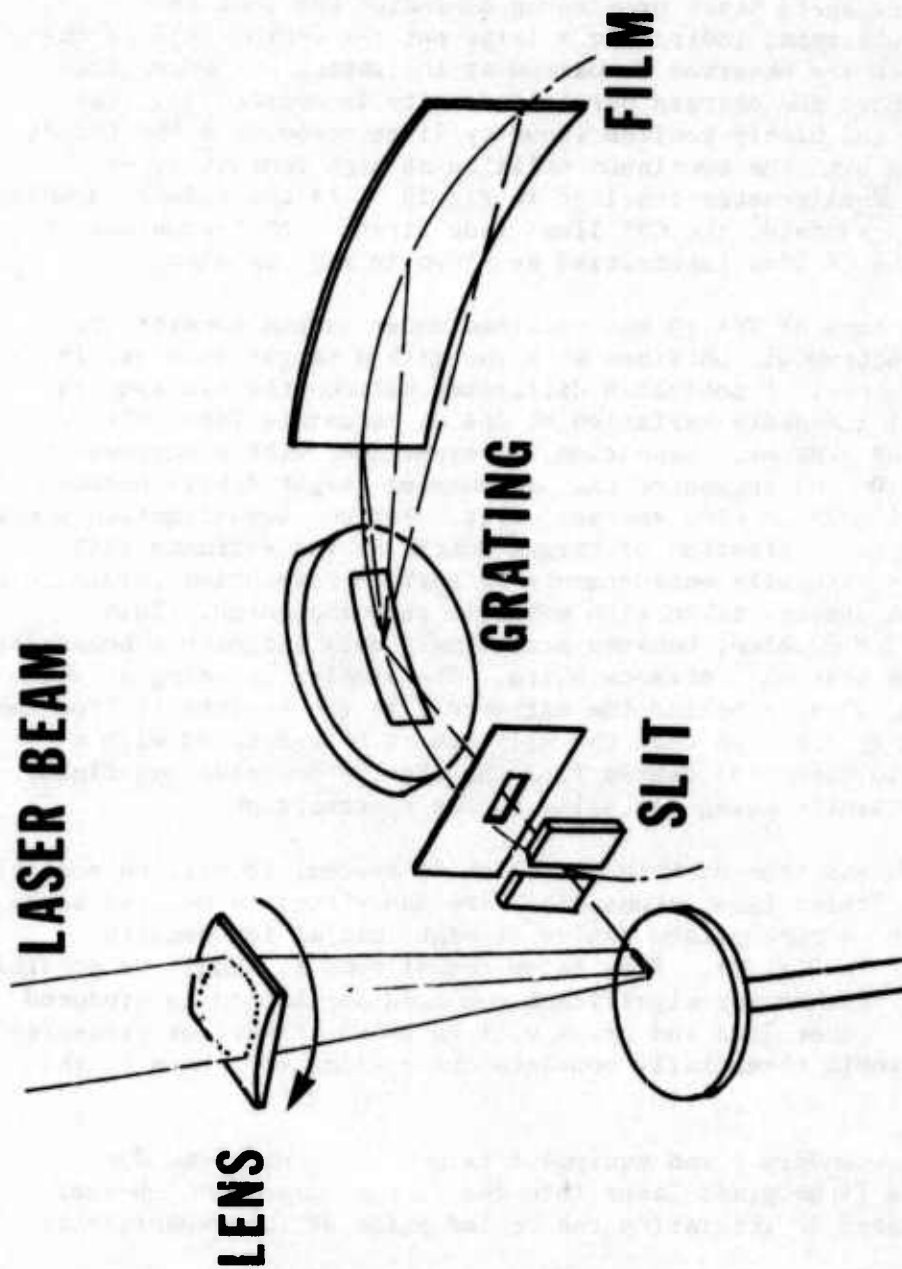
Fig. 18 Schematic diagram of the NRL resonance charge transfer experiment, including the grazing incidence vacuum spectrograph. The horizontal slot provides spatial resolution along the direction of plasma expansion from the target surface. Rotation of the lens permits both axial and radial viewing. The background (atomic) gas is not indicated.

32

2ND ORDER SPECTRUM
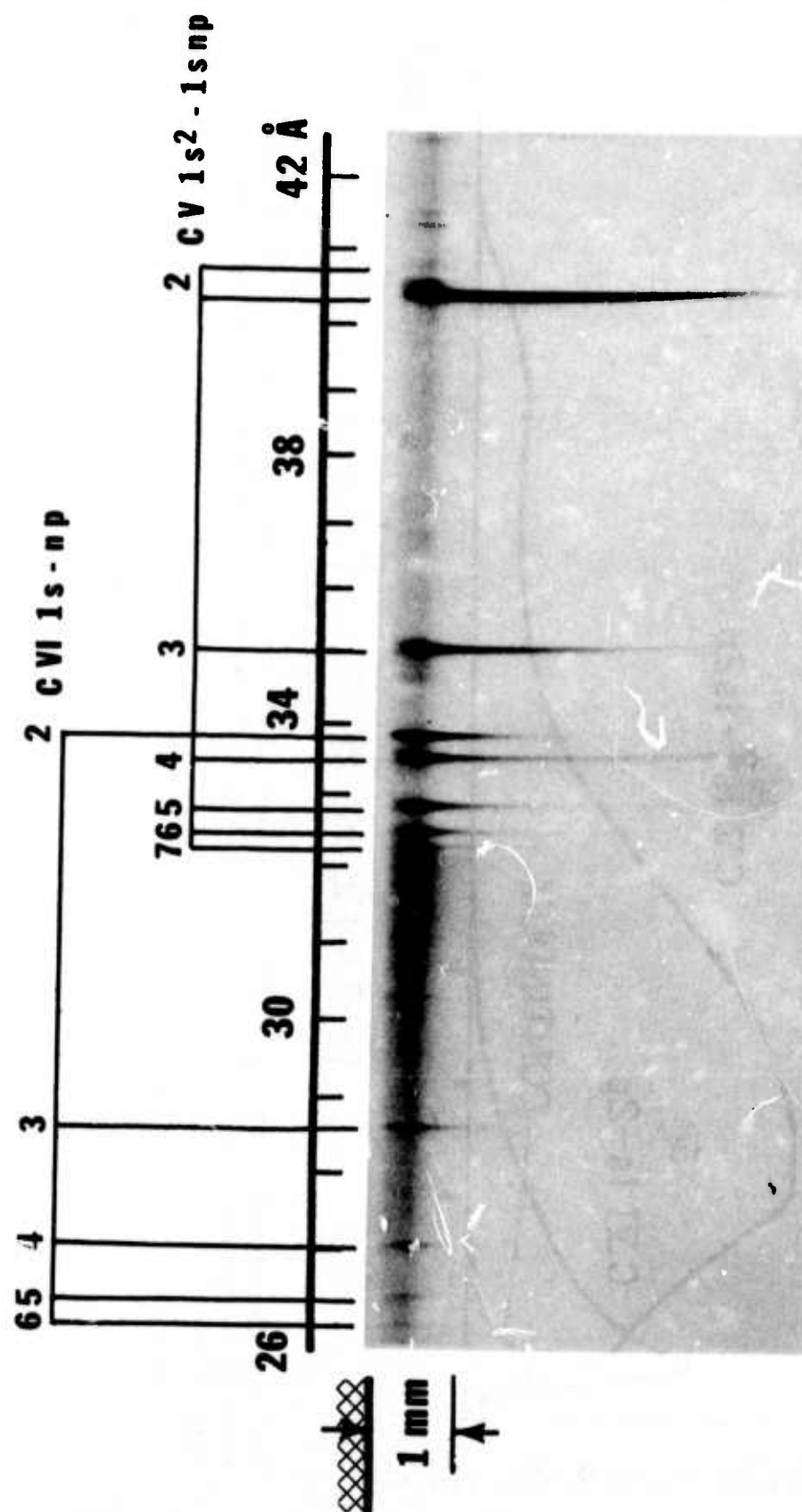
Fig. 19 Spatially resolved CV and CVI grazing incidence spectrum using 400 μm orthogonal slot shown in Fig. 18. No background gas was present.
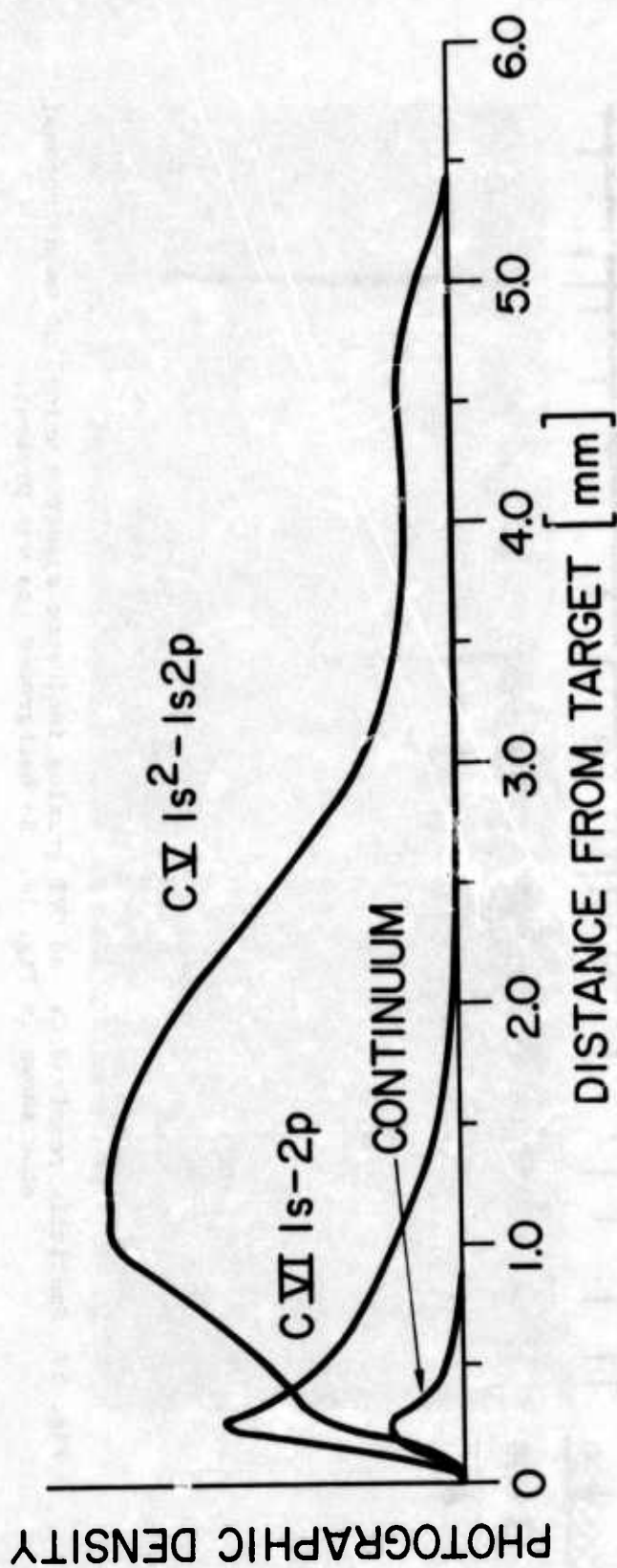
Fig. 20 Densitometer traces of spatially resolved CV and CVI grazing incidence spectral lines along with a typical continuum background. The continuum has been subtracted from the spectral line traces.

34

Press, New York, 1975).

2. R. C. Elton and R. H. Dixon, "X-Ray Laser Research: Guidelines and Progress at NRL", Proceedings Third Conference on Lasers of New York Academy of Sciences (to be published).

IV. COHERENT VUV/SOFT X-RAY PULSES BY NONLINEAR MIXING AND AMPLIFICATION

A. NONLINEAR MIXING

This section describes our approach to the generation of coherent soft-x-radiation through nonlinear mixing processes. The motivation and general technique was described in detail in previous reports and is outlined briefly in Fig. 21. The output of a Nd:YAG mode locked laser is converted to tunable visible radiation by successive frequency doubling and parametric frequency conversion in each of two arms. The tunable visible light in each arm is combined and converted to the vacuum-UV (VUV) region through resonantly enhanced frequency mixing in a suitable metal vapor, and is then amplified in a VUV molecular amplifier as described below. A further stage of resonantly enhanced nonlinear mixing is then used to convert the VUV to the soft x-ray range.

As was outlined in the previous semiannual report, the technique of parametric conversion was chosen to convert the $1.06\ \mu m$ YAG output into tunable visible light because of its potential for generating higher powers and shorter pulse durations with the available laser system. During the previous period, crystals and ovens were obtained for use in the frequency conversion process. During the present period, one arm of the visible radiation generator was set up and preliminary investigation of its operating characteristics was begun. Measurements of conversion efficiency in the first two stages of harmonic generation have been made. The parametric down conversion system has been set up and radiation generated from 4600 to 6300 Å by tuning the crystal temperature from 52 to 70°C.

During the early stages of operation, second harmonic generation was done in a 1" long KDP crystal, phase matched by angle tuning. Pump depletion measurements indicated internal conversion efficiences of 50%, which were consistent with energy measurements of 40 mJ in the second harmonic pulse when reflection losses at the uncoated surfaces were taken into account. The crystal had to be aligned to within $160\ \mu rad$, consistent with the width of the phase matching peak for a crystal of this length. In the latter stages, the 1" crystal was replaced with a 2" long crystal and pump depletion measurements indicated 70% conversion to the second harmonic. Care was taken during these measurements to insure that the waist of the 1.5 cm diameter $1.06\ \mu m$ beam was located at the crystal to avoid reduced conversion due to incomplete phase matching arising from beam divergence.

35

Fig. 21 Schematic diagram for production and amplification of intense picosecond pulses in the VUV from fundamental radiation at 1.06 μ.

Fourth harmonic generation was done on a 1" long crystal of ADP, 90° phase matched by temperature adjustment. Pump depletion measurements indicated 30% conversion from the second harmonic to the fourth harmonic, giving about 12 mJ at 2660 Å. This level of conversion is somewhat less than expected, in view of the excellent conversion achieved in the firs. doubling stage, and sources of the reduced conversion are being investigated. Nonlinear absorption in ADP at 2660 has been reported[1], and a search for intensity-dependent transmission of 2660 Å in a 2" long ADP crystal at 50°C (for both "e" and "o" polarizations) was made at NRL. No nonlinear absorption was observed for incident radiation levels around 100 MW/cm^2. Linear absorption in the crystal was measured at 10%, after calculated Fresnel losses were included, and this level does not seem to be large enough to account for the discrepancy. However, additional qualitative observations were made of second harmonic generation with pump powers at 0.53 μm of the order of 5 GW/cm^2. Significant pump depletion was observed at the phase matching temperature without a corresponding increase in second harmonic signal.

The temperature uniformity of the crystals was measured with the aid of a Mach-Zhender interferometer illuminated with a helium-neon laser. The observed interference pattern indicated that the crystal temperature was uniform across the full aperture of the crystal, and fluctuations in fringe position indicated a short term temperature stability of < .05°C. This fluctuation is well within the phase matching temperature width of ~ 0.2°C, and again appears to be too small to account for the relatively low UV-conversion.

Parametric down conversion of the 2660 Å light to the visible was accomplished in two successive ADP crystals. Visual observation of the generated light was made as the temperature of the crystals was varied from 51.8°C (degeneracy) to 70°C, corresponding to a wavelength interval of 4600 - 6300 Å. Rough estimates of conversion efficiency to the visible indicated that the parametically generated light contained about 7% of the UV pump light, or about 1% of the 1.06 μm light.

The conversion efficiencies and currently available powers in the system are listed in Table 3 and are compared to the expected values listed in the previous semiannual report. The predicted performance levels were quite conservative, especially in the early stages and the performance of the entire system at this stage appears to be well within the initial expectations.

TABLE 3

PARAMETIC OF VUV TUNABLE SOURCE

STAGE	DESIGN VALUES				MEASURED VALUES	
	PULSE ENERGY	PULSE DURATION	η	P(W)	PULSE ENERGY	η
INPUT	180 mJ	30 psec		6×10^9	100 mJ	
1st SH CRYSTAL	90 mJ	30 psec	50%	3×10^9	40 mJ*	50%
2nd SH HARMONIC (Mixing) CRYSTAL	9 mJ	30 psec	5%	3×10^8	12 mJ	15%
TUNABLE LASER OUTPUT	0.09 mJ	10 psec (EST.)	0.05% (EST.)	9×10^6	1 mJ	1%
OUTPUT OF NONLINEAR MIXING CELL	0.03 mJ	10 psec	0.018% (EST.)	3×10^6		

*Discrepanies between energies in successive stages and cumulative efficiences are due to reflection losses at surfaces.

B. VACUUM-UV AMPLIFICATION

As was pointed out in the previous semiannual reports, amplification of the VUV radiation generated by nonlinear mixing of the parametrically generated visible light is desirable to increase the efficiency of further nonlinear processes. Two approaches have been under consideration for amplification in the 1600 - 1700 Å spectral region, namely the electrically excited H_2 laser as an amplifier and the electron-beam pumped noble gas lasers also as amplifiers. The former is much further along in development at NRL, while the latter is very appealing from a wider bandwidth viewpoint. This is illustrated in Fig. 22. Thus, the wider amplifying bands of the noble gases such as Xe, Ar, and
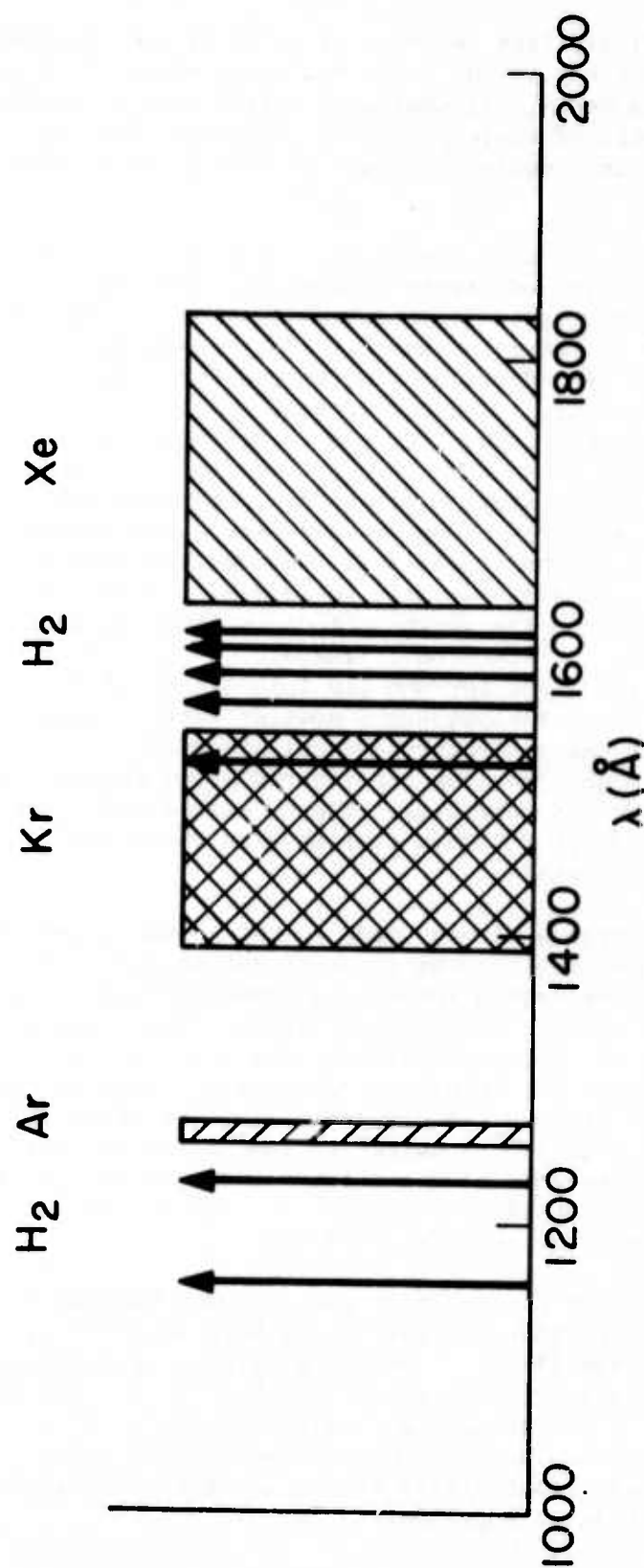
Fig. 22 Diagram of amplification regimes in the VUV showing amplifying lines of molecular H_2 and amplifying bands of noble gas excimer lasers. The boundaries of the amplification regions of Xe, Ar, and Kr are at the one-half widths of the spontaneous emission spectra. [See J. B. Gerardo and A. W. Johnson, IEEE J.Q.E. 9, 748 (1973); P. W. Hoff, J. C. Swingle, and C. K. Rhodes, Appl. Phys. Lett 23, 245 (1973); and W. N. Hughes, J. Shannon, and R. Hunter, Appl. Phys. Lett 24, 488 (1974)]

39

Kr could provide more flexibility in terms of matching the tunable
VUV simultaneously to the amplifying line, and to multiphoton resonances
in appropriate nonlinear media. Estimates of stored energy obtained
from reported measurements of noble gas lasers indicate that the
amplifiers will operate in a depletion mode, providing pulse powers
in the GW range.

Most of the progress for this reporting period has involved the
traveling-wave electron beam and discharge devices described in
previous semiannual reports, with possible application to noble gases,
as well as N_2 and H_2 at increased pressures. The traveling-wave
electron beam system has been described in the previous reports, but
Fig.23 is included here to give a better idea of the operation of the
device. The device consists of two flat plates separated by a
dielectric sheet to form a capacitor. The bottom plate is charged to
extremely high voltage from a storage capacitor. When the charge is
maximum, the dielectric switches along the edge are closed sequentially
making the plates into a transmission line. Each switch generates a
reversed voltage wave which add spatially to form a traveling wavefront.
When the leading edge reaches the first cathode, voltage appears across
the diode causing emission of electrons. These electrons are
accelerated across the diode and through the foil window of the high
pressure gas chamber. There the electrons collide with the gas atoms,
generate secondary electrons and return current electrons, and excite
or ionize the gas. At high pressures the ionized atoms combine with
neutral atoms to form excited molecules. These excited molecules can
be stimulated to emit radiation. When this happens the molecule
dissociates into two atoms again.

Many of the modifications already made to the above system have
been described in the previous reports and will not be repeated here.
Near the end of the last reporting period the traveling-wave electron
beam began operating as expected. Laser experiments were begun, but
the recurrence of numerous minor difficulties and the lack of sufficient
funding to initiate the changes required to properly eliminate these
difficulties considerably slowed the research. At this stage it was
considered to be more profitable to switch to some discharge experi-
ments that could be carried out using the traveling-wave system with
the diode section removed and electrodes added. This was quickly
done and the electron beam section was set aside.

The construction of the discharge section allowed discharge
experiments to be performed that had previously been impossible.
The system now has the capability of operating without windows so
that experiments with laser emission below 1000 Å could be contemplated.
In addition, any pressure can be used in the gas chamber. (The
previous discharge system could not handle pressures above a few
hundred Torr.) With these capabilities the system was ready to carry
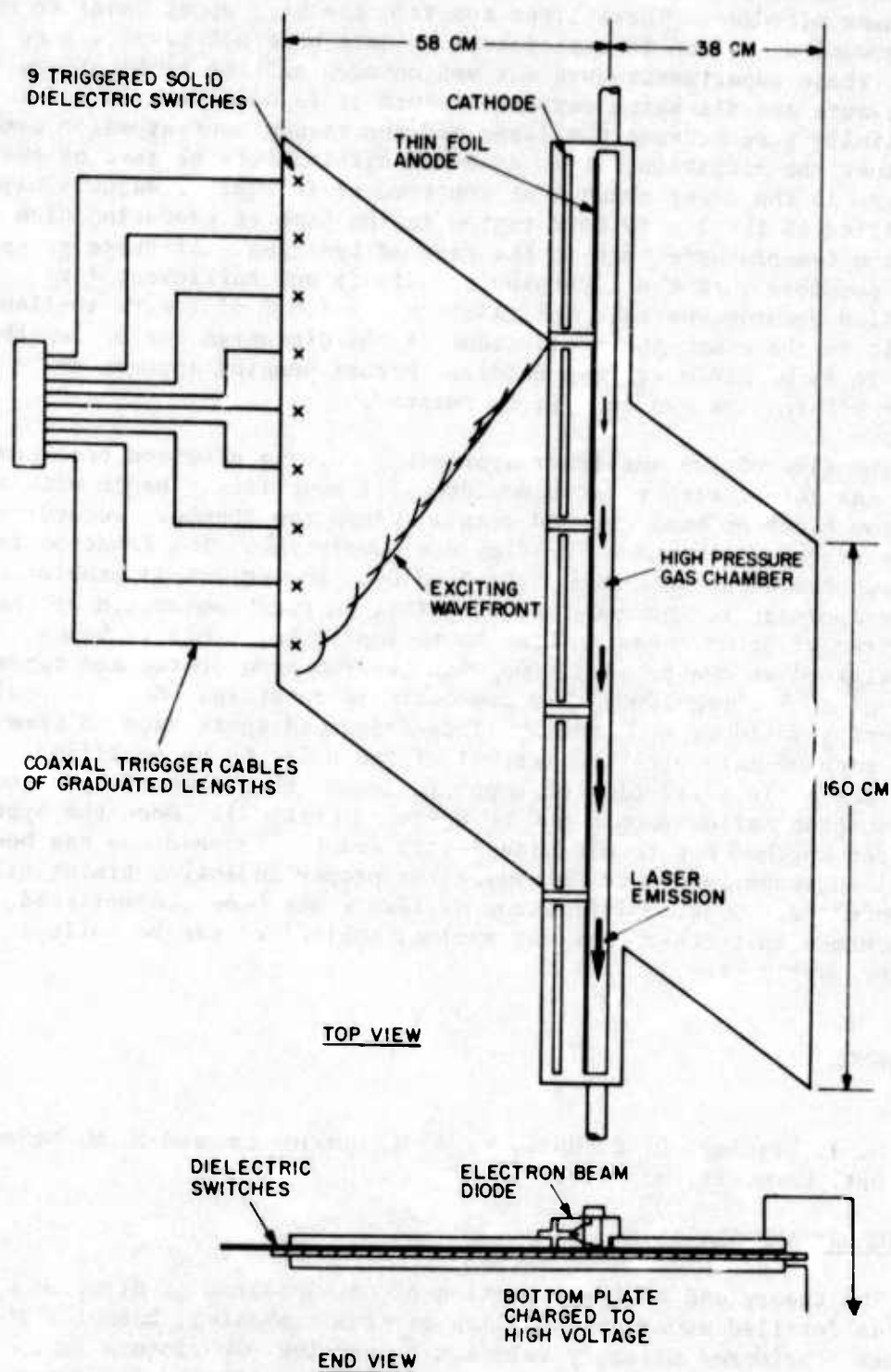out new short wavelength laser experiments.

Fig. 23 Diagram of traveling-wave electron beam device.

The first discharge experiment carried out was an attempt to find vacuum ultraviolet laser lines in the 900 - 980 Å region from molecular nitrogen. These lines are from the $b^1\pi_u$ upper level to the $X^1\Sigma_g^+$ ground state and in experiments to date have not been seen to lase. These experiments have not yet covered all the combinations of pressure and discharge current. Since it is necessary to differentially pump between the laser and the vacuum monochromator used to detect the radiation, it is somewhat difficult to be sure of the pressure in the laser channel at the time of firing. Pressures have been tried in the 1 - 10 Torr region in the hope of producing higher electron temperatures than in the case of hydrogen. At these pressures it is possible that the inversion density is not sufficient for amplified spontaneous emission (ASE) in the 1.6 m of length available. If this is the case, ASE could occur if the discharge can be lengthened or if it is possible to pump harder. Harder pumping appears to be the easier alternative and it will be pursued.

The alternative amplifier approach involving electron beam pumped noble gas lasers with wider bandwidth will most likely begin with a Febetron electron beam pumped coaxial diode gas chamber, according to the proven design of D. Bradley and coworkers[1]. The Febetron is on hand and the diode purchased from Bradley. The principal problem with either approach is the question of jitter in synchronization of the amplifier with the coherent beam to be amplified. This is being investigated at the present time with the Febetron source and appears to be of such a magnitude that operation is possible. Conventional triggering would be replaced by laser-triggered spark gaps to time the production of gain with the arrival of the pulse to be amplified. Since the excited lifetime of xenon is longer than that of hydrogen, the synchronization should not be quite as critical. Once the system has been checked out to minimize jitter and the xenon diode has been installed, experiments to determine the proper injection timing will be conducted. Once amplification at 1720 Å has been accomplished, it is hoped that other rare gas excimer amplifiers can be built at shorter wavelengths.

REFERENCE

1. D. J. Bradley, D. R. Hull, M. H. R. Hutchinson and M. W. McGeoch, Opt. Comm. 11, 335 (1974).

V. THEORY AND ANALYSIS

The theory and analysis portion of this program is directed towards detailed numerical modeling of atomic physics, both for those schemes considered directly relevant to ongoing experiments in the program for guidance and for those considered sufficiently promising as alternative approaches to warrant a somewhat in-depth study. Two

examples from activity during this reporting period follow.

A continuing concern is a monitor of the overall field of short wavelength lasers, to which many participants in the program contribute. A recent overview of the currently popular approaches and an attempt to form a somewhat rough prognosis was completed during this reporting period and included in detail in a conference paper[1], a copy of which is included in the Appendix. The results were described in the Introduction to this report and summarized in Fig. 1. Most of these approaches are being pursued in depth by various groups and it is intended that this sort of prognosis will be continually updated as further data points are provided (not shown in Fig. 1 is the hydrogen laser point at 1600 Å which does indeed match quite well).

V. A. NUMERICAL MODELING OF 3p → 3s LASING

It appears reasonably possible to achieve sufficient gain on 3p → 3s transitions in plasma ions to extend successful visible and near-UV CW ion laser transitions into the vacuum-UV region where reflecting cavities are not available. The basic considerations and some initial results of computations of the 3p → 3s gain coefficient of doubly-ionized oxygen (O III: carbon isoelectronic sequence) as a function of electron temperature and ion density for a simple three-level model which neglected ionization and recombination processes were described in the last semiannual report and elsewhere recently[1,2,3]. It will be recalled that O III was chosen as a test case for carbon-like ions since there is ample atomic data available for this ion without extrapolation. This modeling is relevant to the experiments described in Section II.A. above. The numerical results, which were obtained with a versatile computer code named XRL-1 assembled specifically for modeling x-ray laser schemes showed an increase in gain as the ion density (hence the inversion density) increased. It was pointed out in the preceding report that the gain versus density curve had a portion where the gain coefficient increased as N_i^2 in the low density limit; this slope decreased at intermediate densities so that the gain was approximately proportional to the ion density; and finally, at high densities, collisional mixing of the upper and lower laser levels dominated and wiped out any population inversion. Large gains of the order of a few hundred cm^{-1} were computed with this simple model.

As more physics is added to the XRL-1 computer model, the calculated 3p → 3s inversion density is expected to be less than that computed from the simplified three-level scheme, due to depletion of the upper laser level by atomic processes other than the laser transition (See Fig. 24). Probably the most dominant process contributing to depopulation of the 3p level in the important regions of density and temperature is ionization to the ground state of the next higher species. To test the effect of ionization, a series of runs of the XRL-1 code was made for O III in which the populations of the ground states of

43
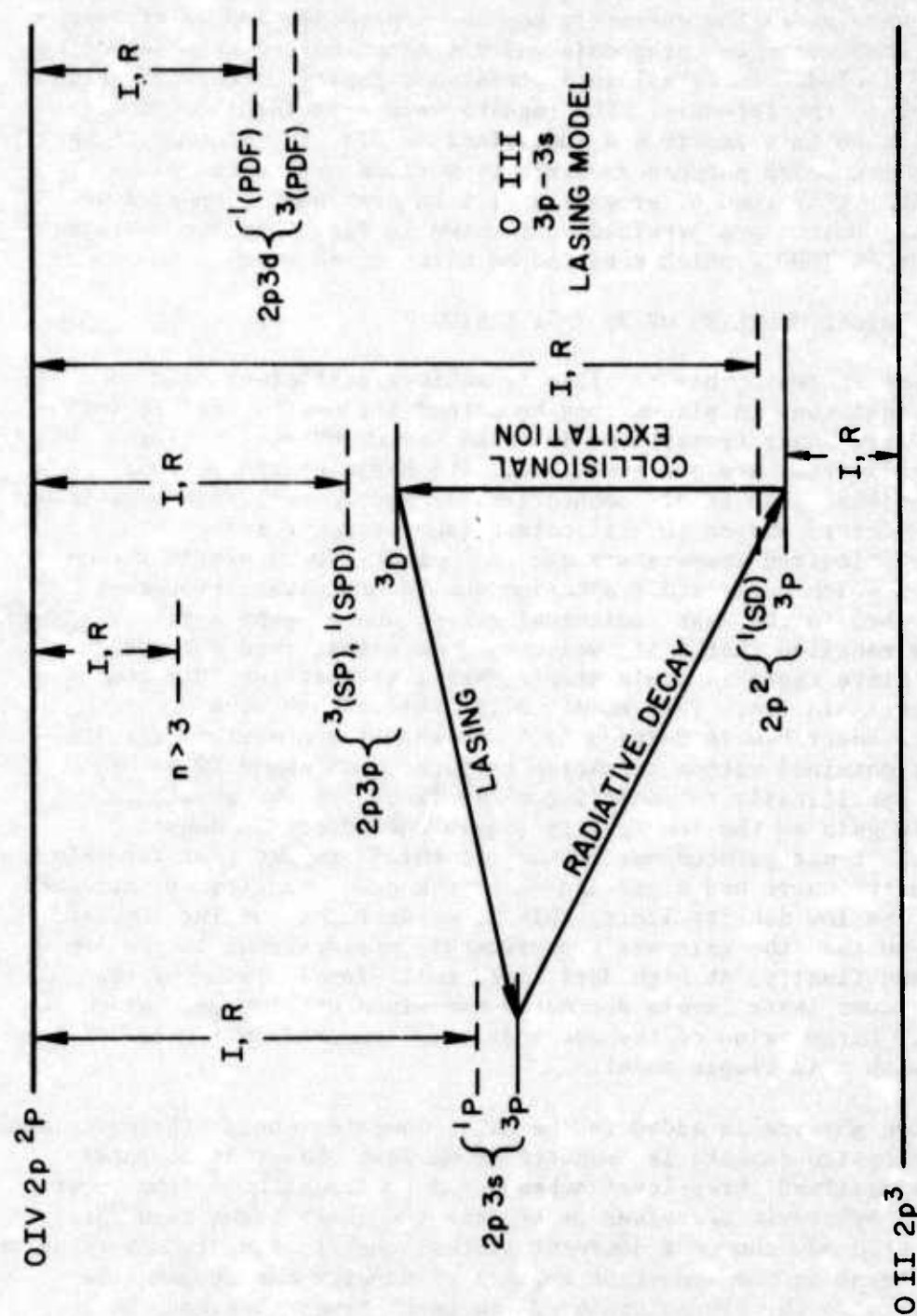
Fig. 24 Energy levels and transitions included in the present numerical model of $3p \to 3s$ lasing. Collisional mixing between all levels shown is considered in the modeling but not indicated by arrows in the figure. The bold arrows show the chief population inversion and lasing transitions. Dashed levels are presently being added to the numerical program.

44

O II and O IV as well as the three O III levels (2p, 3s, 3p) were computed as a function of time.

The atomic processes and energy levels considered by the XRL-1 model are indicated in Fig. 24 and also in Fig. 25, where the arrows (both solid and dashed) indicate the transitions which were taken into account. Where applicable, the following atomic processes were considered: collisional and radiative recombination, collisional ionization, collisional excitation and deexcitation, and radiative decay. All collisional processes are assumed to be dominated by electrons. Other assumptions of the model are listed in Fig. 25.

The curves in Fig. 25 compare the gain coefficient obtained from recent computer runs which have included transitions to and from O II and O IV compared with runs made under the same conditions of density and temperature but with only transitions (solid arrows) between the three O III levels considered. As expected, the inclusion of ionization and recombination does reduce the population inversion by providing an additional sink for atoms excited into the 3p level; but the drop is only about a factor-of-two for what is expected to be the most dominant inversion depletion mechanism, and the remaining gain coefficient is still large.

The addition of more physics and more energy levels to the model and the extension of $3p \rightarrow 3s$ modeling to higher atomic number species such as Mg VII (hence shorter wavelengths) will provide a better grasp on the understanding of the lasing mechanism and pump requirements, as well as guiding the choice of experimental conditions to produce vacuum-UV and soft x-ray lasing.

REFERENCES

1.   R. C. Elton, and R. H. Dixon, "X-ray Laser Research: Guidelines and Progress at NRL", Proceedings Third Conference on Lasers, New York Academy of Sciences, 1975 (to be published).

2.   R. C. Elton, Appl. Optics 14, 97 (1975).

3.   R. C. Elton, "Three Quasi-CW Approaches to Short Wavelength Lasers" in Progress in Lasers and Laser Fusion, p. 117 (Plenum Press, New York, 1975).

V. B.   RECOMBINATION PUMP MODELING

The creation of a population inversion by preferential filling of more highly excited bound states in a free-electron capture (recombination) process has proven attractive to a number of researchers in the short wavelength laser field. In order to better understand the opportunities and limitations with this scheme, computer modeling is necessary, since many competing processes are present of both collisional as well as radiative nature. Therefore, a computer code has been developed[1]

3p → 3s MODELING (OXYGEN III)

PLOTS FOR:

$T_{e,i}$ = 50 eV

$T_{i,i}$ = 1 eV

IONIZATION AND
RECOMBINATION
INCLUDED
(dashed arrows)

I. & R. NEGLECTED

ASSUMPTIONS:
- No Plasma Motion
- Other Excited Terms of O III Ignored
- No Heat Loss
- Energy Absorbed by Inverse Bremsstrahlung
- T_e & T_i Equilibrate
- Electron Collisional Mixing
- α Scales as $T_i^{-1/2}$

PEAK GAIN COEFFICIENT, α [cm^{-1}]

$(N_e N_g)^{1/2}$ [cm^{-3}]
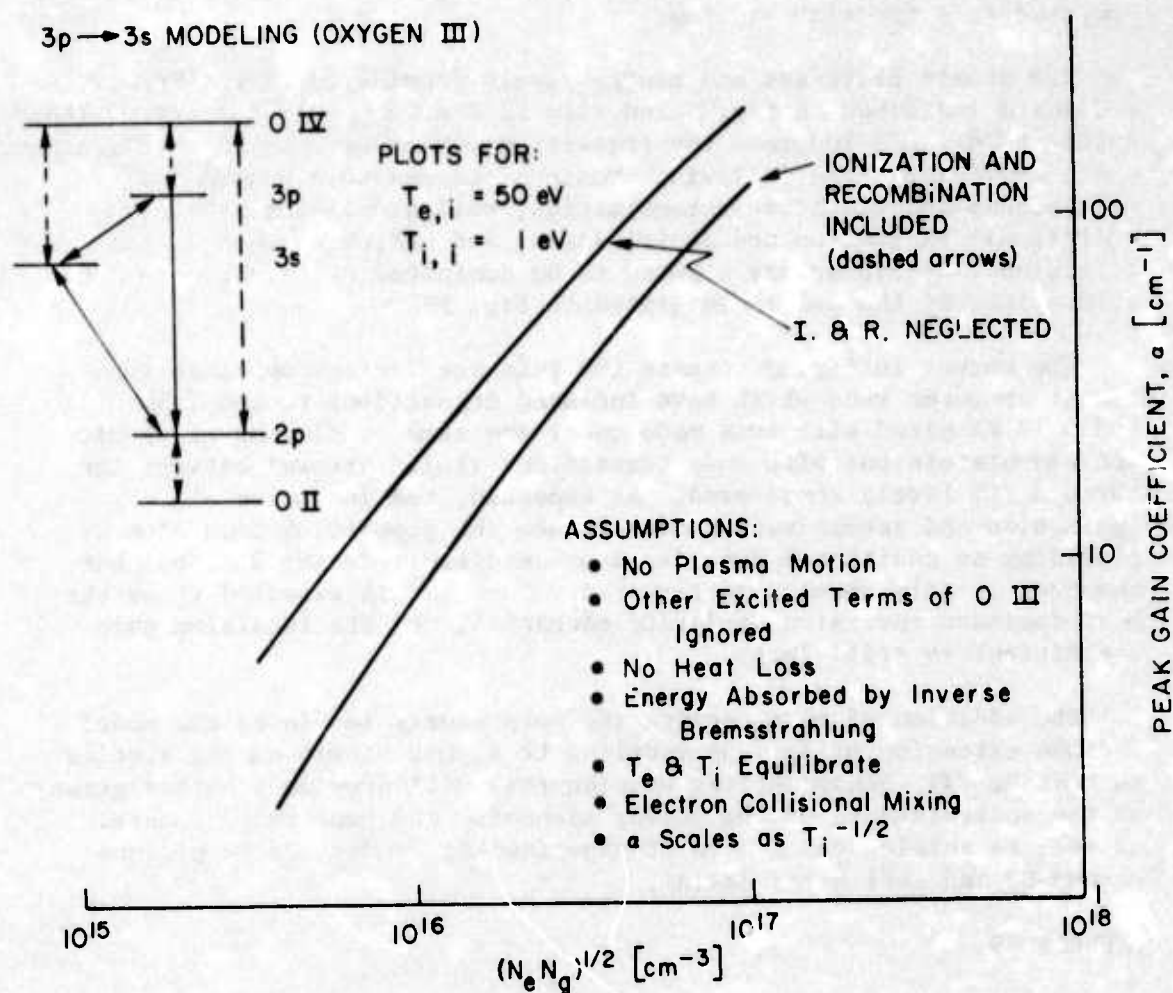
Fig. 25   Computed peak gain coefficient, α, for lasing on O III
3p → 3s line as a function of $\sqrt{N_g N_e}$ where N_g is the ground state density
of the lasing species (O III $2p^2\,^3P$) and N_e is the electron density.
Upper curve is for a three level model considering only those transitions
indicated by the solid arrows while the lower curve shows results of a
five level model accounting for both solid and dashed transitions.

46

to solve the atomic physics associated with such a recombining plasma. The specific intent has been to study the atomic transitions associated with a plasma which is recombining to form hydrogen-like and helium-like ions. It is felt that this approach shows extensive promise in that such a plasma (one which is initially fully ionized) should lase in the infrared and visible as well as the vacuum-UV and x-ray regions. This will make initial testing and diagnostics much simpler (both because the visible spectrum is easier to diagnose and the time scales tend to be longer).

The main process considered is the recombination of a fully ionized plasma via three-body recombination favoring less-bound states, with subsequent cascading of the electrons. The present study is for the initial fill-up stage, where electrons combine with bare nuclei to form hydrogen-like ions which lase for a short time and then equilibrate with the surrounding free electrons. This system could produce a short wavelength laser, but there are three difficulties identified: firstly, the time scale is short enough that, even if lasing occurs, detection will be a problem; secondly, if such a system could be maintained for a longer time, higher inversion densities should result and thus higher gains; finally, plasmas start out at high temperatures and if the system could be cooled (which in general requires a time long compared to atomic transition times) then even higher gains may be achieved. Thus some reasonable cooling scheme needs to be devised. It is well known that plasmas of interest can be generated (temperature $\sim$ 2-5 eV, electron density $\sim 10^{14}$ - 10^{18} cm^{-3}). The problem then arises as to how to cool these plasmas to a temperature such that gain sufficiently large for super-fluorescence may be obtained. This is the project of current interest, namely the long term solution of the rate equations for real experimental conditions wherein a plasma dynamic laser may be obtained.

One further point should be mentioned: it has been estimated that the maximum Z (nuclear charge) which can be utilized, is on the order of 30. This is determined from requiring the gain to be greater than unity and setting the maximum density to be that of a solid ($\alpha \sim 1$ cm^{-1} and $\Delta N \sim 10^{23}$ cm^{-3}). This implies

$$\lambda \sim \frac{\lambda_H}{Z^2} \sim \frac{\lambda_{2,1}}{900} \sim 1 - 2 \text{ Å}$$

which is well within the x-ray region (barring depletion of inversion by radiative recombination preferentially into lower states as discussed in the Introduction above). This means that copper is marginal (Z = 28) as a lasing medium, but that the K_α lines of copper may eventually provide an x-ray laser. The first effects, however, should be a feasibility study of low Z elements in the longer wavelength regions where diagnostics are somewhat simpler.

REFERENCES

1. W. W. Jones and A. W. Ali, Appl. Phys. Lett. (1975); also W. Jones, seminar, General Electric Research and Development Laboratory, July 1975.

VI. SUMMARY

This reporting period has demonstrated a continuing maturity in the program as approaches and options are narrowed and actual vacuum ultraviolet and x-ray measurements on the potential laser devices increases. This trend should continue during the next six months as we somewhat freeze our pump source development and refine our measurement techniques, both to establish current environmental conditions such as temperature and density and to assess the potential of our approaches at this phase.

The most significant results obtained during this period for each of the program areas are as follows.

ELECTRON-COLLISIONAL PUMPING-

1. The short pulse synchronized laser facility was operated as a complete system at full power during this period. Target experiments were performed both with the Q-switched pulse alone and with the two-pulse system. During the present period of plasma diagnostics at the 200 mJ short pulse level, equipment is being assembled for increasing the energy to 2 J and for target isolation against back-reflection.

2. The laser plasma interaction experiments have defined the plasma size and predominant x-ray emitting zones. Vacuum-UV spectra from 3p - 3s transition have been obtained and spatial resolution incorporated. Interferometry for mapping the electron density has been incorporated. Numerical modeling with increased complexity indicates continued promising gain for enhanced electron temperatures.

RESONANT CHARGE TRANSFER-

3. Space-resolved grazing-incidence spectra have been obtained for hydrogenic and helium-like carbon ions. Initial spectra with a helium atmosphere have been obtained also. The debris problem on the entrance slit has been identified and essentially solved. Magnesium target spectra have also been obtained which show Mg VII ions, in support of the 3p → 3s scheme.

NONLINEAR MIXING APPROACH-

4. The components have been assembled and initial doubling

experiments have been completed.

5. Problems in synchronization of a 1600 Å amplifier have been
    identified and laser triggered spark gaps improved. Alternate
    amplifier approaches are being investigated, including noble
    gas lasers.

THEORY, ANALYSIS, AND MODELING-

6. A general atomic physics program for modeling ionic pumping is
    progressing in complexity and is yielding promising gains,
    initially for 3p - 3s transitions. Its versatility should
    make it very useful for future modeling of other promising
    approaches involving ionic transitions.

7. The recombination scheme has been analyzed in more detail as
    far as the atomic physics of the capture process is concerned
    and certain limitations have been better defined.

8. A rather general prognosis analysis has been completed for the
    currently most popular schemes, with an assessment of those
    approaches capable of extrapolation at the lowest possible
    density of amplifying particles and pumping particles (or
    photons), to permit flexibility and avoid high density effects
    on the gain coefficient. A thorough review of the x-ray laser
    research field has also been initiated and is expected to be
    completed for publication in the near future.

In brief, this period has seen a gradual shift in major effort
to more measurements and less apparatus development, a trend expected
to continue for the next period. The charge transfer experiment should
yield much data in the next six months and graduate to the large glass
laser facility for direct laser tests. It is rapidly approaching
a critical proof-of-concept stage. A decision will be forthcoming
soon on the most promising approach to pursue in 1600 Å amplification
and a concentrated effort in this area can be expected in the next period.

Finally, reprints of the important publications and presentation
abstracts are included in the following Appendix, beginning with the
article containing the prognosis survey mentioned above. These re-
present work completed during this period and are included to provide
further details on various portions of the program.

VII. APPENDIX

PUBLICATIONS AND PRESENTATIONS FOR THE REPORTING PERIOD

PUBLICATIONS

"X-Ray Laser Research: Guidelines and Progress at NRL"
by R. C. Elton and R. H. Dixon......................................A1

"Extension of $3p \rightarrow 3s$ Ion Lasers Into The Vacuum Ultraviolet Region"
by R. C. Elton..A25

"X-Ray Emission from Laser-Produced Magnesium Plasmas"
by T. N. Lee and D. J. Nagel..A30

"Two Photon Enhanced Negative Nonlinear Susceptibility of Cesium
Vapor at 1.06 μ", by R. H. Lehmberg, J. Reintjes, and R. C.
Eckardt...A48

"Generalized Adiabatic Following Approximation", by R. H. Lehmberg
and J. Reintjes...A74

PRESENTATIONS

"Generalized Adiabatic Following Approximation", by R. H. Lehmberg
and J. Reintjes...A112

"Negative Nonlinear Susceptibility of Cesium Vapor at 1.06 μ"
by J. Reintjes, R. H. Lehmberg, and R. C. Eckardt...................A113

"X-Ray Lasers: Guidelines and Recent Progress", by R. C. Elton.......A114

"Multiple Micro-Pinch Process in Vacuum Spark Plasma Focus", by
T. N. Lee...A115

"Spectroscopy on Plasmas for Short Wavelength Lasers", by
R. C. Elton...A116

"Atomic Physics in Laser Produced Plasmas", by R. C. Elton...........A117

X-RAY LASER RESEARCH: GUIDELINES AND PROGRESS AT NRL*†

by

R. C. ELTON and R. H. DIXON

Naval Research Laboratory
Washington, D. C.   20375

ABSTRACT

Based upon several general schemes currently considered for
achieving significant gain in the vacuum-UV and x-ray regions,
magnitude estimates of the pumping requirements are deduced and
graphed as guidelines for future research. A high density col-
lision limit is also suggested as a function of wavelength. Recent
progress at NRL in numerical modeling and experiments on two
promising schemes, namely $3p \to 3s$ extrapolation from the near-UV
and resonance charge transfer pumping for the soft x-ray region,
are described.

INTRODUCTION

There have been a number of proposals for x-ray laser schemes in the
past few years, along with some reports of observed gain as well as evidence
for population inversion. While to date there are no verified claims for direct
amplification at wavelengths shorter than 1000 Å, there is continued optimism

A1

that a monotonic advancement towards shorter wavelengths with steadily improving pump sources is possible. It may well be that the plasma devices described here will be integrated with devices based on frequency multiplication schemes (now reaching 887 Å) to obtain a coherent, amplified, short-wavelength beam. With a comprehensive review article in preparation, no attempt at completeness is intended here. What is offered are some generalized extrapolations for certain popular pumping schemes that can also be treated relatively conveniently by simple analytical formulas. While each scheme is sufficiently complex to warrant detailed numerical modeling, a primary intention here is to plot a rough course in somewhat uncertain waters in hopes of avoiding some possible misadventures, while at the same time perhaps anticipating some needed information for support of the mostly-experimental program. Two particular approaches underway at the Naval Research Laboratory will be described as examples, with emphases on some current results in both numerical modeling and experiments.

GENERAL GUIDELINES

Among the numerous proposals for the attainment of net positive gain in the soft x-ray region, there are least five rather basic processes (namely photoionization, electron collisional excitation, charge transfer, dielectronic capture, and recombination) for which sufficiently simple formulations exist to attempt a wavelength projection of the necessary pumping conditions. Since many variables enter and many experimental approaches are possible, rather bold assumptions must be made. Nevertheless, the results are informative guidelines for reasonable experimenting, and should not be assumed overly constraining.

A2

Ignoring the rather distant possibility of future development of collective resonance cavities for this wavelength region, net gain is given by $\exp(\alpha L)$, where L is the lasing-medium length and the small gain coefficient α for amplified spontaneous emission can be written as[1]

$$\alpha = \frac{\lambda^2}{4\pi^2 \Delta\nu} A_{u\ell} \quad \delta \ \Delta N_{u\ell} . \tag{1}$$

(This only includes resonance-absorption beam losses.) Here λ is the laser wavelength, $\Delta\nu$ the line width in frequency units, and the quantities $A_{u\ell}$ and $\Delta N_{u\ell}$ refer to the transition probability and inversion density, respectively, between the upper and lower laser states designated by the appropriate subscripts. Doppler broadening, when assumed, requires the $\delta = (\pi\ell n2)^{\frac{1}{2}}$ factor. The inversion density is given by

$$\Delta N_{u\ell} = N_u - \frac{g_u}{g_\ell} N_\ell = N_o \left(\frac{N_u}{N_o} \right) \left(1 - \frac{g_u}{g_\ell} \frac{N_\ell}{N_u} \right) , \tag{2}$$

where the g's refer to statistical weights and N_o is the density of the initial energy state from which pumping proceeds. Population inversion occurs when $\Delta N_{u\ell}$ is positive, i.e., when $g_\ell N_u > g_u N_\ell$. It is important to notice that inversion can be achieved (and measured) even with low gain αL, since the magnitude of $\Delta N_{u\ell}$ is determined by the initial density N_o and the degree of pumping N_u/N_o (as well as the medium length L). Also, N_o, N_u, and N_ℓ do not have to be of the same species, although rapid re-

A3

generation of the initial state must occur[*]. Assuming that a high degree of inversion can be obtained by some process, the gain coefficient can be approximated by

$$\alpha \lesssim \frac{\lambda^2 \, A_{u\ell}}{4\pi^2 \, \Delta\nu} \, \& \, N_o \left(\frac{N_u}{N_o} \right) . \tag{3}$$

A closely related requirement is the pump irradiance P/a (P the power, a the irradiated area) necessary, which is given simply by [†]

$$\frac{P}{a} \approx \frac{N_u \, A_{u\ell} \, hcL}{\lambda} \div \frac{4\pi^2 \, hc}{5} \, \frac{\alpha L \Delta\nu}{\lambda^3} . \tag{4}$$

Likewise, the pump power density P/aL is a useful source parameter when the gain coefficient α is fixed instead of αL. According to Eq. (3), high gain is achieved at high density and/or a high degree of pumping and in narrow lines, with the required pump power [Eq. (4)] concentrated in a small volume. A comparison of various approaches shows that the potential pump source of greatest irradiance at present appears to be a focused laser beam, generating a high density plasma. For example, 10 percent of the power from a 1 TW laser beam line-focused to 400 μm over a 1 cm length would produce

_____

[*]The time dependence of the inversion will not be further discussed here (see Refs. 1, 2, 7, and 10). If not limited to an equilibration time $\approx A_{u\ell}^{-1}$, i.e., for quasi-cw operation, maintainment of N_o through regeneration must be provided-for.

[†]Where competing transitions (e.g., by collisions) with high depopulation rates $D_{u\ell}$ also exist, $A_{u\ell}$ is replaced by $A_{u\ell}+D_{u\ell}$ in Eq. (4) and P/a is proportional to $D_{u\ell}/A_{u\ell}$ for $D_{u\ell} \gg A_{u\ell}$. Thus, the pumping requirements can greatly increase for relatively weak and "metastable" transitions, even if any could be identified for population inversion.

$P/La \sim 10^{14}$ W/cm^3 in a plasma medium. (Magnitude significances are discussed below.) Vacuum spark discharges can conveniently produce power densities $P/La \sim 10^{15}$ W/cm^3; however the limited length of the $\sim$100 μm spherical plasma does not produced a high, directional, gain factor αL. This simple device is thus more suitable for population inversion experiments under local conditions similar to laser produced plasmas. Electron beams with power comparable to the lasers exist, but the limited focus ($\sim$ 300X larger than the laser focus) and the limited risetimes do not make them as attractive at present. Ion beams appear attractive for pumping targets at near solid densities; however this approach appears to be limited at present to the vacuum-UV region by state-of-the-art beam technology.

Since laser-heated plasmas appear the best candidate at present for high power pumping, it is appropriate to assume $\Delta \nu$ to be the Doppler width, with the possibility of additional density-dependent Stark broadening[2] at the highest densities. Since the Doppler width can be expected to be comparable to the natural width for low-Z innershell lines in cold target atoms,[2] due to the rapid Auger rates present, the assumption of Doppler broadening is probably not limited to the plasma approach. With Doppler broadening, $\Delta \nu / \nu \approx \bar{v}/c$, where $\bar{v}$ is the mean particle velocity. With a typical $\bar{v} \approx 10^7$ cm/sec and $\nu = c/\lambda$, the pump power parameters P/aL and P/a scale as λ^{-4} and specific numbers are shown in Table 1 for a gain factor $\alpha=5$. This indicates a present short wavelength limit of $\lambda \approx 10$ Å due to pump power limitations. The value of $\alpha=5$ is chosen for significant gain over a 1 cm length, which is likely to be both convenient for a focused high power laser beam and necessary for a short pulse single transit (L/c $\sim$30 ps). If N_u/N_o,

A5

which is a measure of pump intensity, is assumed to be given* by $R_{ou}/A_{u\ell}$

where $R_{ou}(\lambda)$ is the rate of pumping events, then the gain factor scales as

$\lambda^3 R_{ou}(\lambda)$. The pump rate per unit volume $N_o R_{ou}$ required for $\alpha=5$ is also

tabulated in Table 1. Since R_{ou} is both density and wavelength dependent,

the remaining goal is to express the wavelength dependence for various pump

methods and derive the necessary density requirements. Expressing R_{ou} as

$N_p r_{ou}$, where N_p is the pump particle (or photon) density and $r_{ou} \doteq \langle \sigma_p v_p \rangle$

the basic rate coefficient, the gain coefficient α depends on the product

$N_o N_p$. A useful parameter (especially for plasmas) emerging from this analysis

is the geometric mean density $(N_o N_p)^{\frac{1}{2}}$; it is this quantity that is plotted

in Fig. 1 versus wavelength for the five rather general pumping schemes given

above and for $\alpha=5$. This parameter is meaningful since both amplification

media and pumping sources ultimately face density limits at short wavelengths.

The relations used for r_{ou} are listed in Table 2, with wavelength expressed

in Ångstrom units. For photoionization, a peak cross section $\propto Z^{-2}$ is assumed[2]

(for Z the target atomic number), multiplied by velocity c, and divided by 100

for ~1% radiation in the rather narrow absorption bands. For dielectronic

capture, the detailed balancing formulation[3] is most appropriate at the high

densities involved, and an autoionization (Auger) rate of 10^{14} sec^{-1} was

assumed. For resonance charge transfer[4] $\sigma_p = \pi a_o^2 z^2$ and $\bar{v} = 10^7$ cm/sec

_____

*As discussed in the footnote to Eq. (4), $A_{u\ell}$ becomes $A_{u\ell}+D_{u\ell}$ for significant

alternate depopulation at a rate $D_{u\ell}$ as, e.g., with weak lasing transitions.

In such a case, R_{ou}, r_{ou}, and $(N_o N_p)^{\frac{1}{2}}$ increase as $D_{u\ell}/A_{u\ell}$ for $D_{u\ell} \gg A_{u\ell}$.

(for plasmas) were assumed. The formulas for excitation and recombination were derived from a collection given in Ref. 5. The conversion to wavelength scaling was achieved with some rather arbitrary (and optimistic) but necessary approximations for shortest wavelengths and a plasma medium. The laser wavelength was taken from Lyman-α scaling as $\lambda = 1216/z^2$ in Ångstrom units, where z is the ion charge. The ionization potential was assumed to be 30 percent higher than the excitation energy interval; the latter was also taken to be 3X the plasma electron temperature and related to wavelength directly by hc/λ.

In addition to the geometric mean pumping densities, also plotted in Fig. 1 is the density above which Stark broadening becomes significant and must be included in the gain formulas. Since Stark widths scale approximately as the density of perturbers, an effect is to cancel one density factor in the gain formula so that the density requirements for a specific gain factor rise more rapidly with shorter wavelength. Also, the onset of significant Stark broadening is associated with strong collisional effects, and indeed a check of several possible pumping schemes at different wavelengths (including the $3p \rightarrow 3s$ numerical modeling described below) verified that the "Stark line" in Fig. 1 represents an approximate upper density limit above which collisional statistical equilibrium (without population inversion) eventually dominates. An immediate implication which follows from Fig. 1 is that compression to supra-solid densities in plasmas, such as planned for laser fusion, will be advantageous mainly for hard x-ray lasing, i.e., $\lambda \leq 10$ Å. Since 10 Å is a present technological limit, it will probably be a new generation of

high power, short pulse lasers with inertial compression that achieves hard x-ray lasing.

Returning to the discussion of various pumping results in Fig. 1, the mean density requirements for the vacuum-UV region ($\lambda \geq 100$ Å) are comparable within an order of magnitude for the fixed gain factor (=5) assumed. Electron collisional excitation is favored, and the density at long wavelengths agrees with the H_2 discharge laser[6] conditions. The mean density derived is extrapolated to values greater than 10^{21} cm^{-3} in anticipation of possible inertial compression. Photoionization could continue to higher densities as indicated, with near solid targets.[2] Collisional (3-body) recombination requires densities close to the Stark-collisional region and has a short wavelength cutoff at ~15 Å (for $N_e = 10^{21}$ cm^{-3}), below which radiative recombination depletes the inversion by preferential lower state population (see Table 2 footnote). This wavelength "cutoff" coincides with a mean density of ~10^{21} cm^{-3} which is also a typical upper value for present laser-produced plasmas.

Resonance charge transfer appears particularly attractive for the shorter wavelengths because of the reduced scaling of mean density and the large absolute cross sections ($\sim a_0^2 z^2$) projected[4] from beam data at lower degrees of ionization. This example shows the general attractiveness of a large-probability pumping process with an increasing cross section at short wavelengths (Table 2). The densities remain reasonable, with a latitude for higher gain coefficients. Wavelengths shorter than 10 Å in plasmas will still depend on future pump sources (Table 1) and proper resonances must be found in an ion/atom mixing zone, as discussed further below.

The estimates plotted in Fig. 1 aid in introducing a discussion of two approaches being followed at NRL with both numerical modeling and experiments. For wavelengths longer than 300 Å, an attempt is underway to achieve population inversion and amplification on $3p \rightarrow 3s$ electron collisionally excited ion transitions, similar to those that lase cw in the near-UV region with resonant cavities. At wavelengths shorter than 400 Å, the resonant charge transfer effect is studied in an interaction region between an expanding plasma and a neutral atmosphere. The presently promising zones are shown by enhanced lines in Fig. 1. A more detailed description accompanied by recent results follows.

RECENT PROGRESS AT NRL

Ion Laser Extrapolation

A large number of ions have $3p \rightarrow 3s$ transitions on which lasing has been demonstrated in the near-UV spectral region in resonant cavities. Recently, it was shown analytically[7] with a simple 3-level scheme that this transition in carbon-like ions could be inverted in a plasma with a sufficient density to achieve amplification without mirrors in the vacuum-UV region. The possibility of achieving extended laser intervals in a quasi-cw mode of operation (through rapid $3s \rightarrow 2p$ decay) was presented, although the time limitations depended on the particular plasma conditions and especially on the ability to maintain a high electron temperature for rapid pumping and large inversion. Following this first anlysis, an existing[8] "hot spot" plasma/atomic NRL code was adapted[9] to include lasing conditions for the O^{2+} ion and the results supported the previous conclusion, i.e., significant quasi-cw gain was

A9

possible at a density of about 10^{15} cm^{-3} with a lasing time 10X the upper
state spontaneous decay li^r time[10]. Meanwhile, a versatile program designed
for expansion of states and extrapolation to short wavelengths has been
assembled[11] and the first tested on O^{2+} ions to show agreement with the earlier
hot-spot results. The levels and transitions included at present are shown
in Fig. 2, as are those to be added (dashed). At present, cooling of the
preferentially-heated electrons is assumed to occur by collisional equipartition
of energy with cooler ions. Expansion, radiative cooling and thermal conductivity
will be added. The latter is expected to be the most limiting as far as the
lasing interval is concerned, but is also a highly uncertain factor since
conduction to a surrounding cooler plasma or target in the presence of self-
generated magnetic fields is not predictable at present. This limitation will
therefore probably be learned from experiments. Present predictions[11] of the gain
factor as a function of density are shown in Fig. 3, where the decrease at
high densities is due to collisional mixing leading finally to a statistical
non-inverted electron distribution. At the highest densities, Stark broadening
will also be included.

An experiment underway to verify these predictions and and supporting
data[10-13] is illustrated in Fig. 4. In essence, a linearly extended medium
with the desired ion concentration is formed by an expanding plasma, created
initially at a target onto which a laser beam is focused with a cylindrical
lens. A second high power, short pulse laser is focused axially into this
plasma to provide rapid and preferential electron heating for population
inversion. The synchronization of these two laser pulses is described else-
where.[11-13] It is intended that net gain will be verified experimentally
by orthogonal intensity measurements on the $3p \rightarrow 3s$ line, after short pulse
pumping in the appropriately designated spatial zone is accomplished.

However, evidence for population inversion will first be sought by relative $3p \to 3s$ and $3s \to 2p$ line intensity measurements. A relative intensity (grazing-incidence) spectrograph calibration over the ~X10 wavelength span involved will be completed by corresponding nearby $3d \to 3_{\uparrow}$ and $3d \to 2p$ lines originating from the same upper level (branching ratio technique), as illustrated in Fig. 5. Initial space resolved (grazing incidence) spectra of an expanding laser-produced magnesium plasma are under study at present to identify the lines from these transitions.

Resonance Charge Transfer in Plasmas

In a scheme similar to that proposed by Vinogradov and Sobel'man[4], a large concentration of resonance charge transfer interactions are sought in the interacting region between an expanding laser-heated plasma and a surrounding neutral gas atmosphere. The energy level structure is shown in Fig. 6 for the exothermic charge transfer transition into n=3 levels, as an example with some parallelism to the $3p \to 3s$ scheme described above (in fact, the same modeling may be extended for this scheme in the future). As shown elsewhere,[10] a simple Landau-Zener theory application for s-s transitions can be applied here and resonances can be expected between hydrogenic and helium-like ionic species of light elements and hydrogen, helium and neon atoms, with laser transitions in the 100-400 Å spectral region on $3 \to 2$, $4 \to 2$, and $4 \to 3$ transitions as a start. Under optimum conditions, gain factors α in the 20-50 cm^{-1} range are predicted.[10]

An experiment designed to test this approach is shown schematically in Fig. 7. Space-resolved grazing-incidence spectroscopy is presently used to

A11

measure relative line intensities and eventually orthogonal laser line emission (by rotating the line-focusing lens). A 6J, 20 ns ruby laser is presently being used for preliminary tests, and a microdensitometer tracing of a typical spectrum obtained with a point focus is shown in Fig. 8. The intense lines identified (in second order) are associated with resonance-series transitions in helium-like C^{4+}(CV) and hydrogenic C^{5+}(CVI) carbon ions, as indicated. Recombination emission beginning at the series limits is also observed. A spatially-resolved spectrum of these lines with limited resolution was obtained using a 300 μm-wide orthogonal slot (as illustrated in Fig. 7) and is reproduced in Fig. 9. The lines are seen to originate in the higher density region near the target surface where Stark broadening dominates and some self-reversal is observed, indicating a large optical depth. As the plasma expands away from the surface, the CVI lines fade first, with recombination supporting the CV line intensities. All of the spectral lines are observed to narrow at increasing distances from the target where the charged particle density is decreasing. These spectra are obtained without a background gas. Examination of the CV lines with 10 torr of helium background gas indicates a narrow ($\lesssim$ 100 μm) reacting zone at about 1.4 mm from the target surface; however, the results are too preliminary to be definitely associated with a particular mechanism.

ACKNOWLEDGEMENTS

the obtainment of the data presented. The close collaboration with Dr. R. A.

Andrews represents an important and significant part of the efforts described.

A13

REFERENCES

1. ELTON, R.C., R. W. WAYNANT, R. A. ANDREWS and M. H. REILLY. 1972. X-Ray
   and Vacuum-UV Lasers, Current Status and Prognosis. Naval Research
   Laboratory Report No. 7412.

2. ELTON, R. C. 1975. Quasi-Stationary Population Inversion on $K\alpha$
   Transitions. Appl. Optics (in press). Also Naval Research Laboratory
   Memorandum Report No. 2906 (October 1974).

3. ANSARI, S. M. R., G. ELWERT and P. MÜCKLICH. 1970. On Dielectronic
   Recombination. Z. Naturforsch. 25a:1781-1797.

4. VINOGRADOV, A. V. and I. I. SOBEL'MAN. 1973. The Problem of Laser
   Radiation Sources in the Far Ultraviolet and X-Ray Regions. Sov. Phys.
   JETP 36(6):1115-1119.

5. ELTON, R.C. 1970. Atomic Processes. In Methods of Experimental Physics,
   Plasma Physics, Vol. 9A, H. R. Griem and R. H. Lovberg, eds., Academic
   Press.

6. WAYNANT, R. W., J. D. SHIPMAN, JR., R. C. ELTON and A. W. ALI. 1971.
   Laser Emission in the Vacuum Ultraviolet from Molecular Hydrogen. Proc.
   IEEE. 59(4):679-684.

7. ELTON, R. C. 1975. Extension of $3p \rightarrow 3s$ Ion Lasers into the Vacuum Ultra-
   violet Region. J. Appl. Optics, 14(1):97-101.

8. WHITNEY, K. G. and J. DAVIS. 1974. Hot-Spot Model of K-Line Emission
   From Laser-Heated Plasmas. J. Appl. Phys. 45(12):5294-5302.

9. ELTON, R. C., T. N. LEE, J. DAVIS, J. F. REINTJES, R. H. DIXON, R. C.
   ECKARDT, K. WHITNEY, J. L. DeROSA, L. J. PALUMBO and R. A. ANDREWS.
   1974. Towards X-Ray Lasers with VUV Amplification on $3p \rightarrow 3s$ Transitions.
   Physica Fennica 9(S1):400.

A14

10. ELTON, R. C. 1975. Three Quasi-CW Approaches to Short Wavelength Lasers. Proceedings Orbis Scientiae II, Center for Theoretical Studies, Univ. of Miami. Plenum Press (in press).

11. ANDREWS, R. A., R. C. ELTON, J. REINTJES, R. C. ECKARDT, R. H. LEHMBERG, R. WAYNANT, T. N. LEE, and L. J. PALUMBO, 1975. DARPA/NRL X-Ray Laser Program Semiannual Technical Report (June - December 1974). Naval Research Laboratory Memorandum Report No. _____.

12. ANDREWS, R. A. 1975. Soft X-Ray Lasers Via Electron-Collisional Pumping. Proceedings Orbis Scientiae II, Center for Theoretical Studies, Univ. of Miami. Plenum Press (in press).

13. ANDREWS, R. A., R. C. ELTON, J. REINTJES, R. C. ECKARDT, R. H. LEHMBERG, R. WAYNANT, T. N. LEE, L. J. PALUMBO, J. M. McMAHON, D. NAGEL, AND W. JONES. 1974. ARPA/NRL X-Ray Laser Program Semiannual Technical Report (January-June). Naval Research Laboratory Memorandum Report No. 2910.

TABLE 1

Volumetric Pumping Requirements for $\eta \sim 5$

λ [Å]:	1	10	100	1000	2000
P/aL [W-cm^{-3}]	10^{18}	10^{14}	10^{10}	10^{6}	10^{5}
$N_o\, r_{ou}(\lambda)$ [cm^{-3}-sec^{-1}]	10^{33}	10^{30}	10^{27}	10^{24}	10^{23}

TABLE 2

Pumping Rate Coefficient Magnitudes Scaled[a]

Process	$r_{ou} \div \langle \sigma_p v_p \rangle$ (cm^3 sec^{-1})
Photoionization	$10^{-12}\,\lambda$
Electron Collisional Excitation	$10^{-13}\,\lambda^{3/2}$
Dielectronic Capture	$10^{-13}\,\lambda^{3/2}$
Collisional Recombination[b,c]	$10^{-13}\,\lambda^{5/4}$
Resonance Charge Transfer	$10^{-6}\,\lambda^{-5/4}$

[a] Wavelength λ in Ångstrom units; $\eta=5$ assumed.

[b] Electron density $N_e \doteq N_p = 10^{21}$ cm^{-3}.

[c] Must exceed radiative recombination for which $r_{ou} \sim 10^{-11}\,\lambda^{-\frac{1}{2}}$; i.e. $\lambda \gtrsim 15$ Å
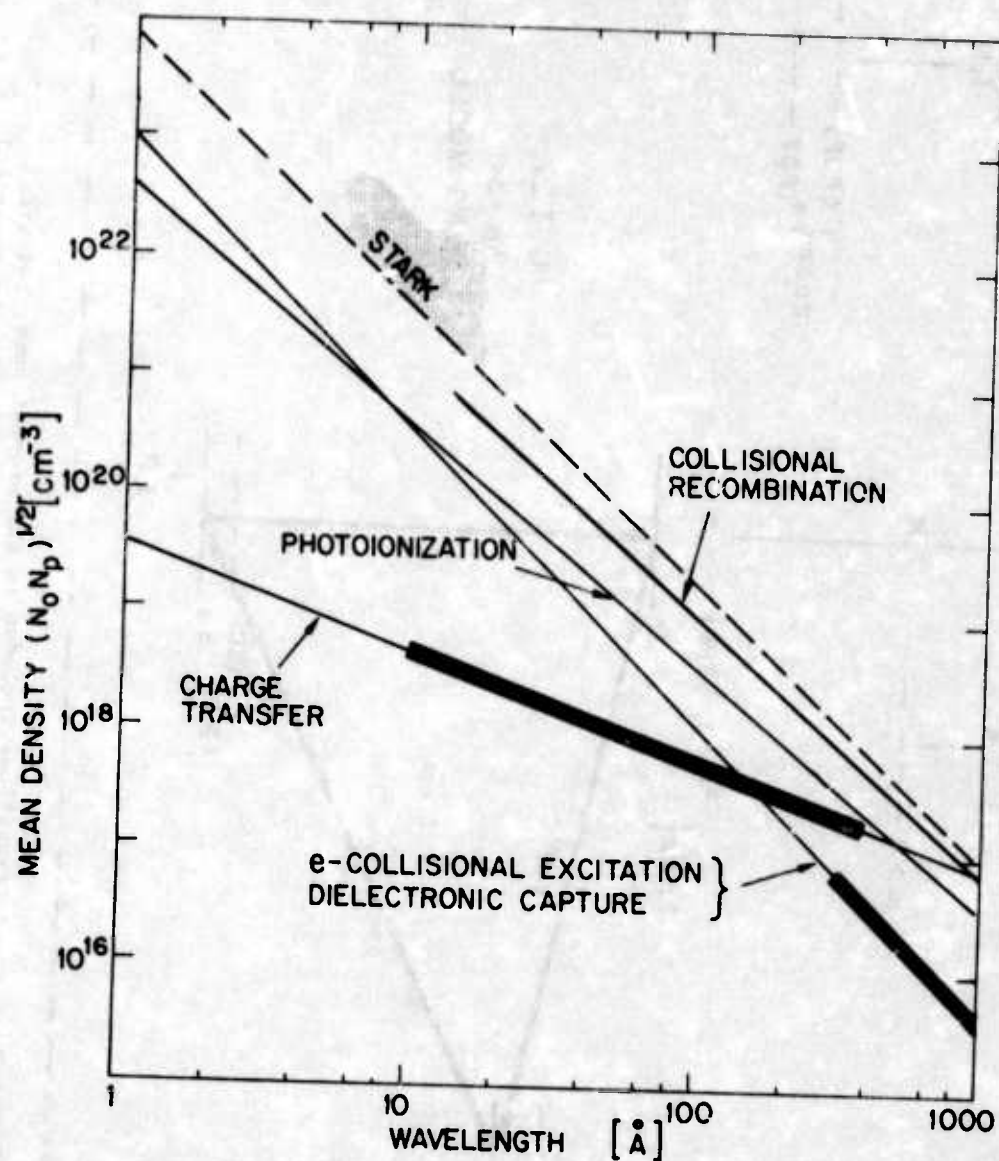
A16

Fig. 1. Mean particle densities (solid lines) versus wavelength for a gain factor of $c = 5$ and for selected pumping mechanisms. Stark broadening becomes important for large charged particle densities (same scale) in the region above the dashed line, also a region of approaching collisional equilibrium. Collisional recombination is plotted for fixed $N_e = 10^{21}$ cm^{-3} and terminates at ~ 15 Å due to dominance of radiative recombination to lower levels (see Table 2 footnote). Heavy lines indicate regions considered promising for present experiments at NRL (described in text).
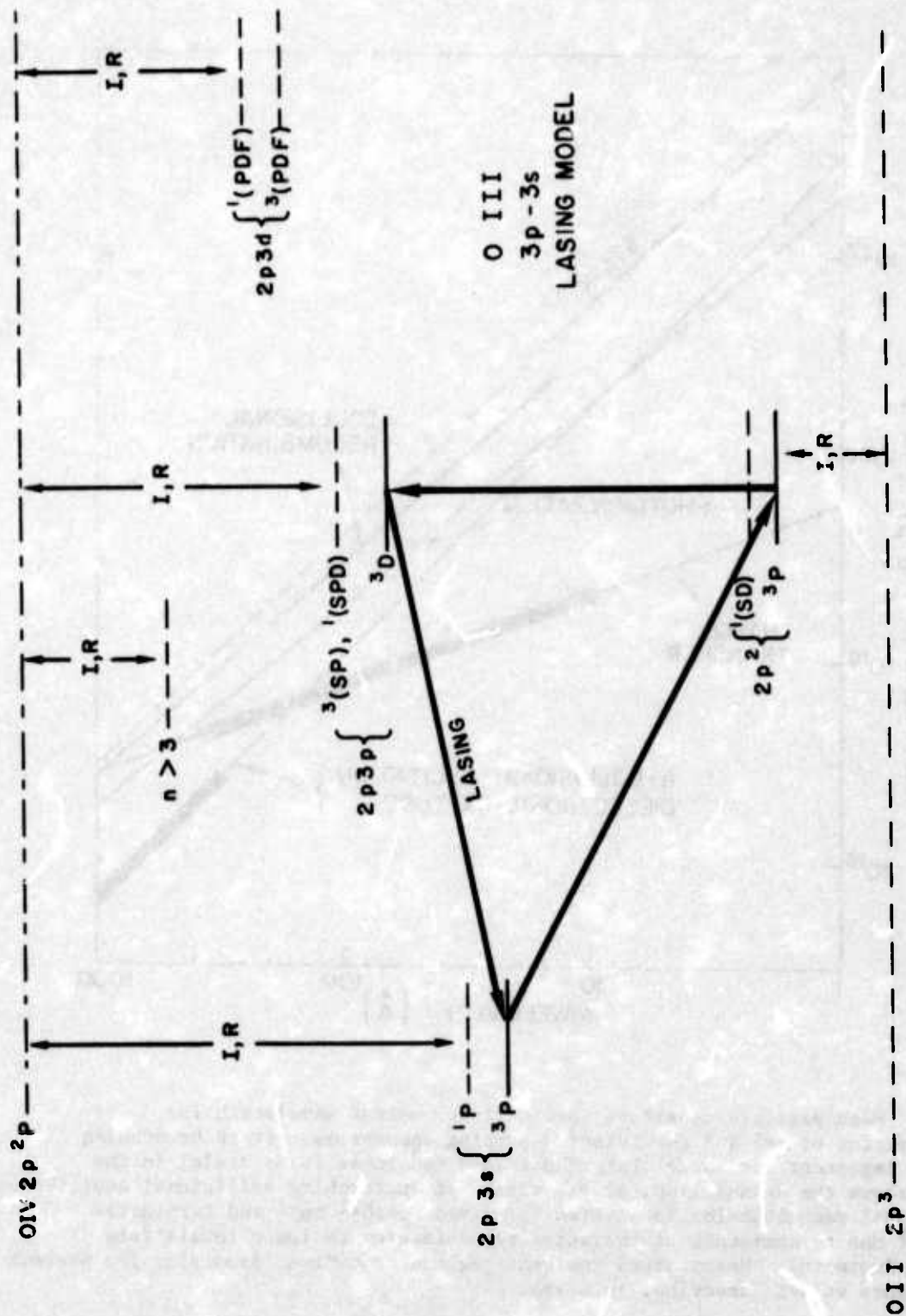
A17

Fig. 2. Energy levels and transitions included in the present numerical model of $^3p \rightarrow 3s$ lasing. Dashed transitions are presently being added to the numerical program.
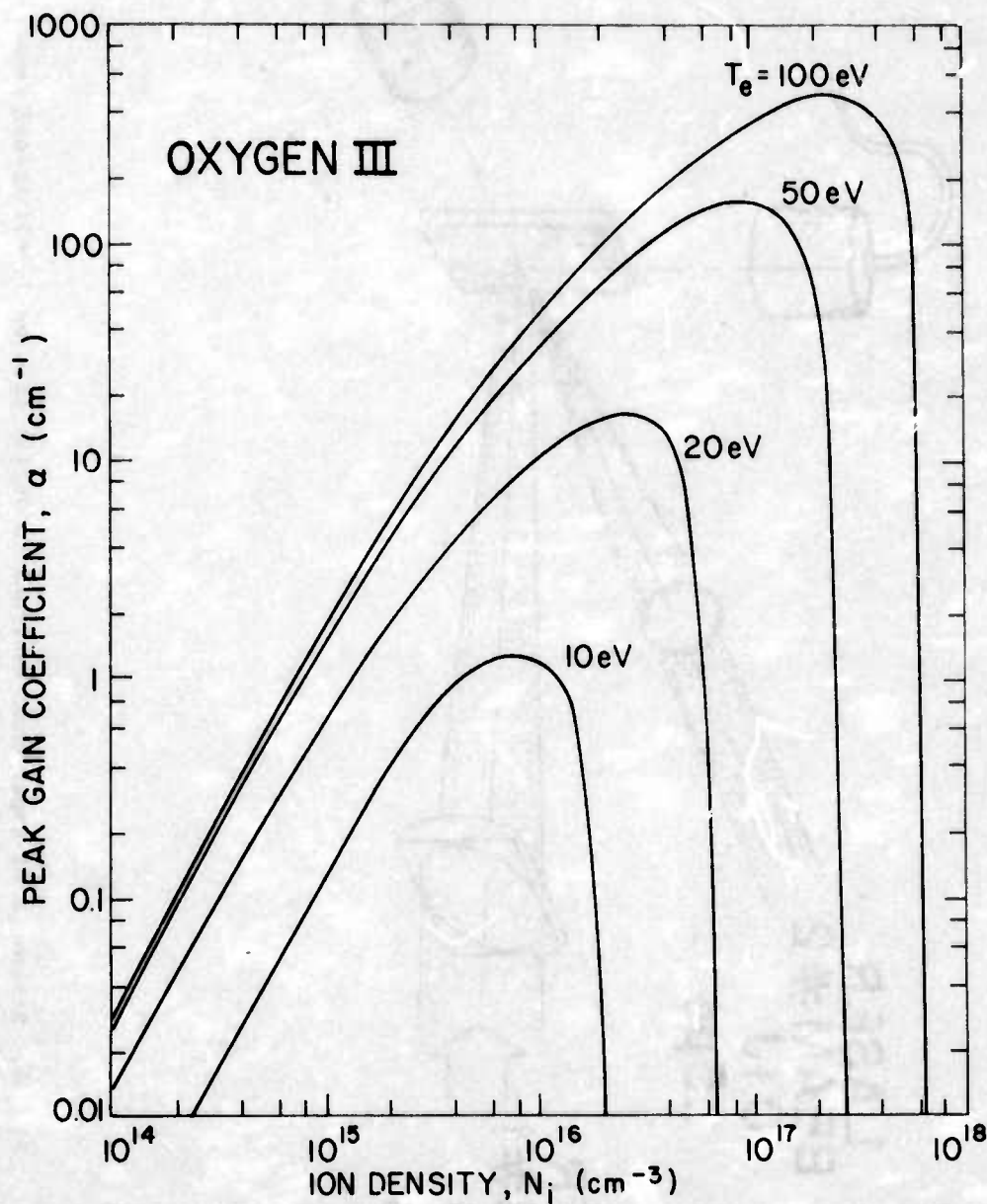
Fig. 3 Gain factor α (cm^{-1}) versus density from numerical model of $3p \rightarrow 3s$ transitions in plasmas. The decrease at high densities is due to increased influence of collisional mixing and finally collisional statistical equilibrium without population inversion. High temperatures produce increased pumping and decreased collisional mixing at a particular density.

A19

LASER BEAM #2
0.1J
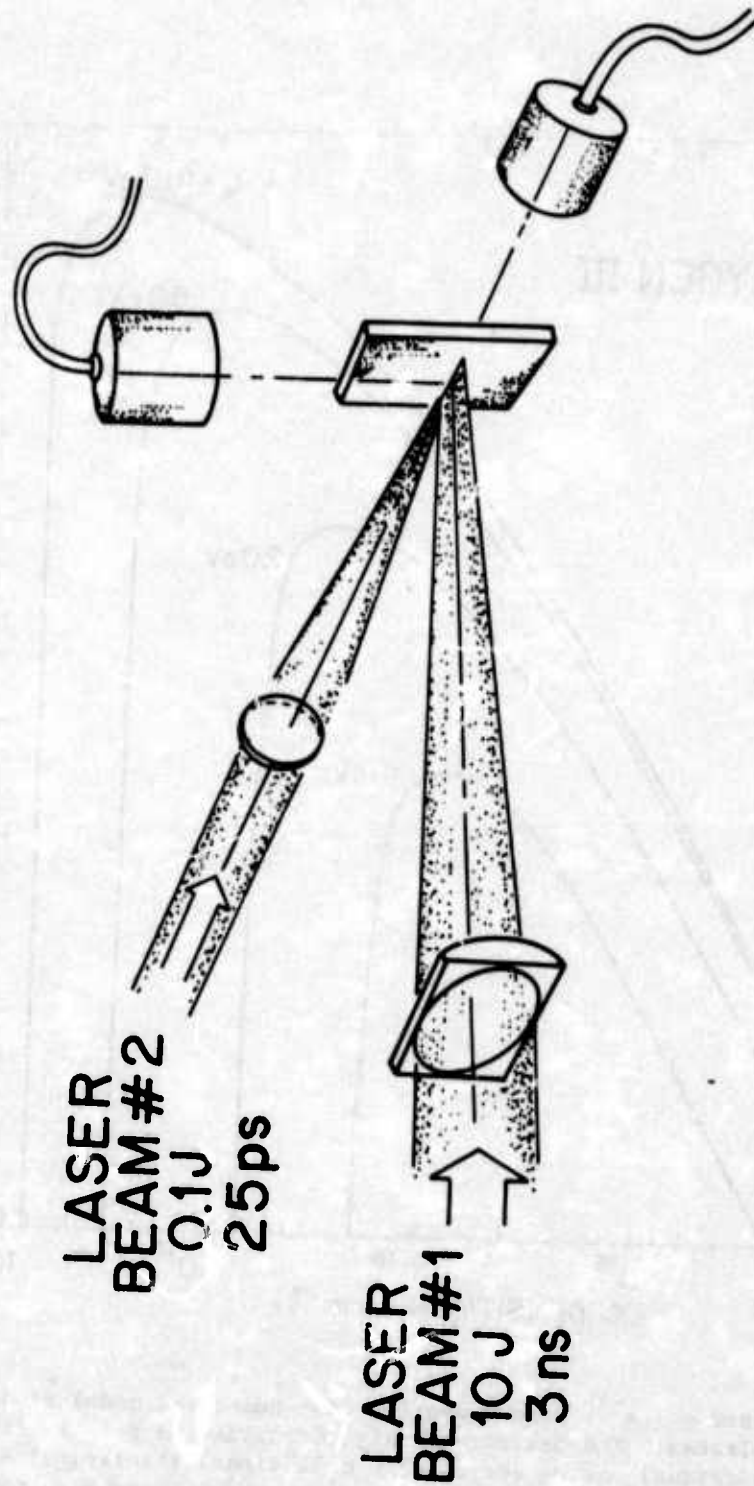25ps

LASER BEAM #1
10 J
3ns

Fig. 4. Schematic of experiment designed to verify gain on $3p \rightarrow 3s$ transitions pumped by electron collisions in a plasma.
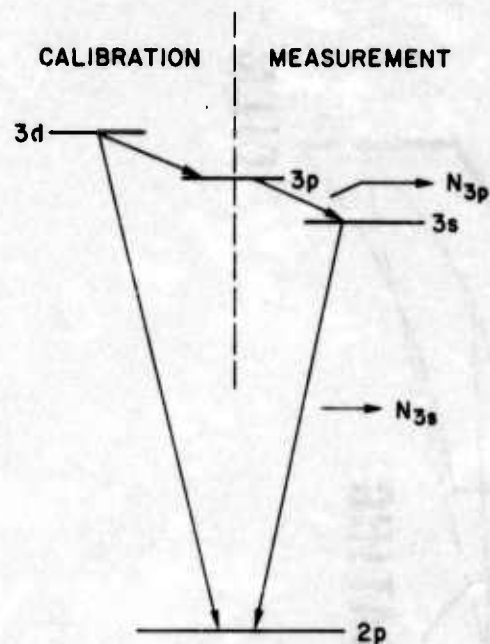
Fig. 5 — Transitions involved in determining the population inversion ratio N_{3p}/N_{3s} from relative line intensities, using branching transitions shown from the 3d level for instrumental calibration
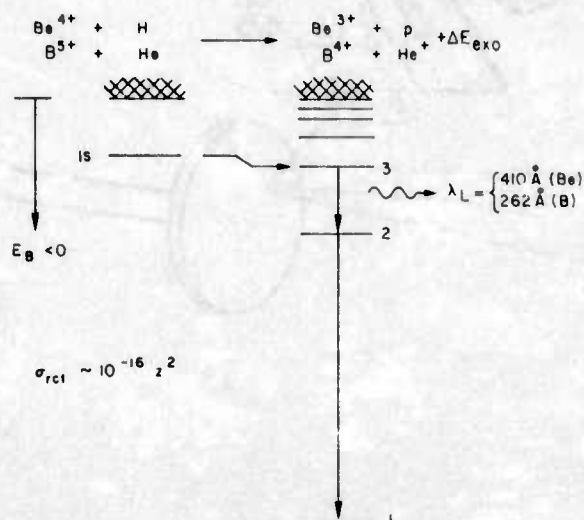

Fig. 6 — Schematic diagram of exothermic s-s resonance charge transfer reaction leading to population inversion between n=3 and n=2 levels in certain helium-like or hydrogenic ions. E_B is the binding energy.
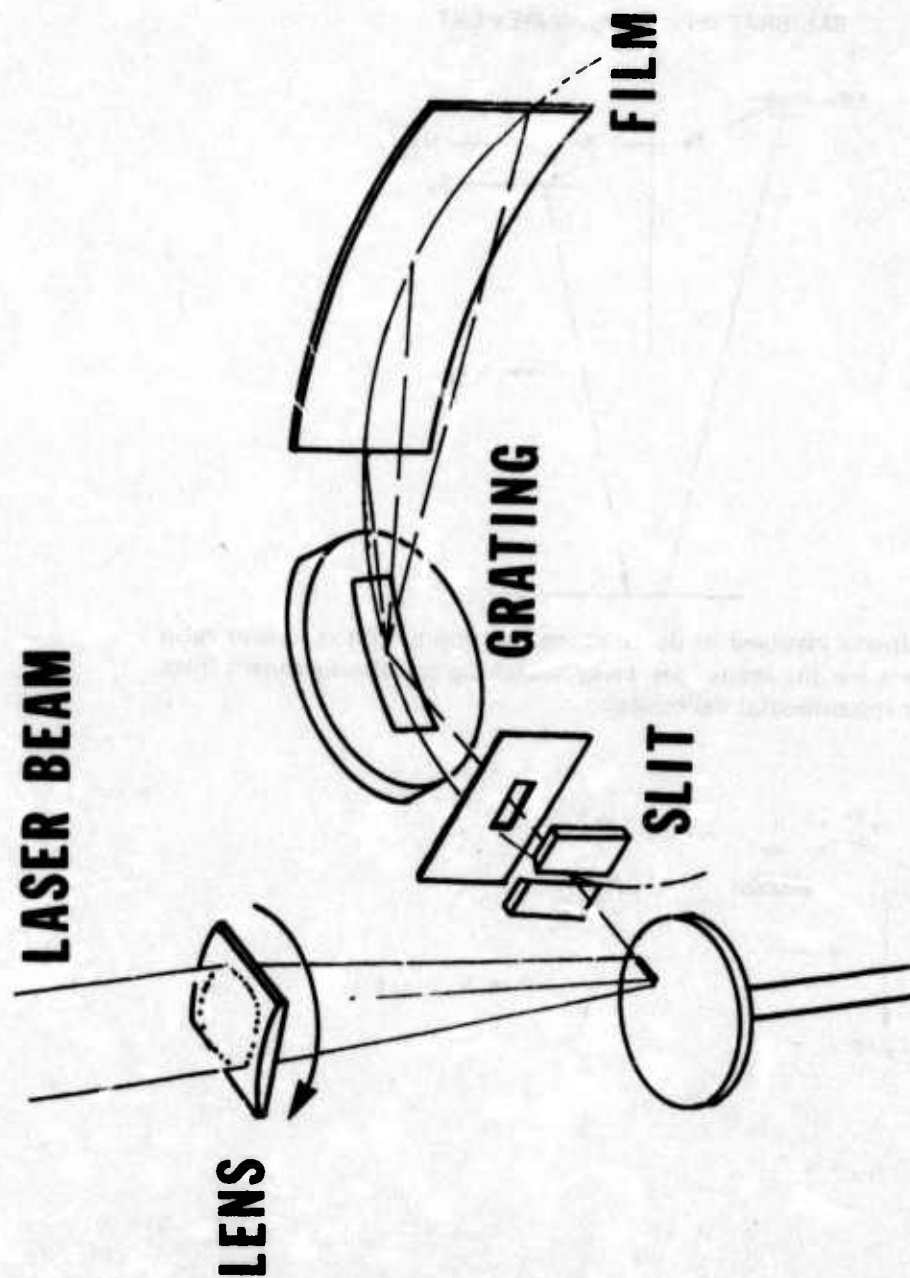
A21

Fig. 7. Schematic diagram of the NRL resonance charge transfer experiment, including the grazing incidence vacuum spectrograph. The horizontal slot provides spatial resolution along the direction of plasma expansion from the target surface. Rotation of the lens permits both axial and radial viewing. The background (atomic) gas is not indicated.
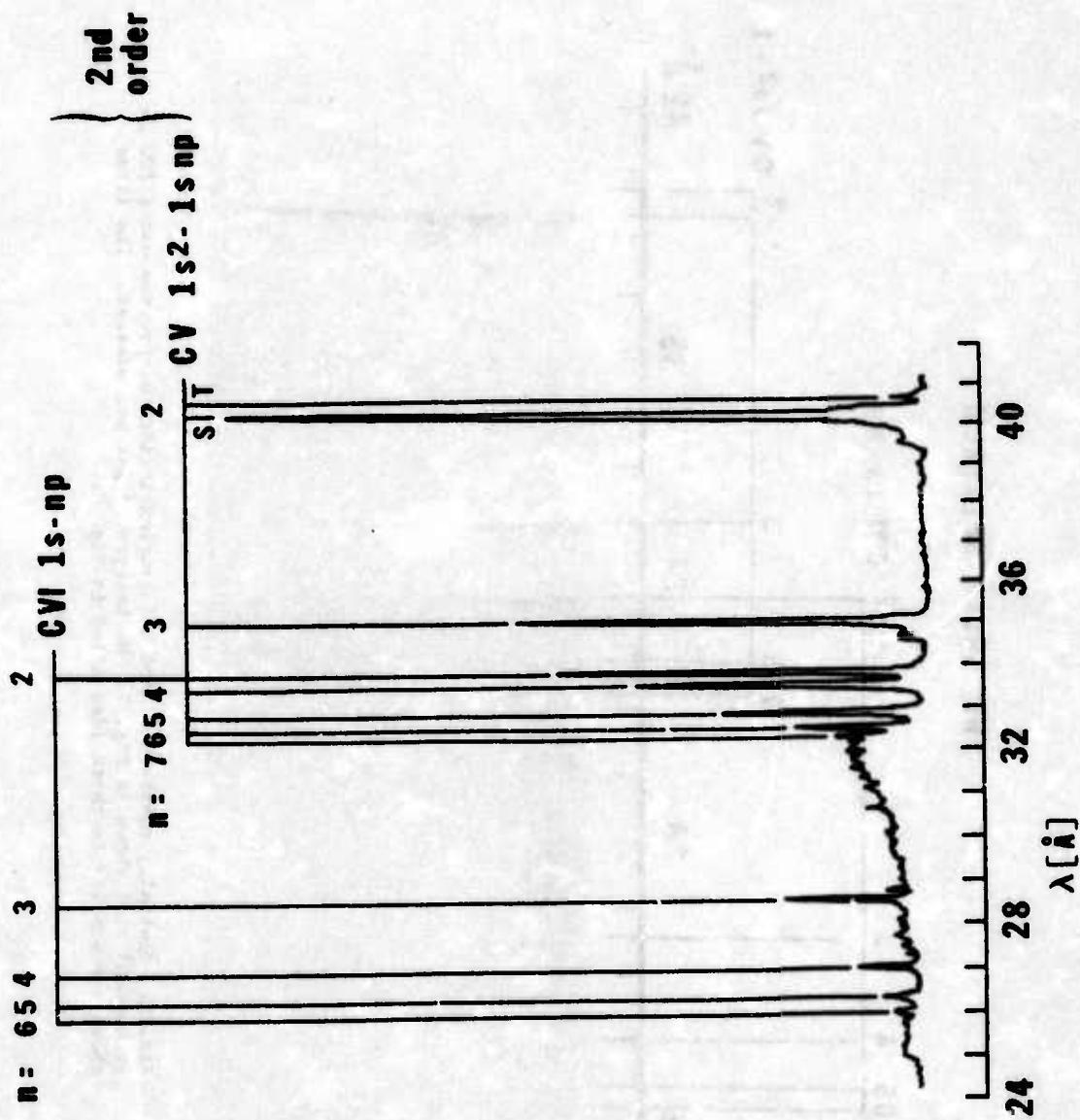
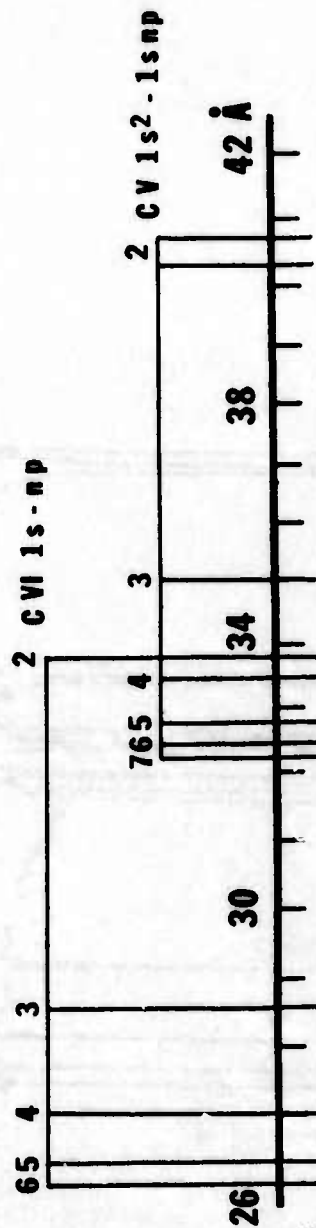Fig. 8. Microdensitometer tracing of a portion of a grazing incidence spectrum showing second order helium-like (CV) and hydrogenic (CVI) resonance series lines. No background gas was present.
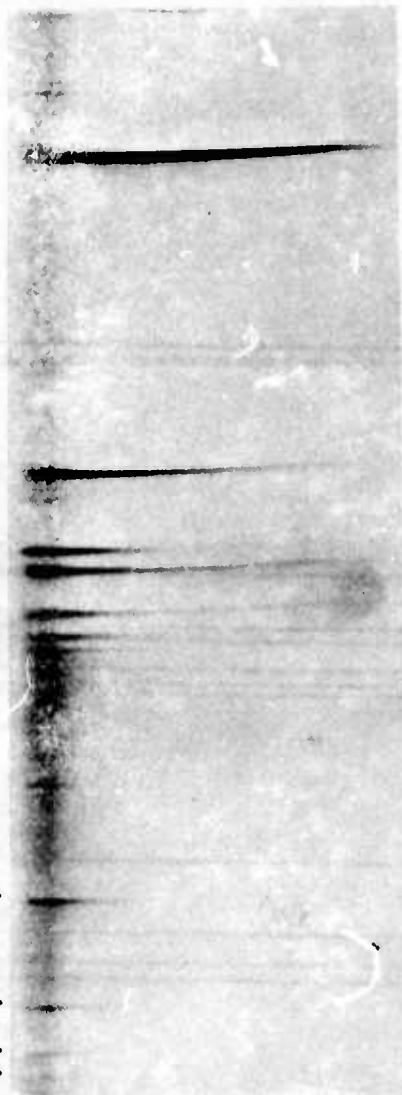
Fig. 9. Spatially resolved CV and CVI grazing-incidence spectrum using 300 μm orthogonal slot shown in Fig. 7. No background gas was present. The lines shown are similar to those identified in Fig. 8.

A 24

Extension of $3p \rightarrow 3s$ Ion Lasers into the Vacuum Ultraviolet Region

R. C. Elton

The feasibility of extending existing near-ultraviolet ion lasers into the vacuum ultraviolet spectral region is analyzed with a simplified three-state model. Single-pass amplification in a laser-produced plasma of reasonable length, pump power, and rise-time requirements is predicted, especially for high electron temperatures. The results are intended to serve as a basis and incentive for detailed numerical modeling and for experiments.

I. Introduction

Lasing in multiply ionized atoms has been demonstrated in the visible and near-ultraviolet spectral regions with gas discharges in resonant cavities.[1] It would he of great interest and importance to translate these results to shorter wavelengths isoelectronically.[2] At vacuum ultraviolet (vuv) wavelengths shorter than 2000 Å, conventional cavities become inefficient, and impractical below 1600 Å. However, for amplification of, for example, a frequency upconverted coherent vacuum-uv beam,[3] a resonant cavity is not required, provided significant gain can be achieved in a single photon pass through an inverted medium of reasonable length. Higher inverted state densities are required for single-pass amplification and for short wavelengths, with an upper density limit set by rapid depletion due to charged particle collisions. Population inversions are often self-terminating in time as equilibrium population distributions are approached, and the required rise time of the pumping source usually decreases with decreasing wavelength according to increasing transition probabilities for spontaneous decay. Also, the higher excitation energy in the heavier elements required for short wavelengths (isoelectric extrapolation) requires increased particle energies and densities for collisional pumping.

With these general guidelines we have attempted to analyze the scalability to shorter wavelengths. The highest degrees of ionization in heavy elements are obtained in high density plasmas, in short bursts, and in small volumes with a limited amount of available energy. A conceivably practical device, compatible with present technology, would be a linear plasma of about 1 cm in length, with the necessary ions and particle densities produced from a solid target by a line-focused laser beam. Longer plasmas may eventually be generated to produce increased overall gain, or perhaps decreased density for improved efficiency, as more powerful lasers are developed. Longer lengths may also become a possibility with axial heating of gaseous media by long wavelength lasers, a concept similar to that proposed for fusion plasma heating.[4] However, absorption and heating is a function of the plasma temperature and density, and uniform heating with narrow channeling[5] must first he proved. For short wavelengths and high Z materials, solid targets are generally more readily available than gases. It therefore seems reasonable to model the present analysis around a transverse irradiated and vaporized solid target plasma medium.

After expansion the initial plasma would be pumped axially with a separate short-pulse laser; this would preferentially heat the electrons, which in turn would produce the inversion by electron-ion collisions. A high electron temperature T_e is often very beneficial in producing a high inversion when, as here, the electron density is limited; also a low ion temperature reduces the (Doppler) line width and increases the possible gain (see Eq. (1) below). Thus, an electron-ion temperature differential is desirable, and this may he achieved by allowing the ions to expand and cool (faster than recombination takes place) and by heating the electrons in times shorter than the electron-ion energy equipartition time.

Considering resonance-line absorption and stimulated emission, the gain in a homogeneous medium of length L is given by $I/I_0 = \exp(\alpha L)$, where α is the gain coefficient[6]:

The author is with the U.S. Naval Research Laboratory, Washington, D.C. 20375.

A 25

$$\alpha = [\lambda^2(\pi \ln 2)^{1/2}/4\pi^2 \Delta \nu] A [N_u - (g_u/g_l)N_l]. \quad (1)$$

Here, λ is the laser wavelength, A the transition probability, $\Delta \nu$ the Doppler line width in frequency units, and g_u, g_l, N_u, N_l he statistical weights and population densities for the upper and lower laser levels, respectively. Photoionization losses are omitted here, since only (K and) L shell electrons are present, and the photon energy of the short wavelength laser lines is insufficient to remove L electrons; likewise competition from Auger decay does not exist. Loss of laser photons through scattering has also been neglected here. A selection of a particular αL product (unity for threshold, ≥ 5 desirable) determines the minimum length of the medium, since the other parameters (e.g., density) are fixed or limited in the medium. Thus, we intend to show that a practical length of the order of 1 cm is reasonable for a particular transition.

Laser transitions between two states, both with $n = 3$ principal quantum number, were chosen for detailed analysis. Electron pumping is assumed to proceed directly from a $n = 2$ ground state of a particular ion through a nondipole transition (slowly decaying) by electron collisions to a $n = 3$ state, followed by lasing through a dipole transition to a lower $n = 3$ state, after which the electron decays more rapidly to the $n = 2$ ground state. (It is not necessary to invoke a seemingly less probable combined ionization-excitation single-step collisional process in the analysis.) Laser transitions from a $n = 4$ upper state (pumped from $n = 2$) to a $n = 3$ lower state would produce shorter wavelength lines. However, the proximity of other $n = 4$ dipole-decaying states limits the maximum electron (and ion) density to too low a value to give reasonable laser lengths. Also, $n = 3$ to $n = 2$ transitions in helium like ions, pumped from the $1s^3$ ground state, were considered; however, the large $1s \rightarrow 3s$ energy gap severely limits the collisional excitation rates (see Eq. (5)) and therefore the available inversion density and the minimum laser length obtainable. (Note that this $3 \rightarrow 2$ laser scheme may prove practical when pumped from above by rapid downward cascading following electron capture.)

Pumping into a $n = 3$ upper laser state that is not dipole-coupled to $n = 2$ levels is one necessary condition for maintaining a large population density, since spontaneous depopulation of this state is limited to the $\Delta n = 0$ laser transition with a relatively low rate. Conversely, the lower laser state population is kept low by a high $n = 3 \rightarrow 2$ dipole depopulation rate. The collisional transition for populating the upper laser state can be monopole; e.g., $2p \rightarrow 3p$ ($2p \rightarrow 3s$ is not followed by $3 \rightarrow 3$ dipole decay). Quadrupole $2s \rightarrow 3d$ excitation is also conceivable. However, in the two instances where this might be particularly important, namely, the lithiumlike and berylliumlike (singlet) ground state ions, an inverted population will not be obtained, since the pumped $3d$ upper laser state has a shorter lifetime than the lower laser state due to a low-lying $2p$ state.

Lasing following monopole $2p \rightarrow 3p$ excitation has been observed in ions belonging to the beryllium (triplet system) through the fluorine isoelectronic sequences.[1] For a particular element (such as oxygen for which data are available), the trend is towards shorter wavelengths (and correspondingly lower gains) for the more highly ionized species (Be like). Also, pumping by collisional excitation becomes more difficult for the larger $2 \rightarrow 3$ energy gap in the highly stripped ions. It is also desirable to have a large energy separation between the upper lasing state and any nearby states that are dipole-coupled to the ground state, in order to reduce collisional-radiative depopulation; here, the boron- and carbonlike ions are slightly favored.

II. Analysis

While observations of lasing in multiply ionized atoms have been reported,[1] no similar attempt towards analysis of the mechanisms and limitations has been found in the literature. The present three-state analysis for carbon-like ions is intended to serve as a guide and stimulus for a more sophisticated and complete time-dependent numerical analysis (presently underway). Pumping is assumed to take place in a $2p^2\,^3P \rightarrow 2p3p\,^3D$ monopole ($\Delta \ell = 0$) transition, followed by lasing in a $2p3p\,^3D \rightarrow 2p3s\,^3P$ dipole transition, with the final state rapidly decaying by a dipole transition to the $2p^2\,^3P$ ground state. Lasing from a $2p3p\,^3S$ upper term is also possible. Two-electron radiative-Auger decay to a $2s2p^3$ configuration is expected to have a negligible effect.[7] Along the isoelectronic sequence, data are generally available up to neon.[7-11] Beyond that, wavelengths are scaled[12] as z^{-1}, where z is the charge seen by the active electron ($z - 1 =$ ion charge). The oscillator strength for the laser transition is extrapolated according to a $Z^{-1.1}$ empirical best fit (Z is the nuclear charge of the ion), and the associated laser transition probability is deduced[3] from $A \propto f/\lambda^2$. The equilibrium kinetic temperature of the plasma in which the ions are produced is taken as $kT \approx 0.25\chi_{z-2}$, where χ_{z-2} is the ionization potential of the next lower ion state. For estimating the excitation rate, and consequently the inversion density, it is assumed that the monopole excitation rate is approximately equal to a corresponding dipole rate. This assumption is supported by experimental and theoretical results[13] on plasma ions and is further discussed below for the high electron temperature situation. For this, the $2p^2\,^3P \rightarrow 2p3d\,^3D$ allowed transition was used and the oscillator strength was extrapolated empirically to unity with higher Z. This oscillator strength, as well as the $n = 2-3$ energy difference ΔE_{23}, are required in the approximation used for calculating the excitation rate in Eq. (5) for $\Delta n \neq 0$ transitions. The energy difference ΔE_{23} was estimated through extrapolation by keeping the ratio $\Delta E/\chi$ constant along the isoelectronic sequence.

In evaluating the collisional mixing rate between the upper laser state and a nearby state that has a short lifetime for dipole decay to the ground state,
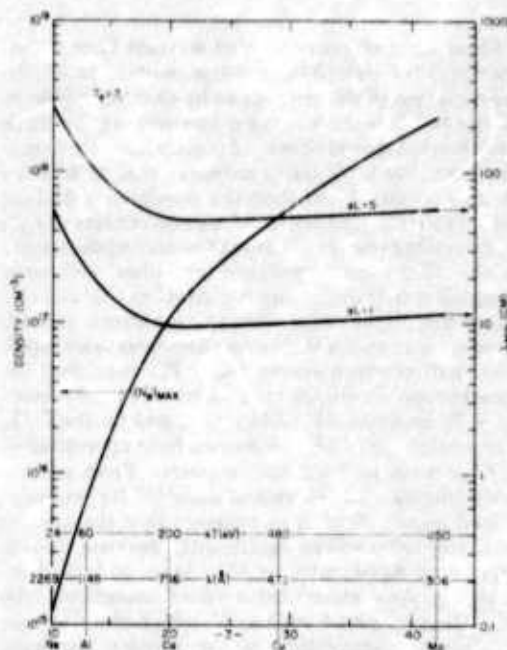
$$v = [6\pi(z - 1)e^2\omega kT_i/M^2]^{1/5}. \qquad (4)$$

Here, M is the ion mass, T_i the ion temperature, and $N_e/(z-1)$ is used for the ion density. The parameter C_i/N_e has also been tabulated[15] and is found to range from about five to two orders of magnitude less than C_e/N_e for the neon to molybdenum ions, respectively.

The maximum electron density is determined by setting the collisional mixing rate equal to the spontaneous emission probability A_{33} for the laser transition. Then, $(N_e)_{max} = A_{33}/(C_eN_e)$, for $C_i \ll C_e$. This density upper limit has been tabulated[15] and is plotted in Figs. 1 and 2. The maximum electron densities shown are quite consistent with those available in an expanding and cooling laser-produced plasma.

If the upper and lower laser terms are assumed to be populated by electron collisions from the $n = 2$ ground state (density $= N_g$) only (see Introduction), final coronal equilibrium values, given in a first approximation by $N_g(C_{23}/A_{32})$, are reached in a characteristic e-folding time of $\sim A_{32}^{-1}$. This time is much shorter for the lower laser level than for the upper, and the lower level reaches a much lower equilibrium concentration more rapidly. The collisional excitation rate C_{23} is calculated with the effective Gaunt factor approximation in the convenient form[16]:

Fig. 1. Minimum length L_{min} for amplification in carbonlike ions with gain $\exp(\alpha L)$ vs atomic number Z, wavelength λ, and temperature, where the electron (kT_e) and ion (kT_i) temperatures are assumed equal. Maximum electron density $(N_e)_{max}$ is also shown

the lower laser state was chosen, since—for the carbon sequence at least—it was close and thereby had a typical overlap. (In carbonlike ions there are six clustered $n = 3$ states that should be properly considered in a more sophisticated collisional analysis.) The electron collisional mixing rate C_e at an electron temperature T_e and density N_e is best estimated for $\Delta n = 0, l = 1 \to l = 0$ transitions from twice the line width given by the portion of Eq. (526) of Ref. 14, which pertains to $l \to l - 1$ transitions:

$$C_e = 6\pi N_e(\hbar m/\pi kT_e)^{1/2}(\hbar/mz)^2 n^2(n^2 - l^2)[l/(2l + 1)]$$
$$\times \ln\{5 - (4.5/z) + \xi^{-1}[(1 + kT_e n^2)/\chi_H z(z-1)]^{-1}\}, \quad (2)$$

where $n = 3, l = 1$, and where $\xi = (z-1) e^2 \omega/m v_e^3$ from Eq. (515) of the same reference. Here, χ_H is the ionization potential of hydrogen and ω is the laser angular frequency. The ratio C_e/N_e has been tabulated[15] for $T_e = T_i$.

The ion collisional mixing rate C_i has also been evaluated by Eqs. (517) and (518) of Ref. 14 (with the former multiplied by the square of the ion charge $(z - 1)^2$ for ions heavier than protons):

$$C_i = [4\pi^2/(2l + 1)] \frac{2}{5} (\hbar n/mz)^2 [N_e/(z - 1)](z - 1)^2$$
$$\times (M/kT_i)\left[l(n^2 - l^2)v \times \exp\left(-\frac{5}{6} Mv^2/kT_i\right)\right], \quad (3)$$
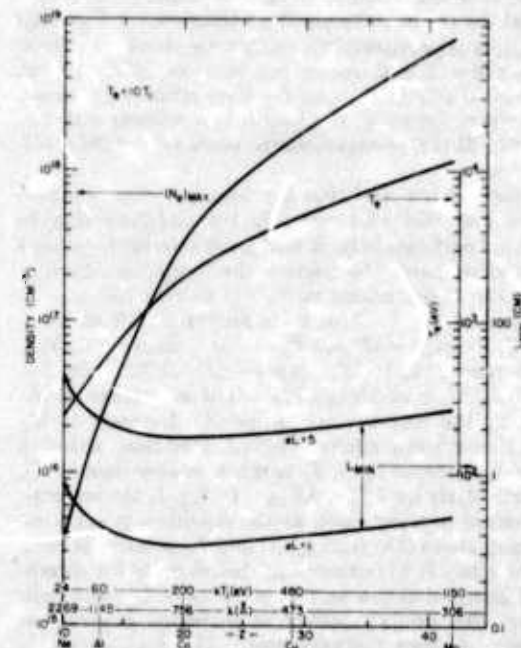
where

Fig. 2. Minimum length L_{min} for amplification in carbonlike ions with gain $\exp(\alpha L)$ vs atomic number Z, wavelength λ, and ion kinetic temperature kT_i. The electronic kinetic temperature kT_e is assumed equal to $10 kT_i$ and is plotted. Maximum electron density $(N_e)_{max}$ is also shown.

$$C_{23} = [1.6 \times 10^{-5} f_{23} \bar{g} \exp(-\Delta E_{23}/kT_e)/\Delta E_{23}(kT_e)^{1/2}]$$
$$\times N_e \ \sec^{-1}, \quad (5)$$

for ΔE_{23} and kT_e in eV and where $\bar{g}$ is the average Gaunt factor (≈ 0.2). By setting $N_g \approx N_e/(z-1)$, the upper laser state density may be calculated and is found[15] to be $\approx 10^{-3} N_g$.

A question remains as to how long an inversion is maintained; i.e., what equilibrium population distribution is reached and in what time interval? At first glance it appears possible that inversion can be sustained for an indefinite period. Clearly, a detailed time-dependent numerical rate equation analysis is needed, including as many effects from other levels (such as cascading) as possible. This refinement is now underway.

III. Results

It is now possible to estimate the minimum length necessary to achieve a particular gain product αL. For Doppler line broadening (Stark broadening is estimated from $0.5C_{23}$ and found to be negligible), this length is given for large inversion by[6]

$$L = (8\pi\alpha L/A_{33}N_u\lambda_{33}^3)(2\pi kT_i/M)^{1/2}. \quad (6)$$

This is plotted as L_{min} vs element, temperature, and wavelength in Fig. 1 for $\alpha L = 1$ and 5, and for $T_e = T_i$. The analysis is carried up to molybdenum ($Z = 42$), which is the heaviest element for which high stages of ionization have been reported.[17] It is seen that the parameters involved scale with Z such that L_{min} is approximately constant for elements heavier than $Z \approx 17$ and never becomes less than 10 cm, which is somewhat long for laser-produced plasmas. However, for neon, the length is consistent with 1-m cavity discharge experiments, since $\alpha I \approx 1.5\%$ is sufficient.

Since it is hoped that the ions may cool in expansion and that subsequently the electrons may be heated preferentially, it is of great interest to observe the effect here. Neglecting the logarithmic term in Eq. (2), C_e/N_e scales as $T_e^{-1/2}$ so that $(N_e)_{max}$ increases as $T_e^{1/2}$. Also, from Eq. (5), C_{23}/N scales as $(\bar{g}/T_e^{1/2})\exp(-\Delta E_{23}/kT_e)$ as does N_u/N_e^2. Therefore, $N_u \propto \sqrt{T_e} \ \exp(-\Delta E_{23}/kT_e)$, and $L \propto (T_i/T_e)^{1/2} \exp(\Delta E_{23}/kT_e)$. The advantage in allowing the ions to cool (while N_e decreases to the maximum value allowed) is indicated here, although the dependence upon T_i is much weaker than on T_e, particularly for $kT_e < \Delta E_{23}$. In Fig. 2, the ion temperature is maintained at the equilibrium value assumed above (i.e., $0.25 \chi_{z-1}$) and T_e is taken as $10T_i$. The effect is to reduce L_{min} below unity for threshold gain and as low as 1.7 cm for $\alpha L = 5$. This indicates the dramatic effect of increased pumping at higher electron temperatures. The L_{min} curves in Fig. 2 are to be shifted downward according to $\sqrt{T_i}$ for significant cooling with frozen-in ions. Just which ions will be most useful (i.e., the carbonlike sequence analyzed here or another sequence) will probably be determined by experiments (presently underway[18]).

There are two concerns that warrant further consideration for high electron temperatures. One is the depopulation of the laser states by electron collisions, the net result being a possible increase in gain length over that estimated above. An estimate[16] for ionization from the $n=3$ states indicates that in all cases the rate is much less than the dominant collisional mixing rate C_e used above. A second concern at high electron temperatures involves the assumption, made above, that the nondipole-transition collisional pumping rate is approximately equal to that of a corresponding dipole transition; i.e., for atoms, at least, the cross section for the former decreases more rapidly at high electron energy (high T_e) than does the cross section for dipole transitions. For the present $T_e = T_i$ analysis, $kT_e/\Delta E_{23} < 1$, and for the $T_e/T_i = 10$ analysis, $kT/\Delta E_{23}$ increases from approximately 3 for neon to 5 for molybdenum. From existing experimental and theoretical data[13,19] for multiply ionized atoms, there is no evidence that the $n=2\to3$ nondipole rates will be significantly less than the corresponding dipole rates for $kT_e/\Delta E_{23}$ up to 5. Furthermore, data exist[20] for $n=3\to3$ transitions with $kT_e/\Delta E_{33}$ varying from 4 to 15, which also shows no significant deterioration in the relative nondipole rates (although the absolute value of the cross section is reduced below that for dipole transitions in this case). Data on relative nondipole excitation rates at high electron temperatures are important, not only to the present analysis, but to other short wavelength ion laser approaches[21] that depend directly on a *weak* monopole excitation rate for the lower laser level at anomalously high electron energies in plasmas.

The required internal pump power density can be found from $N_g C_{23}\Delta E_{23}$, assuming $N_g = N_e/(z-1)$. With a volume determined by the product of the cross-sectional area a and the length L, and assuming a fractional absorption of L/L_{abs} along with a total energy conversion efficiency of η, the axial pumping laser irradiance P/a that is required is given by

$$P/a = N_e C_{23}\Delta E_{23} L_{abs}/\eta(z-1). \quad (7)$$

Here, L_{abs} is the classical inverse-bremsstrahlung absorption length, given by[4]

$$L_{abs} = 5 \times 10^{21} T_e^{3/2}/N_e^2 \lambda^3 (z-1) \ \text{cm} \quad (8)$$

for densities much less than the critical value ($\approx 10^{21}$ cm^{-3} for $\lambda = 1.06 \ \mu m$ radiation) at the plasma frequency. Here, T_e is in eV, λ is in cm, and N_e is in cm^{-3}. Then,

$$P/a = (2 \times 10^{19})[T_e f \exp(-\Delta E_{23}/kT_e)/(z-1)^2\eta]$$
$$\text{W/cm}^2. \quad (9)$$

with Eq. (5). Within the present approximations, P/a is therefore independent of density and medium length.

Numerical results indicate, for an estimated total conversion efficiency of 1%, a required irradiance up to approximately 10^{14} W/cm^2 for the ions indicated in the figures, and for $T_e = 10T_i$. This may be obtained with a 0.1-J, 10-psec laser focused to a 100-μm diam. The 1% efficiency estimate is arrived at by assuming 10% for laser heating and 10% for excitation of the particular upper configuration, in competition both with other excitation modes and with ionization (ionization from the $n = 2$ orbit proceeds at a rate[16] comparable to that for excitation to $n = 3$ levels for the enhanced electron temperature case).

IV. Discussion

The experimental scheme proposed above involves the transverse generation and subsequent expansion of a cylindrical plasma and the additional heating and pumping by an axial laser beam. A Maxwellian electron distribution has implicitly been assumed in the analysis. The electron equilibration time scales as $N_e{}^{-1}T_e{}^{3/2}$ and reaches the nanosecond range for the high electron temperature cases, which is comparable both to the upper laser state lifetimes and the collisional excitation times. Electron-ion equipartition times are, however, still much longer, so that high T_e/T_i ratios may be maintained. A more sophisticated analysis will either have to account for this relatively slow electron equilibration or depend upon electron heating at higher densities with an associated risk of excessive cooling during the ensuing expansion phase. The latter approach would not require additional pump irradiance, according to the present analysis; however, a complicated dynamic numerical plasma model would be required for analysis. Experiments will undoubtedly be done with various heating times.

V. Summary

The present three-state analysis indicates that it is promising to extrapolate successful near-ultraviolet ion laser transitions into the vacuum-uv region for amplification, by using expanding laser-produced cylindrical plasma as an initial medium that is subsequently pulse-heated axially with available lasers to increase the electron temperature for efficient pumping. The particular ion species that are generated and maintained in a frozen-in state will be identified in experiments. The added effects of other levels, as well as the true time dependence of the gain, will hopefully evolve from a numerical model presently under development. Such modeling of increasing sophistication will require more refined extrapolation methods and more basic data, particularly as it proceeds to higher Z elements.

References

1. R. S. Pressley, Ed. *Handbook of Lasers*, (Chemical Rubber Co., 1972) p. 242; C. K. Rhodes, IEEE J. Quantum Electron. **QE-10**, 153 (1974); Y. Hashino, Y. Katsuyama, and K. Fukuda, Japan J. Appl. Phys. 11, 967 (1972); 12, 470 (1973), for recent low-Z ion lasing in a z-pinch discharge.
2. M. Duguay, Laser Focus **9**, 45 (1973); R. A. Andrews, NRL Memo. Rept. 2677 (1973).
3. S. E. Harris, A. H. Kung, and J. F. Young, J Opt. Soc. Am. **64**, 556 (1974).
4. J. M. Dawson, A. Hertzberg, R. E. Kidder, G. C. Vlases, H. G. Ahlstrom, and L. C. Steinhauer, *IAEA Symposium on Plasma Physics and Controlled Fusion Research, Madison* (IAEA, Vienna, 1971), p. 673.
5. L. C. Steinhauer and H. G. Ahlstrom, Phys. Fluids 14, 1109 (1971).
6. R. C. Elton, R. W. Waynant, R. A. Andrews, and M. H. Reilly, "X-Ray and Vacuum-UV Lasers: Current Status and Prognosis," NRL Rept. 7412, (May 2, 1972).
7. R. L. Kelly with L. J. Palumbo, "Atomic and Ionic Emission Lines Below 2000 Å, NRL Rept. 7599 (1973).
8. C. E. Moore, "Atomic Energy Levels" NSRDS-NBS 35 (Dec. 1971); NSRDS-NBS 3 (1965–1971); NBS Circular 488.
9. W. L. Wiese, M. W. Smith, and B. M. Glennon, "Atomic Transition Probabilities, Vol. 1 Hydrogen through Neon" NSRDS-NBS-4 (May 1966); W. L. Wiese, M. W. Smith and B. M. Miles, "Vol. II, Sodium through Calcium" NSRDS-NBS 22 (October 1969).
10. W. L. Wiese, Appl. Opt. 7, 2361 (1958).
11. M. W. Smith and W. L. Wiese, Astrophys. J. **23**, 103 (1971).
12. B. Edlen, in *Handbuch der Physik* (Springer Verlag, Berlin, 1964), Vol. 27, p. 80.
13. H.-J. Kunze, Space Sci. Rev. 13, 565 (1972).
14. H. R. Griem, *Broadening of Spectral Lines by Charged Particles in Plasmas* (Academic Press, New York, 1974).
15. R. C. Elton, NRL Memo. Rept. 2799 (May 1974); Proceedings IV Int. Conf. on Vacuum-Ultraviolet Radiation Physics, Hamburg, 1974.
16. R. C. Elton, in *Methods of Experimental Physics-Plasma Physics*, H. R. Griem and R. H. Lovberg, Eds. (Academic Press New York, 1970), Vol. 9A.
17. J. J. Turechek and H.-J. Kunze (to be published).
18. T. N. Lee, J. Davis, J. F. Reintjes, R. H. Dixon, R. C. Eckardt, K. Whitney, J. L. DeRosa, R. A. Andrews, and R. C. Elton, Bull. Am. Phys. Soc. 19, 558 (1974); Proc. VIII IEEE International Quantum Electronics Conf. (1974).
19. H.-J. Kunze and W. D. Johnson, III, Phys. Rev. A **3**, 1384 (1971); W. D. Johnson III and H.-J. Kunze, Phys. Rev. A **4**, 962 (1971).
20. R. U. Datla, H.-J. Kunze, and D. Petrini, Phys. Rev. A **6**, 38 (1972).
21. T. C. Bristow, M. J. Lubin, J. M. Forsyth, E. B. Goldman, and J. M. Sources. Opt. Commun. 5, 315 (1972).

X-Ray Emission from Laser-Produced Magnesium Plasmas

T. N. Lee and D. J. Nagel

Naval Research Laboratory, Washington, D. C. 20375

ABSTRACT

Characteristics of the x-ray emission produced by focusing a 0.5 GW laser to about 10^{12} W/cm^2 on magnesium metal targets were measured. Approximately 0.01% of the incident laser energy of 10 J was emitted in a 11 nsec (FWHM) pulse of x-rays with photon energy in the range 1.3 - 1.8 keV.

INTRODUCTION

Reliable, easy-to-maintain lasers with powers up to about 1 GW are becoming increasingly available. When focused, such lasers produce power densities in the 10^{11}-10^{12} watts/cm^2 range. Plasmas produced from solid targets irradiated with such power densities typically have peak electron temperatures near 100 eV ($\sim 10^6$ K). Thus they are convenient laboratory sources of vacuum ultraviolet and soft x-radiation. There are a number of plasma light sources, for example, θ-pinch machines, which are capable of producing plasmas of hotter than 10^6 K. Such plasmas are large in volume but the electron density is smaller by many orders of magnitude than the density of laser-produced plasmas. In addition, the low-density plasma machines use gases for heating and therefore are limited to elements which occur in gases or can be made in convenient gaseous compounds. Advantages of laser-plasmas over discharge sources (including vacuum and sliding sparks) are: (a) spectra of all elements can be excited, (b) the spectra are relatively free of impurity lines, (c) the number of ionization stages contributing to a spectrum is small and somewhat controllable, and (d) size of the radiating plasma is small enough so that entrance slits may be eliminated for x-ray spectroscopy in some cases. Hence laser-plasmas are useful to generate data for interpretation of spectra from other sources. Their radiation is also convenient for testing and calibration of spectrographs and detectors.

The physics and diagnostics of high temperature laser plasmas are presently receiving intense study. Central problems include coupling of

A31

laser energy into the target plasma, and the division of that energy into thermal conduction losses, plasma expansion and radiation. Plasma temperatures and densities are desired as a function of laser pulse, focusing and target parameters. In this regard, several studies at laser powers similar to those in this work have already been made. In particular, Stumpfel et al.[1] used a grazing-incidence monochromator to do time-dependent studies of radiation down to 35 Å from Mg plasmas generated by a 0.5 GW laser. They found ionization stages through Mg X and suggested that He-like Mg XI ions should exist in plasmas produced by few-joule, ~ 20 nsec laser pulses. Recently, Peacock et al.[2] made a spectroscopic study of the satellite lines near the resonance lines of He-like Mg ions in plasmas produced using a Nd-laser at about 1 GW. Donaldson et al.[3] did a comprehensive study of lighter-atom plasmas which were generated with laser powers up to 2 GW.

In this work,[4] we investigated several characteristics of the plasma x-ray emission produced by focusing a 0.5 GW (18 nsec FWHM) ruby laser beam (0.69 μm) onto Mg-targets, namely the x-ray yield as a function of the lens-target distance, the time histories and correlation between laser and x-ray signals, the x-ray conversion efficiency, x-ray pinhole photographs and the x-ray spectrum in 7 Å - 10 Å region. Non-uniformity of the laser power distribution is evidenced by post-shot microscopy of the targets. Comparisons of the present results with x-ray emission produced by 1 nsec Nd laser pulses (1.06 μm) of similar energy are made.

EXPERIMENTAL ARRANGEMENT

The experimental arrangement is shown schematically in Fig. 1. A Korad K2 ruby laser system consisting of a Q-switched oscillator produced

pulses with energies up to 10 J. The beam divergence was 8 mrad.

A beam splitter and an S-1 response photo-diode were used to monitor the laser pulse signal shape and the power. The laser beam (3.5 cm in diameter) was focused by a 5 cm diameter, 20 cm focal length lens, which was mounted on a micrometer translation stage outside of a vacuum window. Flat Mg-targets, polished with abrasive paper, were placed at 45 degrees to the incident beam in a 3×10^{-2} torr vacuum. A silicon p-i-n x-ray detector located at about 60 degrees to the beam, and *(15 degrees from the target normal)* 10 cm from the focus, and covered with a light-tight 25 μm beryllium window, was used to monitor x-ray pulses. Prior to emplacement of the spectrometer shown in Fig. 1, an x-ray camera with a 25 μm pinhole 2 cm from the focus viewed the plasma 90 degrees to the beam *and 45 degrees to the target normal.* It yielded 2X magnification. The simple slitless x-ray spectrometer at 90 degrees to the laser beam *and 45 degrees to the target normal* consisted of a flat rubidium acid phthalate (RAP) crystal (2d spacing: 26.121 Å) with its center 4 cm from the plasma. Kodak No-Screen x-ray film behind 12 μm beryllium foil 6 cm from the crystal center recorded the spectrum.

EXPERIMENTAL RESULTS

In order to provide as much plasma x-radiation as possible, the effect of laser beam focusing on the x-ray yield was examined by varying the lens-target spacing. The result is shown in Fig. 2 where the relative x-ray intensity as measured with the p-i-n detector is given as a function of lens displacement near the focal point. The measurements were taken by both increasing and decreasing the lens-target distance. In doing the "through focus" measurements, we found the laser power and x-ray intensity both

A33

reproducible from shot to shot to within ± 10%. The curve obtained here has a single, roughly symmetrical peak in constrast to recent work[5] using deuterium targets where the soft x-ray intensity vs. target position for 3 nsec, 10 GW pulses was found to have two peaks. As can be seen in Fig. 2, the x-ray intensity is not highly sensitive to the focusing within ± 0.5 mm of the optimum point. However, the x-ray signal shows a rapid decrease to both sides of the peak. The half-width (~ 2 mm) of the profile is considerably narrower than that expected from the beam divergence of the present laser-lens system. This apparent discrepancy can be rationalized if one assumes that most of the x-radiation detected originates from much smaller areas - hot spots - within the focal region. This assumption is consistent with the target damage which will be described below. Actually little x-ray emission was detected when there was no hot spot mark within a focal crater. Another reason for the narrower profile may be the existence of a power density threshold which must be exceeded to produce measurable x-ray intensity.

The p-i-n detector, cables, and Tektronix 7904 oscilloscope have a combined rise time of about 2 nsec. Hence, the p-i-n detector signal approximated the time history of the x-ray emission. The x-ray pulse, and the laser pulse as measured with the photodiode, are shown in Fig. 3. The FWHM of the x-ray emission is much narrower (~ 11 nsec) than that of the laser pulse. This result is consistent with the absence of x-ray emission until laser light intensity reaches a certain threshold as mentioned above. For lasers with 1 nsec pulses and intensities greater than 1 GW[6] and 5 nsec, 4 GW pulses,[7] the x-ray pulse width is approximately equal to the laser pulse width, in contrast to the results shown in Fig. 3. The time correlation between the

laser and x-ray signals was made by feeding a commo.*high frequency sinusoidal signal to the Z-axis (intensity) terminal of two oscilloscopes. The two signals peaked simultaneously to within 3 nsec.

The approximate x-ray conversion efficiency was obtained from the p-i-n signal using the detector sensitivity calculated from the manufacturer's specifications. *and the known Be window thickness.* Assuming isotropic emission into 4π, the efficiency for conversion of the 6943 Å laser light to x-ray line radiation near 9 Å (see below) was 0.007%. This x-ray conversion efficiency is much smaller than that obtained with laser pulses of about 1 nsec where more than 1% [8,9] of the incident energy can be converted into x-rays with energies greater than 1 keV. The total energy in the radiation was 7×10^3 ergs compared to 10^7 ergs of x-rays from a 1 nsec, 10 J (10 GW) laser pulse. [9]

Nevertheless, the x-ray intensity was enough to obtain x-ray photographs of the plasma through a 25 μm pinhole with a single exposure on Kodak No-Screen film behind a 12 μm Be window. An example is shown in Fig. 4. The time-integrated image consists of a more intense region which is elongated along the direction of the incident laser beam and the less intense, apparently more tenuous, radially-expanding plasma. The elongated hot region probably results from interaction of the beam with the expanding plasma during the relatively long pulse. Pinhole x-ray pictures from plasmas produced by short (< 1 nsec) laser pulses [10,11] are more symmetrical.

The x-ray spectrum from the Mg-plasmas was obtained in order to know what ionization stages can be achieved with such a low power laser. Fig. 5 (top) shows a microdensitometer scan of an x-ray spectrum obtained in a 25 shot exposure. The ions and transitions labeled in the figure were identified using tabulated wavelengths for Mg-ion radiation. [12] Three

A35

transitions ($np \to 1s$, $n = 2$, 3, and 4) in two ionization states, He-like Mg XI and Li-like Mg X, make up most of the spectrum. Free-to-bound Mg XI recombination radiation appears at the short-wavelength end of the spectrum. One of the weak peaks to the short wavelength side of the Mg XI $1s^2$-$1s2p$ line is ascribed to a transition in doubly-excited Mg XI. The weak lines on the longer wavelength side of Mg X $1s^2 2\ell$ - $1s2\ell 2p$ lines, may be from Zn[9] which was found by optical spectrographic analysis to be present in the target material at the 0.2% level. Relatively strong Zn-$L\alpha$ emission from a low-level contamination of a Henke tube system was also reported previously.[13] The spectrum produced by the ruby laser is compared with the Mg-spectrum obtained from a MgO target with a 0.9 nsec, 2.2 GW glass laser (shown in lower part of Fig. 5). Rather broader lines in the former spectrum are due to the multiple exposure (during which plasma position might have changed from shot to shot) and also due to the large plasma size produced by the present laser. The H-like Mg Lyman α line, one of the prominent features in the spectrum produced by the higher-power Nd laser, is absent in the spectrum obtained with the 18 nsec, 0.5 GW laser.

The approximate peak temperature of the Mg plasma might have been determined from the ratio of the $1s$-$2p$ lines from H- and He-like ions by use of a coronal model.[14] However, the absence of the Lyman α line only allows an upper limit of 300 eV to be set on the effective plasma temperature. The spectrum in figure 5 (top) shows that the average ionization stage is between 9 and 10. According to a coronal model[15], this implies an electron temperature near 80 eV. In a separate study[16] of the dependence of x-ray emission on the atomic number of the target, which was done with the same laser used for this work, temperatures of about 70 eV were found. These can be compared with temperatures near 750 eV which are produced by focusing 0.9 nsec, 7 J pulses ($\sim 2 \times 10^{14}$ W/cm^2) on Al.[14]

It is generally difficult to measure the exact size of the focal spot which is needed for the determination of the average laser power density at the target. Furthermore, the laser intensity is usually not uniform over beam diameter. The focus may contain hot spots which are the predominant x-ray sources, as mentioned earlier. In order to examine this possibility, the target craters produced by a single shot were observed with a scanning electron microscope. [17] Fig. 6 is a typical crater which shows the effects of nonuniform power density within a focal spot, i.e., relatively deep areas due to higher-than-average power density within the larger crater. The diameter of the overall crater is about 1.5 mm whereas the hot spot measures about 150 to 200 μm. The focal pattern is believed to be caused by the extremely nonuniform laser beam as witnessed by burn patterns of annular or horse-shoe shapes. Since the beam energy is divided into the larger crater and the hot spots, an upper limit of the beam power density at the hot spot is estimated to be roughly 10^{12} watt/cm^2.

DISCUSSION AND SUMMARY

Some characteristics of the Mg-plasma x-ray emission produced by focusing an 18 nsec, 0.5 GW ruby laser beam onto magnesium slab targets have been described. The unexpectedly strong dependence of the x-ray emission on the lens-target distance is believed to be due to most x-radiation originating at hot spots. Results of the focal hot spots are actually observed in photographs taken with a scanning electron microscope. Determination of the power density of the laser beam therefore requires care since the power concentration at the hot spots is higher than the rest of the crater area.

A37

for conversion of laser light to x-rays above 1 keV which

The rather low ~~x-ray conversion~~ efficiency obtained in this experiment
is thought to be caused by the following: (a) the existence of ~ threshold
laser energy below which no significant x-radiation is emitted, i.e., the
x-ray pulse width is much narrower than the laser pulse width (see Fig. 3),
(b) some fraction of the beam energy is lost in the focal spot other than the
hot spots, and (c) the electron temperature is not high enough to give in-
tense x-rays such as the series of line radiation and the continuum associated
with the H-like Mg XII ions. The x-ray time history, the pinhole x-ray
photographs, the target damage, and the spectrum are all consistent with
this picture.

The electron temperature of the Mg-plasma is estimated in this work
to be ~~less than 300~~ *approximately 80* eV. The lower temperature obtained with the present
laser compared to that of 1 nsec Nd-laser of comparable energy can be
understood at least qualitatively from a power law relationship[3] between
the temperature and the laser beam power density.

Regardless of the lower x-ray conversion efficiency compared to
sophisticated, expensive and hard-to-maintain lasers of 10 to 100 GW, the
present results indicate that a small, low power laser (≤ 0.5 GW) produces
plasmas which emit enough soft x-rays to be useful as laboratory light source
for spectroscopy, for calibration of x-ray detectors and for radiography of
high speed phenomena. [18]

ACKNOWLEDGMENTS

REFERENCES

[1] C. R. Stumpfel, J. L. Robitaille, and H. Z. Kunze, J. Appl. Phys. $\underline{43}$, 902 (1972).

[2] N. J. Peacock, M. G. Hobby, and M. Galanti, J. Phys. B $\underline{6}$, L 298 (1973).

[3] T. P. Donaldson, R. J. Hutcheon, and M. H. Key, J. Phys. B $\underline{6}$, L 298 (1973).

[4] T. N. Lee and D. J. Nagel, Bull. Am. Phys. Soc. $\underline{18}$, 684 (1973).

[5] F. Floux, D. Cognard, A. Saleres, and D. Redon, Phys. Lett $\underline{45A}$, 483 (1973).

[6] D. J. Nagel and J. F. Holzrichter, unpublished.

[7] M. H. Key et al., Appl. Phys. Lett. $\underline{25}$, 335 (1974).

[8] P. J. Mallozzi et al., in M. S Feld et al., (Eds.) Fundamental and Applied Laser Physics, (Wiley and Sons, New York, 1973), p. 165.

[9] D. J. Nagel et al., Phys. Rev. Lett. $\underline{33}$, 743 (1974).

[10] J. F. Holzrichter, C. M. Dozier, and J. M. McMahon, Appl. Phys. Lett. $\underline{23}$, 687 (1973).

[11] T. N. Lee et al., Bull. Am. Phys. Soc. $\underline{19}$, 558 (1974).

[12] R. L. Kelly and L. J. Palumbo, NRL Report No. 7599, Naval Research Laboratory, Washington, D. C. (1973).

[13] L. J. Palumbo, PhD Thesis, Georgetown University (1971).

[14] B. M. Klein et al., Bull. Am. Phys. Soc. $\underline{18}$, 685 (1973).

[15] D. Mosher, Phys. Rev. A10, 2330 (1974)

[16] R. D. Bleach and D. J. Nagel, unpublished.

[17] K. Vogel and P. Backlund, J. Appl. Phys. $\underline{36}$, 3697 (1965).

[18] See, for example, S. K. Handel and B. Stenerhag in N. R. Nilsson and L. Hogberg (Eds.) High Speed Photography (Wiley and Sons, New York, 1968), p. 253.

See next sheet for
full names for references
7, 8, 9, 11 and 14

Full Names for References

7 M.H. Key, K. Eidman,
   C. Dorn + R. Sigel

8 P.J. Mallozzi, H.M. Epstein, R.G. Jung,
   D.C. Applebaum, B.P. Fairand +
   W.J. Gallagher.

9 D.J. Nagel, P.G. Burkhalter, C.M. Dozier,
   J.F. Holzrichter, B.H. Klein, J.M. McMahon,
   J.A. Stamper, + R.R. Whitlock

11 T.N. Lee, J. Davis, J.F. Rientjes, R.H. Dixon,
    R.C. Eckardt, K. Whitney, J.L. De Rosa,
    R.A. Andrews + R.C. Elton

14 B.M. Klein, C.M. Dozier,
    D.J. Nagel, + R.R. Whitlock.

A40

FIGURE CAPTIONS

1. Schematic diagram of experimental arrangement.

2. X-ray signal measured with p-i-n detector vs. relative lens displacement.

3. Time histories and correlation between laser and x-ray pulses. The peak alignment is uncertain to $\pm$ 1.5 nsec.

4. Densitometer scan of x-ray photograph taken with 25 μm pinhole, showing density contours. Outer contour extends 1 mm from the target surface which is indicated by the dashed line.

5. Mg spectrum taken with 0.5 GW ruby laser in 25 shots compared with spectrum produced by a single 2.2 GW shot of a Nd:glass laser.

6. Scanning electron micrographs of the Mg target. Top: Overall oblique view of the focal area showing two deep craters due to hot spots. Center: View down into the larger of the two craters which is approximately 175 μm in diameter. Bottom: Enlargement of the region between the two craters.
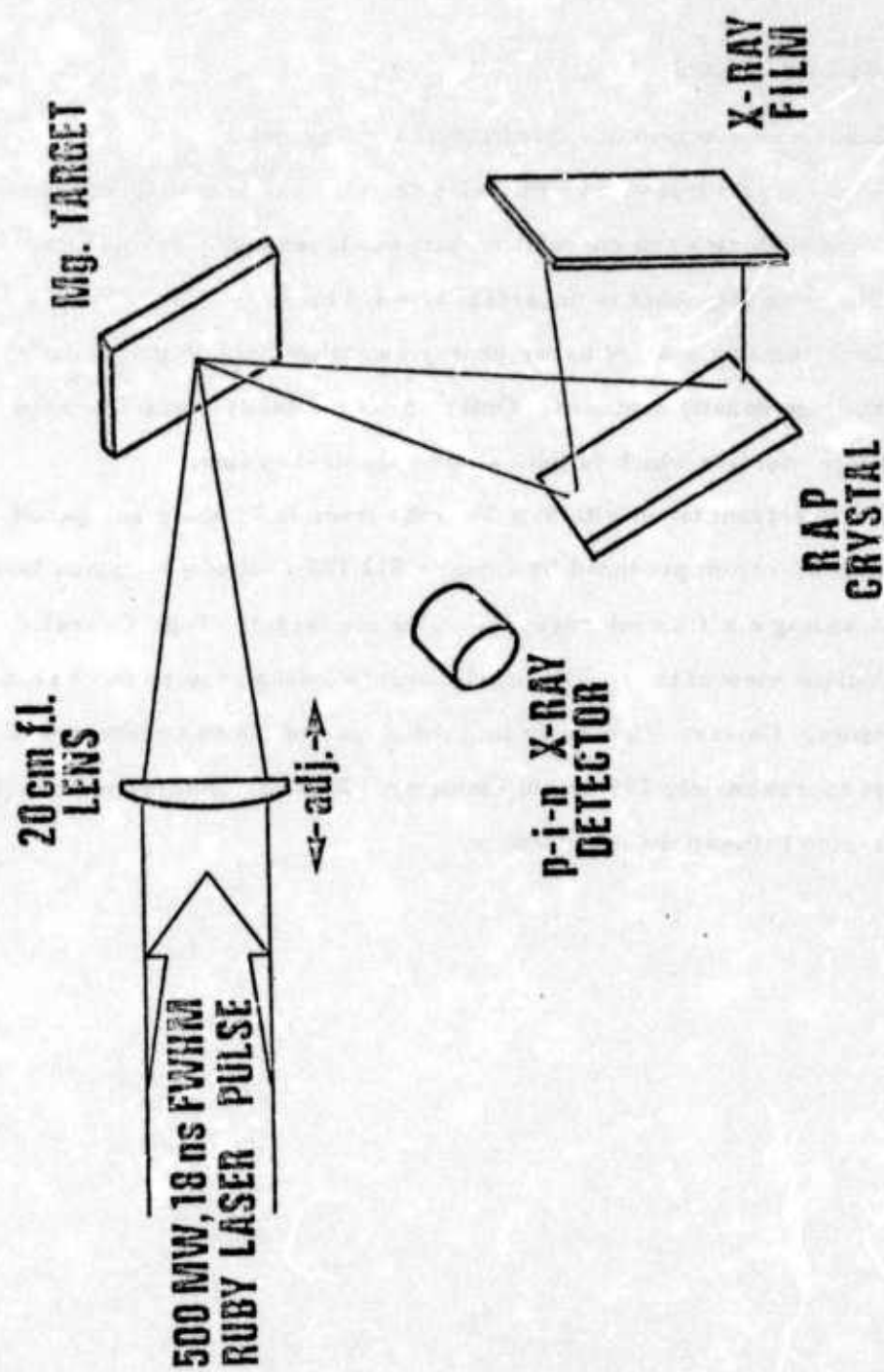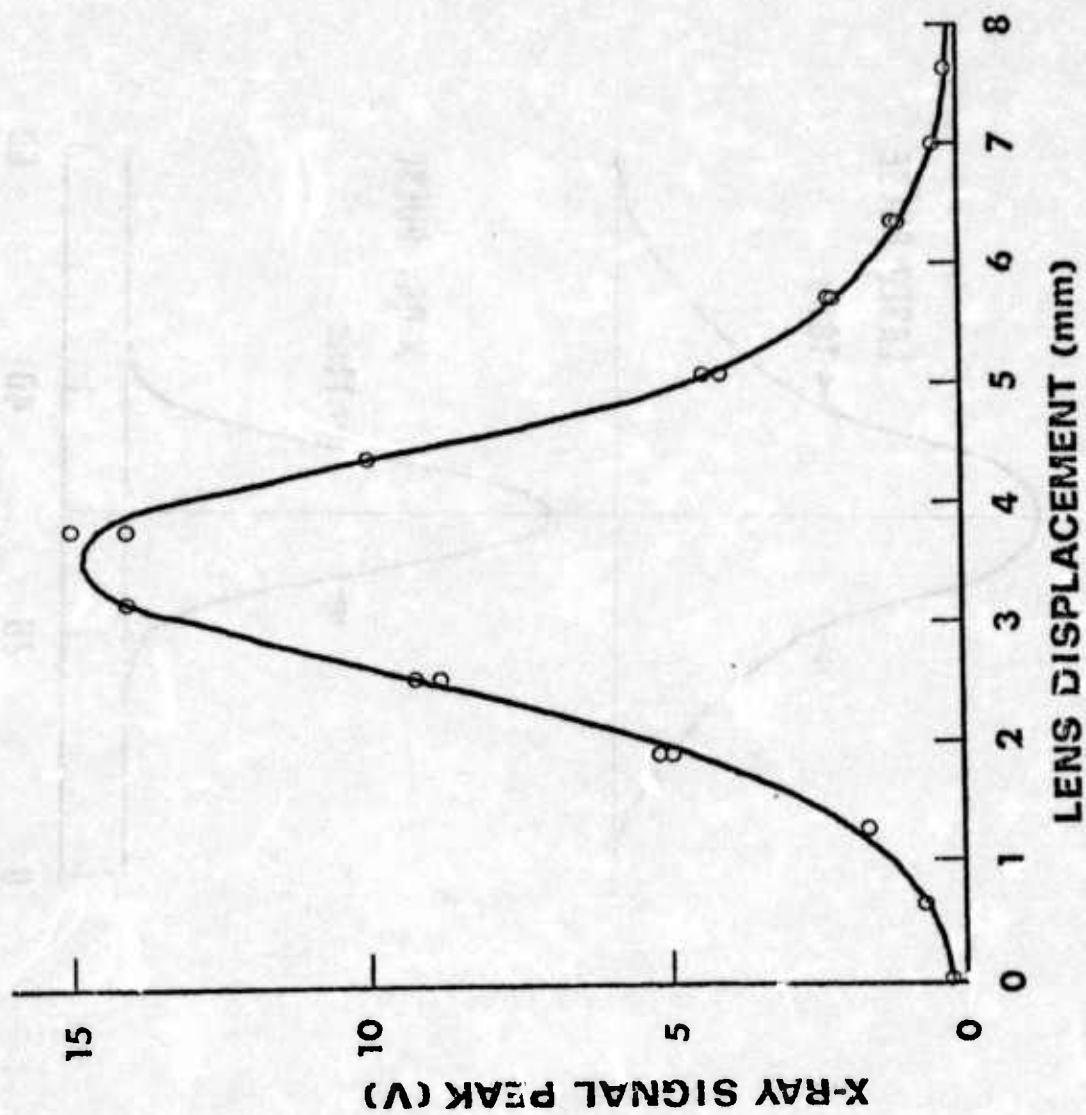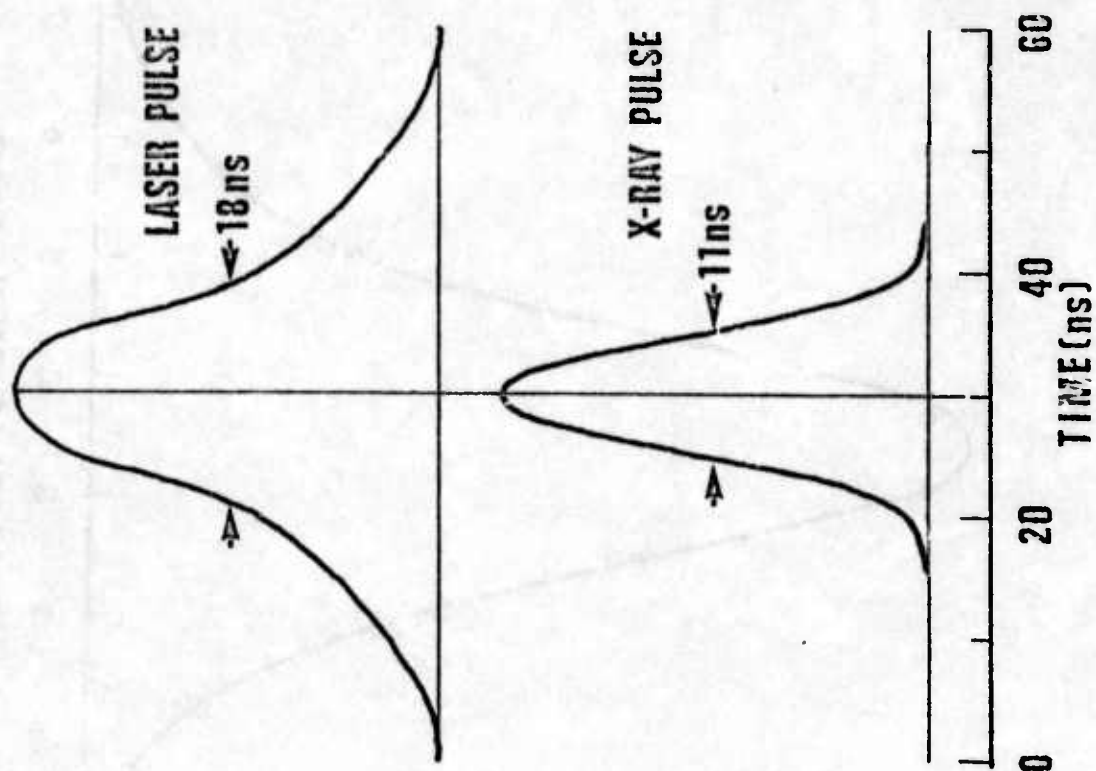
Mg. TARGET

X-RAY FILM

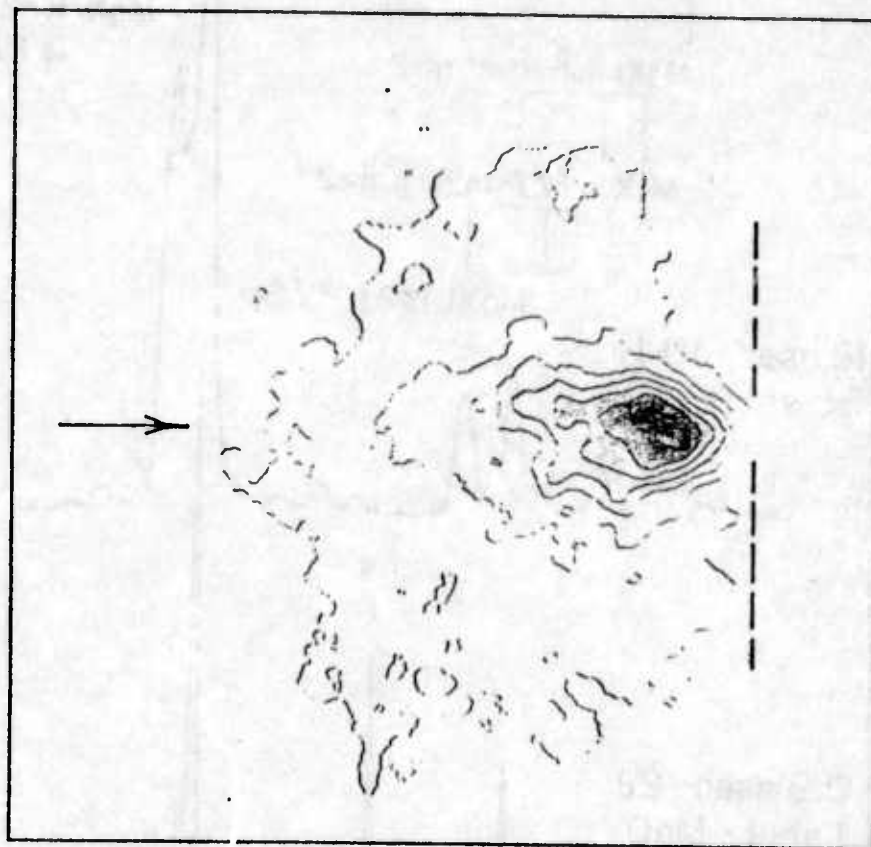RAP CRYSTAL

20 cm f.l. LENS

← adj. →

p-i-n X-RAY DETECTOR

500 MW, 18 ns FWHM RUBY LASER PULSE

Figure 1

A42

Figure 2

LASER PULSE
←18ns→

X-RAY PULSE
←11ns→

TIME [ns]

0   20   40   60

Figure 3

A44

Figure 4

Figure 5

Figure 6

A47

TWO PHOTON ENHANCED NEGATIVE NONLINEAR SUSCEPTIBILITY
OF CESIUM VAPOR AT 1.06μ[*]

R. H. Lehmberg, J. Reintjes, and R. C. Eckardt

Naval Research Laboratory
Washington, D. C.   20375

ABSTRACT

We outline a theory of the nonlinear susceptibility of Cs at 1.06μ, and present the first measurement of the negative nonlinear refractive index n_2 responsible for the self defocusing that is observed. For linearly polarized light, the theoretical value of n_2 is -1.93×10^{-30}N, in good agreement with our measured value of $-(1.4 \pm .2) \times 10^{-30}$N. The main portion comes from a two-photon resonance between the 6s and 7s levels. An additional negative term arises from induced population changes between 6s and 6p. By comparing the measured values of n_2 for linearly and circularly polarized light, we obtained the two photon contribution $n_{20} = -(1.2 \pm 0.2) \times 10^{-30}$N, in good agreement with the theoretical value of -1.55×10^{-30}N. In our experiments, where the (35 psec) pulses are shorter than the 6s-6p inverse linewidth, the nonlinear susceptibility depends primarily on the instantaneous intensity; however, with longer pulses, one obtains additional contributions proportional to time integrals over the intensity. Since the useful output power from large Nd laser systems is limited by self focusing due to the laser glass, our results suggest the possibility of increasing this power by using Cs vapor for compensation.

I. INTRODUCTION

In recent years, a number of authors have observed self-focusing,[1-3] self-defocusing,[4] and other nonlinear dispersive effects[5,6] due to the electronic nonlinear susceptibility in atomic vapors. These effects have been attributed to intensity dependent population changes associated with single-photon resonances in a two-level system. Recently, we reported the observation of self-defocusing of mode locked pulses at 1.06μ in cesium vapor,[7] and attributed it primarily to a two-photon resonance between the 6s and 7s levels. Since the useful output power from large Nd laser systems is ordinarily limited by self focusing in the laser glass, observation of self defocusing at 1.06μ raises the possibility of increasing this power by using Cs vapor for compensation.

In this paper, we outline a complete theory of the nonlinear dispersion, and present the first measurement of the negative nonlinear refractive index n_2 responsible for the self-defocusing. We show that, in general, the nonlinear change in refractive index $\delta n^{NL}(t)$ can be expressed as the sum of an instantaneous intensity dependent contribution, plus terms involving time-integrated intensities. For linearly polarized light at 1.06μ, the instantaneous portion arises primarily from the two photon resonance, while the integral terms arise entirely from redistribution of population in the first excited state. Under the conditions in our experiment, the instantaneous term is predominant, and the measurements are in good quantitative agreement with the two photon resonance interpretation.

A50

II. THEORY

The lowest order nonlinear refractive properties of an isotropic medium can be found from the polarization

$$P_z^{(3)}(t) = N \sum_{\alpha\beta} \mu_{\alpha\beta} \; \rho_{\alpha\beta}^{(3)}(t) \tag{1}$$

induced by the optical field

$$E_z(t) = \frac{1}{2} \mathcal{E}(\omega,t) \, e^{-i\omega t} + \frac{1}{2} \mathcal{E}(-\omega,t) \, e^{+i\omega t}. \tag{2}$$

Here, N is the atomic density, $\mu_{\beta\alpha} = e \, z_{\beta\alpha}$ are the atomic dipole matrix elements between states $|\alpha\rangle$ and $|\beta\rangle$, $\rho_{\alpha\beta}^{(3)}(t)$ are the corresponding third order density matrix elements, and $\mathcal{E}(\omega,t) = \left[\mathcal{E}(-\omega,t)\right]^*$ is the slowly varying optical field amplitude. The density matrix elements are obtained by solving the Boltzmann equations

$$\dot{\rho}^{(n)}(t) = -(i/\hbar)\left[H_0, \rho^{(n)}(t)\right] - (i/\hbar)\left[V(t), \rho^{(n-1)}(t)\right] + \left\{\dot{\rho}^{(n)}(t)\right\}_R, \tag{3}$$

for $n = 1, 2, 3$, subject to the condition $\rho_{00}^{(0)} = 1$. Here,

$$H_0 = \sum_{\alpha} \hbar\omega_{\alpha 0} \; |\alpha\rangle\langle\alpha|, \qquad V(t) = - \sum_{\alpha,\beta} E(t) \, \mu_{\alpha\beta} |\alpha\rangle\langle\beta|, \tag{4}$$

$|0\rangle$ is the ground state, $\hbar\omega_{\alpha 0}$ is the energy difference $\epsilon_\alpha - \epsilon_0$ between $|\alpha\rangle$ and $|0\rangle$, and $\left\{\dot{\rho}^{(n)}(t)\right\}_R$ describes the atomic relaxation. If we write $\rho_{\alpha\beta}^{(3)}(t)$ in terms of its slowly varying amplitudes $\sigma_{\alpha\beta}^{(3)}(\omega,t) = \left[\sigma_{\beta\alpha}^{(3)}(-\omega,t)\right]^*$,

$$\rho_{\alpha\beta}^{(3)}(t) = \frac{1}{2} \sigma_{\alpha\beta}^{(3)}(\omega,t) \, e^{-i\omega t} + \frac{1}{2} \sigma_{\alpha\beta}^{(3)}(-\omega,t) \, e^{+i\omega t} + \text{3rd harmonic terms}, \tag{5}$$

A51

then the nonlinear contribution to the refractive index is

$$\delta n^{NL}(t) = 2\pi\ N \sum_{\alpha,\beta}\ \mu_{\beta\alpha}\ \ \sigma^{(3)}_{\alpha\beta}(\omega,t)\big/ \mathcal{E}(\omega,t) \quad . \tag{6}$$

The number of matrix elements contributing to the solution of equations (3) can be reduced by examining the lower lying energy levels of Cs, shown in Fig. 1. Around 1.06 μ, $\delta n^{NL}(t)$ is determined almost entirely by the $|6s\rangle \equiv |0\rangle$, $|6p\rangle \equiv |1\rangle$ and $|7s\rangle \equiv |2\rangle$ levels. This is due partly to the nearby one and two photon resonances with 6p and 7s, respectively, (i.e., $\omega_{10} - \omega$, $|\omega_{20} - 2\omega| \ll \omega$) and partly to the large 6s – 6p and 6p – 7s oscillator strengths. To a good approximation, therefore, one can ignore all other levels and all nonresonant contributions to $\delta n^{NL}(t)$. We also make the following additional simplifications: (i) the LS splitting of the 6p level is ignored; (ii) all longitudinal relaxation processes, except for collision-induced transitions among the 6p sublevels are neglected; and (iii) the atomic and laser linewidths are neglected in comparison to the detuning frequencies $\omega_{10} - \omega$ and $|\omega_{20} - 2\omega|$. Assumption (i) is reasonable around 1.064 μ, where $(\omega_{10} - \omega)/2\pi c = 2149$ cm^{-1} and the L–S splitting is only 544 cm^{-1}. Assumption (ii) requires that either the pressure broadening be large in comparison to the radiative linewidth for the 6p levels, or the optical pulsewidth t_p be short in comparison to the radiative lifetime of 6p. Assumption (iii) is valid for $t_p \geq 10^{-13}$ sec and atomic densities $N \leq 10^{19}$ cm^{-3}.

The solution of Eqs. (3), (5) and (6) for linearly polarized light, which is outlined in the appendix, yields the result

$$\delta n^{NL}(t) = n_2 \langle E^2(t) \rangle - \Gamma_{10}\, n_{10} \int_{-\infty}^{t} \langle E^2(t') \rangle \, dt'$$

$$+ \gamma \int_{-\infty}^{t} e^{-(3/2)\Gamma'(t-t')} \langle E^2(t') \rangle \, dt'$$

$$- \tfrac{1}{2}\,\Gamma'\Gamma_{10}(n_{10} + n_{12}) \int_{-\infty}^{t} e^{-(3/2)\Gamma'(t-t')} dt' \int_{-\infty}^{t'} \langle E^2(t'') \rangle \, dt'', \qquad (7)$$

where $\langle\ \rangle$ denotes an average over an optical cycle [e.g., $\langle E^2(t) \rangle = \tfrac{1}{2}|\mathcal{E}(\omega,t)|^2$], Γ_{10} is the dephasing rate of the 6s – 6p transition, and Γ' is the collisional mixing rate of the 6p sublevels. The remaining parameters are given by expressions (A12) – (A14). At 1.06 μ, where nonresonant contributions are small, these are well approximated by

$$n_2 = n_{20} - n_{10} \quad , \qquad\qquad (8)$$

$$\gamma = -\,(\Gamma_{10} - \tfrac{1}{2}\Gamma')\,(n_{10} + n_{12}) \quad , \qquad\qquad (9)$$

where

$$n_{20} \equiv \frac{2\pi\, N\, \mu_{01}^2\, \mu_{12}^2}{\hbar^3\,(\omega_{10} - \omega)^2(\omega_{20} - 2\omega)} \quad , \qquad\qquad (10a)$$

$$n_{10} \equiv \frac{2\pi N\, \mu_{01}^4}{\hbar^3(\omega_{10} - \omega)^3} \; , \qquad n_{12} \equiv \frac{2\pi\, N\, \mu_{01}^2\, \mu_{12}^2}{\hbar^3(\omega_{10} - \omega)^2(\omega - \omega_{21})} \; . \quad (10\ b,\ c)$$

Expression (8), or its more general version (A12), has been derived by other authors for quasi cw conditions,[8] or for the special case where the atomic relaxation arises entirely from radiative processes[9] (i.e., where $\Gamma' = 0$ and Γ_{10} is half the radiative damping rate of 6p). Under these conditions

A53

the integral terms do not appear,[10] at least for processes up to third order. In the collision dominated regime, where Γ_{10} is large in comparison to radiative damping rates, the integral terms must, in general, be retained.

For circular polarization,

$$\vec{E}(t) = \tfrac{1}{2}\,\hat{r}_-\,\mathcal{E}(\omega,t)e^{-i\omega t} + \tfrac{1}{2}\,\hat{r}_+\,\mathcal{E}(-\omega,\,t)\,e^{i\omega t}, \tag{11}$$

where $\hat{r}_{\pm} \equiv 2^{-\frac{1}{2}}(\hat{x} \pm i\,\hat{y})$. Solution of Eqs. (3), (5) and (6) again gives Eq. (7), but expressions (8) and (9) are replaced by

$$n_2 = -\,n_{10} \tag{12}$$

$$\gamma = -\,(\Gamma_{10} - \tfrac{1}{2}\Gamma')\,n_{10} - (\tfrac{1}{2})\,\Gamma' n_{12} \quad . \tag{13}$$

The n_{20} term does not contribute in this case because the corresponding virtual transition $6s \rightarrow 6p \rightarrow 7s$ requires a zero net angular momentum transfer from the light to the atom, whereas two photons of circularly polarized light must transfer $\Delta J = \pm 2$.[11]

Numerical values of n_{20}, n_{10}, and n_{12} can be calculated using the 6s – 6p oscillator strength measured by Korff and Breit,[12] and the 6p – 7s oscillator strength calculated by Stone.[13] The matrix elements are (in atomic units) $\mu_{01} = 3.05$ and $u_{12} = 2.44$, and the results are $n_{20} = -1.55 \times 10^{-30} N$, $n_{10} = 0.29 \times 10^{-30} N$, and $n_{12} = 0.16 \times 10^{-30} N$ esu for $\lambda = 1.064\ \mu$.

The main term of interest here is the two photon contribution n_{20}, which arises primarily from the second order polarization $\rho_{20}^{(2)}(t)$.[14] At $1.06\ \mu$, terms such as n_{20} are positive in most substances, and are generally

A54

accepted as being responsible for the self focusing observed in materials such as laser glass.[15] In Cs vapor at 1.064 μ, however, n_{20} is large and negative due to the strong resonant enhancement by the two-photon denominator $(\omega_{20} - 2\omega)/2\pi c = -260$ cm^{-1}.

The n_{10} and n_{12} terms arise from pulse-induced population of 6p, which is weakly enhanced by the nearby single photon 6s-6p resonance $\left[(\omega_{10} - \omega)/2\pi c = 2149 \text{ cm}^{-1}\right]$ As Eq. (7) indicates, this can result in both instantaneous and time-integrated contributions to $\delta n^{NL}(t)$. The instantaneous portion is due to coherent population changes and can be obtained from the adiabatic following model proposed by Grischkowsky.[1] The integral terms are due to incoherent population changes, and can be significant if the pulse duration t_p is comparable to Γ_{10}^{-1}.

If $t_p \ll \Gamma_{10}^{-1}$, Γ^{-1}, the integral terms will be negligible, and Eq. (7) reduces to

$$\delta n^{NL}(t) = n_2 \langle E^2(t) \rangle \quad . \tag{14}$$

One can therefore measure n_{20} by measuring n_2 for linear and circular polarization, and using Eqs. (8) and (12); i.e.,

$$n_{20} = n_2(\text{linear}) - n_2(\text{circular}). \tag{15}$$

III. EXPERIMENT

In order to measure n_2, we studied the self-defocusing of mode locked Nd:YAG pulses in a 100 cm long cesium vapor cell at several densities between $N = 0.08 \times 10^{17}$ cm^{-3} and 0.32×10^{17} cm^{-3}. The density was controlled by adjusting the temperature of a cesium reservoir (260 - 305°C), while the main cell was held at 460°C in order to minimize linear absorption from Cs dimers. The input radiation consisted of single pulses of FWHM intensity

duration t_p = 35 psec (determined by measurements with a 5 psec resolution streak camera) with peak on-axis intensities around 6 GW/cm^2. The input beam, which was well collimated (radius of curvature R_o = 20 m), had the form of an Airy profile truncated at the first minimum.

The beam energy entering the cell was measured with a calorimeter and was monitored with a calibrated photodiode. Its 1/e intensity radius was a_o = 0.58 mm. Simultaneous energy measurements at the output end of the cell showed that insertion loss due to the Cs was < 5% for all of the data that was used in determining n_2. The energy profile at the output end was recorded by imaging the exit window onto a silicon photodiode array of 25 μ resolution. Figure 2a shows typical oscilloscope traces of these output profiles for the case N = .32 x 10^{17} cm^{-3}.

At low intensities, the beam profile was identical to that obtained with linear propagation in an empty cell. At intermediate intensities, the beam size increased, but its smooth characteristic shape was retained. At the highest intensities used, further increase in beam size was observed, accompanied by beam distortion and the appearance of ring structure near the axis. This behavior is similar to that observed in the self defocusing experiments of Grischkowsky and Armstrong.[4] All of the data that was used in determining n_2 was taken at the intermediate intensities where there was no beam distortion.

In analyzing the data, the output profile of the beam was calculated from a solution of the wave equation in the paraxial ray approximation.[16] Using Equation (14), along with a constant shape assumption, and approximating the shape of the input beam with a Gaussian distribution, we obtain for the intensity profile at the end of the cell

$$I(r,t) = \left[P(t)/\pi a^2(t)\right] \quad \exp\left[-r^2/a^2(t)\right] . \qquad (16)$$

Here $P(t)$ is the input beam power and $a(t)$ is a time dependent radius given by[16]

$$a^2(t) = a_o^2\left\{(1 + z/R_o)^2 + \left[1 - P(t)/P_c\right](\lambda z/2\pi a_o^2)^2\right\}, \qquad (17)$$

where z is the length of the Cs cell, a_o and R_o are the input radius and beam curvature, respectively, and $P_c \equiv \lambda^2 c/32\pi^2 n_2 < 0$. The energy profile was then obtained by numerically integrating expression (16) over the pulse duration. For each data point, measured values of a_o, R_o and $P(t)$ were used and the value of n_2 was chosen to give the best theoretical fit to the measured energy distribution at the half-maximum points. This procedure is justified by the good overall agreement between the calculated and experimental profiles, as illustrated by the examples shown in Fig. 2b.

IV. RESULTS

The results of our measurements for linearly and circularly polarized light are shown as a function of density in Fig. 3, and are compared with the theory in Table 1. The first column of Table 1 gives the experimental value of n_2/N obtained using Eq. (14), as described above. Column B gives an adjusted experimental value which approximately accounts for the effects of the integral terms in Eq. (7), as will be discussed later. Column C gives the theoretical values for n_2/N obtained from Eqs. (8) and (12) using the calculated values of n_{20} and n_{10}. The values shown in Column D are calculated from the exact expressions (A12 and A17). The good agreement between columns C and D justifies our earlier neglect of such terms. Finally, the last column gives the value of n_2/N obtained from the susceptibility calculations of Miles and Harris.[17]

The agreement between our theory and the measurements shown in column A appears quite adequate, especially since it compares an ab-initio calculation with an absolute measurement; however, the fact that $|n_2 \text{ (measured)}|$ < $|n_2 \text{ (theory)}|$ for linear polarization, whereas $|n_2 \text{ (measured)}|$ > $|n_2 \text{(theory)}|$ for circular polarization requires further comment. The discrepancy appears to stem from the integral terms of Eq. (7). In analyzing the data, we have effectively treated the integral terms as instantaneous, and lumped them into an effective contribution to the measured value of n_2. One can estimate the relative importance of these integral terms by averaging their contribution to $\delta n^{NL}(t)$ over the incident intensity, and comparing this to a similar average for the $n_2 \langle E^2(t) \rangle$ contribution; i.e., we consider the quantity

$$Q \equiv \int_{-\infty}^{\infty} \left[\delta n^{NL}(t) - n_2 \langle E^2(t) \rangle \right] \langle E^2(t) \rangle \, dt \bigg/ \int_{-\infty}^{\infty} n_2 \langle E^2(t) \rangle^2 \, dt, \qquad (18)$$

using Eq. (7). The corrected values of n_2 (measured) would then be approximately $(1 + Q)^{-1}$ times the numbers shown in column A of Table 1. For $N = 0.32 \times 10^{17} \text{cm}^{-3}$, the transverse relaxation time is $\Gamma_{10}^{-1} \approx 80$ psec.[18] Assuming that $\Gamma' \approx \Gamma_{10}$,[19] we then obtain Q(linear) ≈ 0.09 and Q(circular) ≈ 0.5. The integral terms therefore contribute little in the case of linear polarization, but they result in a significant correction for circular polarization because $|n_2|$ is relatively small. The corrected values of n_2, which are given in column B of Table 1, are approximately 20 - 25% smaller than the theoretical values. It is possible that a systematic error of this magnitude could arise from inaccuracy in the measurement of the atomic density or the pulse energy.

The experimental value of the two-photon term n_{20} can be found immediately from Eq.(15). From either column A or B of Table 1, we obtain $n_{20} \approx (1.2 \pm .2) \times 10^{-30}$ N esu, in good agreement with our calculated value of -1.55×10^{-30} N. The fact that this result is independent of the integral terms is not surprising,

since most of the integral contribution cancels in the expression n_2(linear) – n_2(circular).

V. REFERENCES

1. D. Grischkowsky, Phys. Rev. Lett. $\underline{24}$, 866 (1970).

2. S.A. Akhmanov, A.I. Kovrigin, S.A. Maksimov, and V.E. Ogluzdin, ZhETF Pis. Red. $\underline{15}$, 186 (1972) (JETP Lett. $\underline{15}$, 129 (1972)).

3. J.E. Bjorkholm and A. Ashkin, Phys. Rev. Lett. $\underline{32}$, 129 (1974).

4. D. Grischkowsky and J. A. Armstrong, Phys. Rev. A$\underline{6}$, 1566 (1972).

5. V.M. Arutyunyan, N.N. Badalyan, V.A. Iradyan, and M.E. Movsesyan, Zh. Eksp. Teor. Fiz. $\underline{58}$, 37 (1970) (JETP $\underline{31}$, 22 (1970)).

6. D. Grischkowsky, E. Courtens, and J.A. Armstrong, Phys. Rev. Lett. $\underline{31}$, 422 (1973).

7. R.H. Lehmberg, J. Reintjes, and R.C. Eckardt, Appl. Phys. Lett. $\underline{25}$, 374 (1974).

8. N. Bloembergen and Y.R. Shen, Phys. Rev. $\underline{133}$, A37 (1964).

9. B.J. Orr and J.F. Ward, Molec. Phys. $\underline{20}$, 513 (1971).

10. R.H. Lehmberg and J. Reintjes, Bull. Am. Phys. Soc. $\underline{20}$, 635 (1975); submitted to Phys. Rev. A

11. P.P. Bey and H. Rabin, Phys. Rev. $\underline{162}$, 794 (1967).

12. S.A. Korff and G. Breit, Rev. Mod. Phys. $\underline{4}$, 471 (1932).

13. P.M. Stone, Phys. Rev. $\underline{127}$, 1151 (1962).

14. The contribution due to $\rho^{(2)}_{(20)}(t)$ is $n_{20} + \frac{1}{2} n_{12} \approx -1.47 \times 10^{-30} \, N \approx n_{20}$.

15. J.T. Fournier and E. Snitzer, IEEE J. Quantum Electron. QE-10, 473 (1974).

16. S.A. Akhmanov, R.V. Khokhlov and A.P. Sukhorukov, in Laser Handbook, Vol. 2, edited by F.T. Arecchi and E.O. Schulz-Dubois (North-Holland, Amsterdam, 1972).

17. R.B. Miles and S.E. Harris, IEEE J. Quantum Electron. $\underline{QE-9}$, 470 (1973).

18. This was obtained by taking the weighted average of the $6p\ ^2P_{1/2}$ and $6p\ ^2P_{3/2}$ linewidths measured by C.L. Chen and A.V. Phelps, Phys. Rev. $\underline{173}$, 62 (1968).

19. P.R. Berman and W.E. Lamb, Jr., Phys. Rev. $\underline{187}$, 221 (1969); C.G   rington, D.N. Stacey, and J. Cooper, J. Phys. B $\underline{6}$, 417 (1973).

20. M.D. Crisp, Phys. Rev. A $\underline{8}$, 2128 (73).

To obtain the solution of Eqs (3), we use the harmonic expansions of $\rho_{\alpha\beta}^{(n)}(t)$, as in Eq. (5); i.e.,

$$\rho_{\alpha\beta}^{(3)}(t) = \tfrac{1}{2}\sigma_{\alpha\beta}^{(3)}(\omega,t)\, e^{-i\omega t} + \tfrac{1}{2}\sigma_{\alpha\beta}^{(3)}(-\omega,t)\, e^{i\omega t}$$

$$+ \text{ third harmonic terms,} \qquad\qquad \text{(A1a)}$$

$$\rho_{\alpha\beta}^{(2)}(t) = \sigma_{\alpha\beta}^{(2)}(0,t) + \tfrac{1}{2}\sigma_{\alpha\beta}^{(2)}(2\omega,y)\, e^{-2i\omega t} + \tfrac{1}{2}\sigma_{\alpha\beta}^{(2)}(-2\omega,t)e^{2i\omega t}, \quad \text{(A1b)}$$

$$\rho_{\alpha\beta}^{(1)}(t) = \tfrac{1}{2}\sigma_{\alpha\beta}^{(1)}(\omega,t)\, e^{-i\omega t} + \tfrac{1}{2}\sigma_{\alpha\beta}^{(1)}(-\omega,t)\, e^{i\omega t}, \qquad\qquad \text{(A1c)}$$

where α and β refer to states $|0\rangle$, $|1\rangle$ or $|2\rangle$, and the amplitudes $\sigma_{\alpha\beta}^{(n)}(n'\omega,t) = \left[\sigma_{\beta\alpha}^{(n)}(-n'\omega,t)\right]^{*}$ will vary in times on the order of the pulse-width t_p. Substituting Eqs (A1) into (3) [and dropping the time label for brevity], one obtains

$$\dot{\sigma}_{\alpha\beta}^{(3)}(\omega) + [i(\omega_{\alpha\beta} - \omega) + \Gamma_{\alpha\beta}]\, \sigma_{\alpha\beta}^{(3)}(\omega)$$
$$= 2i\,\mathcal{E}(\omega)\, s_{\alpha\beta}^{(2)}(0) + i\,\mathcal{E}(-\omega)\, s_{\alpha\beta}^{(2)}(2\omega), \qquad\qquad \text{(A2a)}$$

$$\dot{\sigma}_{\alpha\beta}^{(2)}(0) + (i\omega_{\alpha\beta} + \Gamma_{\alpha\beta})\, \sigma_{\alpha\beta}^{(2)}(0)$$
$$= \tfrac{1}{2} i\,\mathcal{E}(\omega)\, s_{\alpha\beta}^{(1)}(-\omega) + \tfrac{1}{2}i\,\mathcal{E}(-\omega)\, s_{\alpha\beta}^{(1)}(\omega) + \delta_{\alpha\beta} \sum_{\gamma}{}' W_{\gamma}\, \sigma_{\gamma\gamma}^{(2)}(0), \quad \text{(A2b)}$$

$$\dot{\sigma}_{\alpha\beta}^{(2)}(2\omega) + [i(\omega_{\alpha\beta} - 2\omega) + \Gamma_{\alpha\beta}]\, \sigma_{\alpha\beta}^{(2)}(2\omega) = i\,\mathcal{E}(\omega)\, s_{\alpha\beta}^{(1)}(\omega), \qquad \text{(A2c)}$$

$$\dot{\sigma}_{\alpha\beta}^{(1)}(\omega) + [i(\omega_{\alpha\beta} - \omega) + \Gamma_{\alpha\beta}]\, \sigma_{\alpha\beta}^{(1)}(\omega) = (i/\hbar)\,\mathcal{E}(\omega)\, \mu_{\alpha\beta}\, (\delta_{\beta 0} - \delta_{\alpha 0}), \quad \text{(A2d)}$$

where

$$s_{\alpha\beta}^{(n)}(n'\omega) \equiv (1/2\,h) \sum_{\gamma} \left[\mu_{\alpha\gamma}\, \sigma_{\gamma\beta}^{(n)}(n'\,\omega) - \sigma_{\alpha\gamma}^{(n)}(n'\,\omega)\, \mu_{\gamma\beta} \right], \qquad (A3)$$

$\Gamma_{\alpha\beta} = \Gamma_{\beta\alpha}$ is the relaxation rate of $\rho_{\alpha\beta}(t)$, and W_{γ} describes collisional mixing of states such as the 6p sublevels. It is evident from these equations that the nonresonant contributions could be eliminated at the outset simply by dropping all terms except $\sigma_{10}^{(3)}(\omega)$, $\sigma_{21}^{(3)}(\omega)$, $\sigma_{\alpha\alpha}^{(2)}(0)$, $\sigma_{20}^{(2)}(2\omega)$, and $\sigma_{10}^{(1)}(\omega)$. In this treatment, however, we will retain the nonresonant terms and present the complete expressions for the coefficients of $\delta n(t)$ in order to assess the accuracy of Expression (10).

For all cases except the zero frequency diagonal terms, $\dot\sigma_{\alpha\alpha}^{(2)}(0)$, Eqs. (A2) have the general form

$$\dot\sigma(t) + (i\,\Omega + \Gamma)\,\sigma(t) = R(t) \quad , \qquad |\Omega| \gg \Gamma, \qquad (A4)$$

with the formal solution for $\sigma(-\infty) = R(-\infty) = 0$ [20],

$$\sigma(t) = \int_{-\infty}^{t} dt'\, e^{-(i\Omega + \Gamma)(t-t')}\, R(t')$$

$$= -\sum_{m=0}^{\infty} \left(\frac{-1}{i\,\Omega + \Gamma} \right)^{m+1} \frac{d^n R(t)}{dt^n} \quad . \qquad (A5)$$

For example, (A2d) yields the result

$$\sigma_{\alpha\beta}^{(1)}(\omega,t) = -(i/h)\,\mu_{\alpha\beta}\,(\delta_{\beta o} - \delta_{\alpha o}) \sum_{m=0}^{\infty} \left[\frac{-1}{i(\omega_{\alpha\beta} - \omega) + \Gamma_{\alpha\beta}} \right]^{m+1} \frac{\partial^m \mathcal{E}(\omega,t)}{\partial t^m} \quad . \qquad (A6)$$

A62

Since Ω represents $\omega_{\alpha\beta}$, ω, $\omega_{\alpha\beta} \pm \omega$, or $\omega_{\alpha\beta} \pm 2\omega$, and $\left| (1/R) \, dR/dt \right|$ will be on the order of the laser linewidth, postulate (iii) of Sec. II leads to the condition $\left| (1/R) \, dR/dt \right| \ll \left| \Omega \right|$. Therefore, only the lowest order terms of Eq. (A5) must be kept, and in most cases, only the zero order term will be needed. According to postulate (iii) this can be further simplified by dropping Γ in comparison to $i\,\Omega$. The resulting expressions

$$\sigma_{\alpha\beta}^{(3)} (\omega,t) = \frac{2\,\mathcal{E}(\omega,t) \, s_{\alpha\beta}^{(2)} (0,t) + \mathcal{E}(-\omega,t) \, s_{\alpha\beta}^{(2)} (2\omega,t)}{\omega_{\alpha\beta} - \omega} \tag{A7a}$$

$$\sigma_{\alpha\beta}^{(2)} (0,t) = \frac{\mathcal{E}(\omega,t) s_{\alpha\beta}^{(1)} (-\omega,t) + \mathcal{E}(-\omega,t) \, s_{\alpha\beta}^{(1)} (\omega,t)}{2\,\omega_{\alpha\beta}} \;, \quad (\omega_{\alpha\beta} \neq 0), \tag{A7b}$$

$$\sigma_{\alpha\beta}^{(2)} (2\omega,t) = \frac{\mathcal{E}(\omega,t) \, s_{\alpha\beta}^{(1)} (\omega,t)}{\omega_{\alpha\beta} - 2\omega} \;, \tag{A7c}$$

are identical to the usual cw solutions.

The solution of the zero frequency diagonal equations $\dot{\sigma}_{\alpha\alpha}(0,t)$ requires somewhat greater care. Following the postulates of Sec. II, we consider only the ground state $|0\rangle = |6s\rangle$ and the magnetic sublevels of 6p, which are denoted by $|6p_{+1}\rangle \equiv |a\rangle$, $|6p_0\rangle \equiv |b\rangle$ and $|6p_{-1}\rangle \equiv |c\rangle$. For linearly polarized light, the state labelled $|1\rangle$ corresponds to $|b\rangle$, which is the only sublevel radiatively coupled to $|0\rangle$. Equations (A2b) and A3) then lead to the results

A63

$$\dot{N}_o = - (i/4\hbar) \, \mu_{01} \, \mathcal{E}(\omega) \left[\sigma_{01}^{(1)} (-\omega) - \sigma_{10}^{(1)}(-\omega) \right] - c.c., \tag{A8a}$$

$$\dot{N}_b = \Gamma' \, (\tfrac{1}{2} N_a + \tfrac{1}{2} N_c - N_b) - \dot{N}_o , \tag{A8b}$$

where $N_\alpha = \sigma_{\alpha\alpha}^{(2)} (0)$, and Γ' is the collisional mixing rate of the 6p sublevels.
The terms $N_a + N_c$ can be eliminated from (A8b) by using the identity
$N_a + N_b + N_c + N_o = 0$, which follows from the assumption that no other levels are
occupied to second order. Then

$$\dot{N}_b = - \frac{3}{2} \Gamma' \, N_b - \tfrac{1}{2} \Gamma' \, N_o - \dot{N}_o . \tag{A9}$$

The right hand side of (A8a) can be evaluated by substituting the expansion
(A6) for $\sigma_{01}^{(1)} (-\omega)$ and $\sigma_{10}^{(1)}(-\omega)$. The formal solution represented by equation (A6)
constitutes an expansion in time derivatives of the optical field, as has been
pointed out by Crisp.[20] According to postulate (iii), the zero order term of
(A6) is always much larger than the remaining terms; and thus the solutions
(A7a-c) give results to order zero in the time derivative expansion. When terms
involve the diagonal matrix elements at zero frequency, however, cancellations
occur in combining the contributions with their complex conjugates, leaving
integral expressions that are of lower order in the time derivative expansion.
Consequently, in evaluating such quantities, the first order term in (A6) must
be kept to insure retention of all terms of order zero in the time derivative
expansion. Equation (A8a) then becomes

$$\dot{N}_o = - \frac{\mu_{01}^2 \, (\omega_{10}^2 + \omega^2)}{2\hbar^2 (\omega_{10}^2 - \omega^2)^2} \left[2\Gamma_{10} \, |\mathcal{E}(\omega)|^2 + d \, |\mathcal{E}(\omega)|^2 / dt \right] , \tag{A10}$$

where we have again neglected Γ_{10} in comparison to $\omega_{10} \pm \omega$.

The solutions of (A9) and (A10) are then

$$\sigma_{00}^{(2)}(0,t) = N_0(t) = - \frac{\mu_{01}^2 (\omega_{10}^2 + \omega^2)}{2\hbar^2 (\omega_{10}^2 - \omega^2)^2}$$

$$\times \left[|\mathcal{E}(\omega,t)|^2 + 2\Gamma_{10} \int_{-\infty}^{t} |\mathcal{E}(\omega,t')|^2 dt' \right] \tag{A11a}$$

$$\sigma_{11}^{(2)}(0,t) = N_b(t) = \frac{\mu_{01}^2 (\omega_{10}^2 + \omega^2)}{2\hbar^2 (\omega_{10}^2 - \omega^2)^2}$$

$$\times \left[|\mathcal{E}(\omega,t)|^2 + (2\Gamma_{10} - \Gamma') \int_{-\infty}^{t} e^{-(3/2)\Gamma'(t-t')} |\mathcal{E}(\omega,t')|^2 dt' \right.$$

$$\left. + \Gamma' \Gamma_{10} \int_{-\infty}^{t} e^{-(3/2)\Gamma'(t-t')} dt' \int_{-\infty}^{t'} |\mathcal{E}(\omega,t'')|^2 dt'' \right] . \tag{A11b}$$

Combining Eqs (6), (A11), (A7) and the zero order term of (A6), one obtains Eq. (7) after some rather tedious algebra. The complete coefficients are

$$n_2 \equiv \frac{2\pi N \mu_{01}^2 \mu_{12}^2}{\hbar^3} \left[\frac{1}{(\omega_{10} - \omega)^2 (\omega_{20} - 2\omega)} + \frac{1}{(\omega_{10} + \omega)^2 (\omega_{20} + 2\omega)} \right.$$

$$\left. + \frac{4\omega_{10}^2}{\omega_{20}(\omega_{10}^2 - \omega^2)^2} \right] - \frac{4\pi N \mu_{01}^4 (3\omega_{10}^2 + \omega^2) \omega_{10}}{\hbar^3 (\omega_{10}^2 - \omega^2)^3} , \tag{A12}$$

$$\gamma = - (\Gamma_{10} - \tfrac{1}{2}\Gamma')(n_{10} + n_{12}), \tag{A13}$$

$$n_{10} \equiv \frac{8\pi N \mu_{01}^4 (\omega_{10}^2 + \omega^2)\omega_{10}}{\hbar^3 (\omega_{10}^2 - \omega^2)^3} , \quad n_{12} \equiv \frac{8\pi N \mu_{01}^2 \mu_{12}^2 (\omega_{10}^2 + \omega^2) \omega_{21}}{\hbar^3 (\omega_{10}^2 - \omega^2)^2 (\omega^2 - \omega_{21}^2)} . \tag{A14}$$

At 1.06μ, where $\omega_{10} - \omega$, $\omega - \omega_{21}$ and $\omega_{20} - 2\omega$ are small in comparison to

A65

ω_{10} ~ ~, $\omega + \omega_{21}$ and ω_{20}, expressions (A13) and (A14) are well approximated by Eqs (8) and (10).

In the case of a circularly polarized field [Eq. (11)], one can derive the nonlinear refractive properties from arguments similar to those given above if Eq. (6) is replaced by

$$\delta n^{NL}(t) = 2\pi N \sum_{\alpha\beta} \mu^-_{\beta\alpha} \sigma^{(3)}_{\alpha\beta}(\omega,t)/\mathcal{E}(\omega,t) \quad , \tag{A15}$$

and the interaction portion of (4) is replaced by

$$V(t) = - \sum_{\alpha\beta} \mu^+_{\alpha\beta} |\alpha\rangle\langle\beta| \; \tfrac{1}{2}\mathcal{E}(\omega,t) \; e^{-i\omega t} - c.\,c., \tag{A16}$$

where $\mu^{\pm}_{\beta\alpha} \equiv 2^{-\frac{1}{2}} (ex \pm iey)_{\beta\alpha}$. For $\gamma \equiv 0$ or 2, the only nonvanishing matrix elements are $\mu^+_{a\gamma} = (\mu^-_{\gamma a})^*$ and $\mu^+_{\gamma c} = (\mu^-_{c\gamma})^*$, and these have the absolute values $|\mu^+_{a\gamma}| = |\mu^+_{\gamma c}| = \mu_{\gamma 1} = \mu_{1\gamma}$. These considerations again lead to Eq. (7), with the coefficients

$$n_2 = - \frac{2\pi N \mu^4_{01} (3\,\omega^2_{10} + 5\,\omega^2)\,\omega_{10}}{h^3 (\omega^2_{10} - \omega^2)^3}$$

$$+ \frac{2\pi N \mu^2_{01} \mu^2_{12}}{h^3 \omega_{20}(\omega^2_{10} - \omega^2)} \left[\frac{3\omega^2_{10} + \omega^2}{\omega^2_{10} - \omega^2} + \frac{\omega_{10}\,\omega_{21} + \omega^2}{\omega^2 - \omega^2_{21}} \right] \quad , \tag{A17}$$

$$\gamma = - \frac{\pi N \mu^4_{01} [\Gamma_{10} (4\omega^2_{10} + 12\omega^2) - \Gamma' (\omega^2_{10} + 7\,\omega^2)]\,\omega_{10}}{h^3 (\omega^2_{10} - \omega^2)^3}$$

$$-\frac{\pi N \mu_{01}^2 \mu_{12}^2 \left[(4\Gamma_{10} - \Gamma')(\omega_{10}^2 + \omega^2) \omega_{21} - (4\Gamma_{10} - 3\Gamma') 2\omega^2 \omega_{10} \right]}{h^3 (\omega_{10}^2 - \omega^2)^2 (\omega^2 - \omega_{21}^2)} \qquad \text{(A18)}$$

and expressions (A14). In the near-resonant approximation, these results reduce to Eqs (12), (13), and (10).

FIGURE CAPTIONS

FIGURE 1   Energy level diagram of Cs, showing the three levels $|6s\rangle = |0\rangle$, $|6p\rangle = |1\rangle$ and $|7s\rangle = |2\rangle$ primarily responsible for self defocusing at 1.064 µ. The dotted lines show the position of the laser fundamental at 1.064 µ and its two-photon level at .532 µ.

FIGURE 2   Spatial profiles of the pulse at the exit window of the Cs cell.

        a. Oscilloscope traces of photodiode array measurement at low, intermediate, and high intensity.

        b. Comparison between theoretical profiles (solid lines) and measured profiles (dotted lines) at intermediate pulse energies.

FIGURE 3   Effective nonlinear refractive index n_2 vs. atomic density N for linearly and circularly polarized light at 1.064 µ.

TABLE 1

$$\frac{n_2}{N} \times 10^{30} \text{ (esu)}$$

	EXPERIMENTAL		THEORETICAL		MILES & HARRIS
	(A)	(B)	(C)	(D)	(E)
↑	−1.5 ± 0.02	−1.4 ± 0.2	−1.84	−1.93	−0.66
↻	−0.35 ± 0.04	−0.23 ± 0.03	−0.29	−0.28	

(A) Experimental values obtained from analysis of data that ignores the integral terms of Equation (7).

(B) Experimental values including an adjustment to approximately account for the integral terms.

(C) Theoretical calculation using resonant approximation [Eqs. (8), (10) and (12)].

(D) Theoretical calculation including antiresonant terms. [Eqs. (A12) and (A17)].
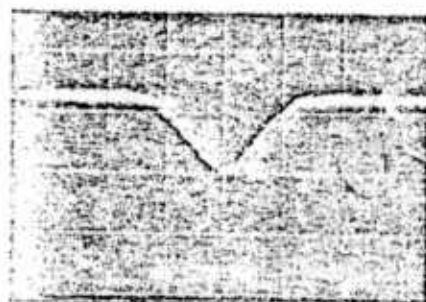
(E) Theoretical calculation of Ref. 17.
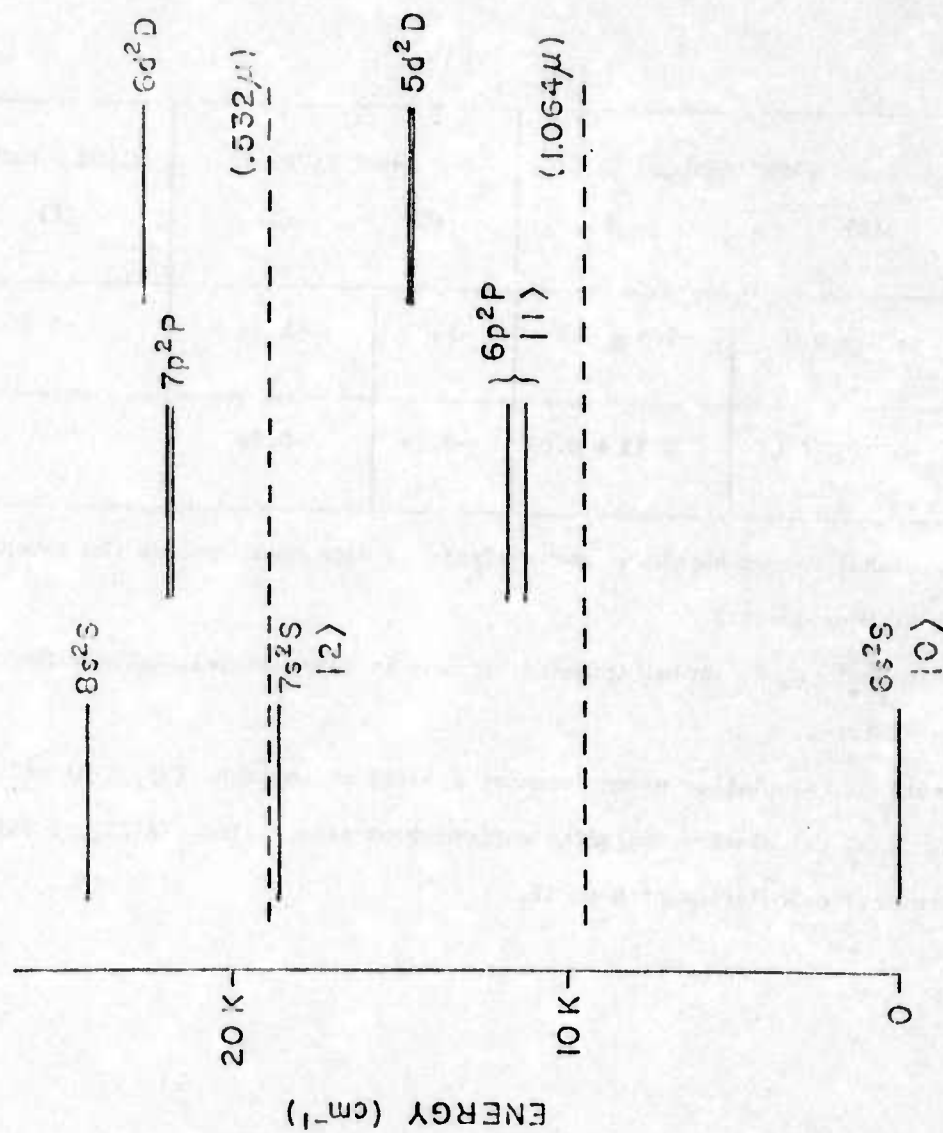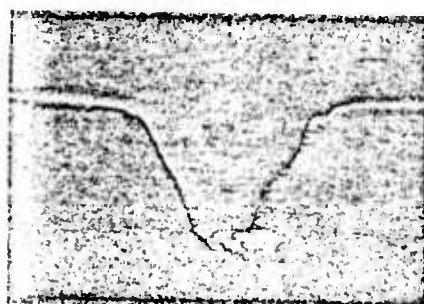
Figure 1

ENERGY (cm^{-1})
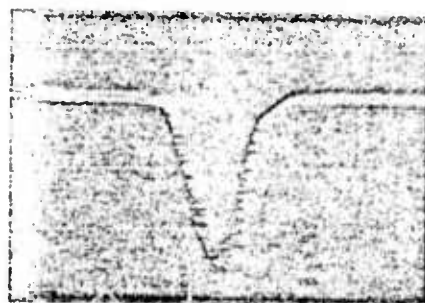
(a)
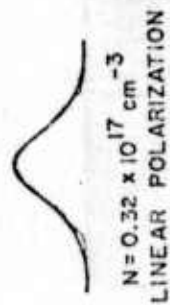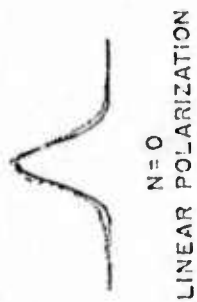$0.027 \times 10^{10} \, W/cm^2$

(b)
$0.64 \times 10^{10} \, W/cm^2$

(c)
$1.9 \times 10^{10} \, W/cm^2$

|←—5mm—→|

MEASURED BEAM PROFILE
AT OUTPUT WINDOW OF CELL

Figure 2a

BEAM PROFILES
AT OUTPUT WINDOW OF CELL

Figure 2b

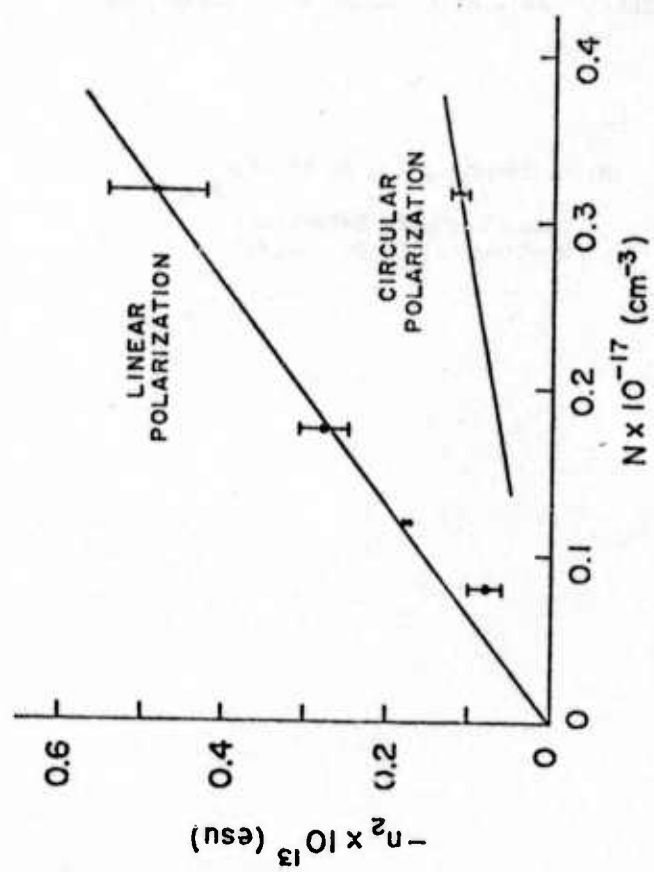Figure 3

GENERALIZED ADIABATIC FOLLOWING APPROXIMATION

by

R. H. Lehmberg and J. Reintjes

Naval Research Laboratory
Washington, D. C.   20375

A 74

ABSTRACT

The response of a two-level atom to a smoothly varying near-resonant driving pulse can be described by the usual adiabatic following approximation if the conditions T_1^{-1}, $T_2^{-1} \ll t_p^{-1} \ll \Omega(t)/2\pi$ are satisfied throughout the pulse. Here, $\Omega(t) = [\Delta^2(t) + p^2 \mathcal{E}^2(t)/\hbar^2]^{\frac{1}{2}}$ is the atomic precession frequency, $\Delta(t)$ the detuning, $\mathcal{E}(t)$ the field envelope, t_p the effective pulsewidth, and T_1, T_2 the atomic level and phase relaxation times. From Bloch's equations, we have developed a generalized version of this approximation applicable to cases where T_1 and T_2 can be comparable to or less than t_p. It allows the condition T_1^{-1}, $T_2^{-1} \ll t_p^{-1}$ to be replaced by the weaker requirement T_1^{-1}, $T_2^{-1} \, p^2 \mathcal{E}^2(t)/\hbar^2 \Omega^2(t) \ll \Omega(t)$. If $T_1 \gg t_p$, the atomic Bloch vector remains aligned nearly parallel to the effective driving field $(\mathcal{E}(t), 0, \hbar\Delta(t)/p)$ in the rotating reference frame (as in the pure adiabatic following case); however, it decays in length if T_2 is comparable to t_p. The approximation bridges the gap between pure adiabatic following behavior for $t_p^{-1} \gg T_1^{-1}$, T_2^{-1} and rate equation behavior for $t_p^{-1} \ll T_2^{-1} \approx \Omega(t)$, thereby allowing a more complete description of phenomena such as adiabatic inversion and resonantly enhanced self focusing and defocusing.

A75

I.   INTRODUCTION

In recent years, there has been a considerable interest in phenomena arising from the nonlinear interaction between short light pulses and near-resonant two level atoms.[1-11] Such phenomena include resonantly enhanced self focusing and defocusing,[1-5] spectral broadening due to self phase modulation,[6] optical shock formation,[7] and atomic population inversion due to adiabatic[8-10] or nearly adiabatic[11] rapid passage. Under suitable conditions many near-resonant effects can be described quite simply within the framework of the vector model of the atom by applying the adiabatic following (AF) approximation[1,2,12,13] to the Bloch equations. In this approximation, the atomic Bloch vector remains aligned nearly parallel to an effective driving field that is the vector sum of the optical field $E(t)$ and a fictitious field proportional to the detuning Δ. The conditions required for its validity are (i) the effective driving field must change direction slowly in comparison to the precession rate of the Bloch vector, and (ii) the atomic population and phase relaxation times T_1, T_2 must be long in comparison to the pulsewidth t_p.

Crisp[13] has shown that the near-resonant behavior of a two level atom can be expressed in terms of a series in inverse powers of Δ. The adiabatic following approximation is then equivalent to retaining only the first two terms of this series. In his actual derivation of the AF approximation, Crisp neglected atomic relaxation entirely. He also assumed that $|\Delta|$ remains large and constant, thereby excluding the condition encountered in adiabatic passage experiments,[8-10] where a chirped pulse can sweep through the resonance and still maintain a large precession frequency.

A76

In this paper, we derive a generalized adiabatic following (GAF) approximation that includes the effects of atomic relaxation, and is applicable even if T_1 and T_2 are comparable to or shorter than t_p. Moreover, it is applicable to adiabatic passage experiments as well as to those in which Δ remains large throughout the pulse. It reduces to the adiabatic following result for T_1, $T_2 \gg t_p$, and to ordinary rate equations when $T_2 \ll t_p$ and the optical field remains small. If $T_1 \gg t_p$, but $T_2 \approx t_p$, the atomic response can be described physically in terms of a Bloch vector that remains nearly parallel to the effective driving field (as in the adiabatic following case), but decays in length while the pulse is present. For the case of an unchirped pulse, this means that the atom will not return to its initial state immediately after the interaction has ceased; similarly for a chirped pulse is an adiabatic passage experiment, the atom will undergo only a partial population inversion. With the theory presented here, one can easily calculate this partial inversion without solving the complete Bloch equations.

The GAF approximation enables one to generalize many of the earlier calculations on the near-resonant third order susceptibility. For either of the extreme cases, T_1, $T_2 \gg t_p$ or T_1, $T_2 \ll t_p$, the nonlinear refractive index is purely intensity - dependent;[1,2,4] however, in general, the GAF approximation introduces additional terms that are proportional to the time-integrated intensity.[14] One interesting exception to this occurs in the case where the relaxation is due only to spontaneous emission ($T_2 = 2T_1$). Under these conditions we show that Grischkowsky's[1,2] lowest order nonlinear susceptibility remains valid even if $t_p \gg T_2$.

The paper is divided into five sections. Section II presents the Bloch-Maxwell equations describing the atom-field interaction, and reviews the ordinary adiabatic following approximation. In Section III, we derive the CAF approximation, and discuss the special cases mentioned in the preceding paragraphs. Section IV addresses the question of stability of the CAF approximation in response to a perturbation, such as a small but rapid change that may occur in a limited region of the pulse. In Section V, we compare our results to the numerical solutions of Bloch's equations under a variety of conditions, and relate these results to the theory presented in Sections III and IV.

II. VECTOR MODEL

Consider the interaction between an intense optical pulse $E(t,z)$ and an atom with energy levels $|a\rangle$ and $|b\rangle$ corresponding to a transition frequency $\omega_{ab} = h^{-1}(\epsilon_a - \epsilon_b)$. For a linear polarization, we write

$$E(t,z) = \mathcal{E}(t,z) \cos \psi(t,z) \quad , \tag{1}$$

where $\mathcal{E}(t,z)$ is the field envelope,

$$\psi(t,z) \equiv \omega_o t - k_o z + \varphi(t,z) \quad , \tag{2}$$

ω_o is the nominal optical carrier frequency, $k_o \equiv \omega_o/c$, and $\varphi(t,z)$ is a phase factor that will describe the frequency modulation of the pulse. We will assume that $\mathcal{E}(t,z)$ and $\varphi(t,z)$ remain slowly-varying in comparison to the optical frequency oscillation; i.e.,

A78

$$\left| \partial \mathcal{E}/\partial t \right| \ll \omega_o \left| \mathcal{E} \right| \quad , \qquad \left| \partial \omega/\partial t \right| \ll \omega_o \tag{3a}$$

$$\left| \partial \mathcal{E}/\partial z \right| \ll k_o \left| \mathcal{E} \right| \quad , \qquad \left| \partial \omega/\partial z \right| \ll k_o \tag{3b}$$

The instantaneous carrier frequency

$$\omega(t,z) = \partial \psi/\partial t = \omega_o + \partial \omega/\partial t \tag{4}$$

is therefore well defined, and remains close to ω_o. We also assume that the pulse remains in near resonance with the atom; i.e., the detuning

$$\Delta(t,z) \equiv \omega_{ab} - \omega(t,z) \tag{5}$$

satisfies the criterion $\left| \Delta \right| \ll \omega_{ab}$.

Expression (1) can be regarded as a linear superposition of two counterrotating circularly polarized waves of frequency $\omega(t,z)$. The response of an atom at point z can be conveniently described by writing the Schroedinger equation for the density matrix elements $\rho_{\alpha\beta}(t,z)$ in a reference frame $\hat{e}_1$, $\hat{e}_2$, $\hat{e}_3$ rotating with one of these components. The other component will introduce only a small second harmonic contribution that can be ignored if $\left| \Delta \right| \ll \omega_{ab}$. Using Crisps notation[13,15]

$$X(t,z) \equiv \rho_{ab}(t,z) + \rho_{ba}(t,z) \quad , \quad Y(t,z) \equiv i\left[\rho_{ab}(t,z) - \rho_{ba}(t,z) \right], \tag{6a,b}$$

$$Z(t,z) \equiv \rho_{aa}(t,z) - \rho_{bb}(t,z) \quad , \tag{6c}$$

and adding the usual population and phase relaxation rates $\Gamma_1 = 1/T_1$ and $\Gamma_2 = 1/T_2$, respectively, one then obtains the Bloch equations[13,15]

A79

$$\partial X / \partial t = -\Gamma_2 X - \Delta Y \tag{7a}$$

$$\partial Y / \partial t = \Delta X - \Gamma_2 Y + \omega_1 Z \tag{7b}$$

$$\partial Z / \partial t = -\omega_1 Y - \Gamma_1 (Z + 1) \ . \tag{7c}$$

Here,

$$\omega_1(t,z) = p \, \mathcal{E}(t,z) / \hbar \ , \tag{8}$$

and p is the dipole matrix element between states $|a\rangle$ and $|b\rangle$. In deriving (7c), we have also assumed that $\rho_{aa} + \rho_{bb} = 1$.

The quantities X and Y represent the polarization components in the rotating frame that are, respectively, in phase and in quadrature with the optical field. The total polarization in the laboratory frame is thus given by[15]

$$P(t,z) = \mathcal{P}_1(t,z) \cos \psi(t,z) - \mathcal{P}_2(t,z) \sin \psi(t,z), \tag{9}$$

where

$$\mathcal{P}_1(t,z) \equiv Np \ X(t,z) \quad , \quad \mathcal{P}_2(t,x) \equiv Np \ Y(t,z) \ . \tag{10a,b}$$

The dispersive properties of the medium are described by $\mathcal{P}_1$, while the losses are described by $\mathcal{P}_2$. As an example, one can write the refractive index as

$$n(t,z) = 1 + 2\pi \, \mathcal{P}_1(t,z) / \mathcal{E}(t,z). \tag{11}$$

In calculating the local response of the atom to the optical field, the z coordinate label is not needed, and will be dropped in the subsequent discussion.

If $\Gamma_1 = \Gamma_2 = 0$, then Eqs (7) describe a Bloch vector $\vec{R}(t) = \hat{e}_1 X(t) + \hat{e}_2 Y(t) + \hat{e}_3 Z(t)$ precessing around an effective driving field $\hat{e}_1 \mathcal{E}(t) - \hat{e}_3 \hbar\Delta(t)/p$ in the fictitious space $\hat{e}_1$, $\hat{e}_2$, $\hat{e}_3$; i.e.,

$$\vec{\dot{R}} = \vec{\Omega} \times \vec{R}, \tag{12}$$

where

$$\vec{\Omega}(t) \equiv -\hat{e}_1 \omega_1(t) + \hat{e}_3 \Delta(t) \tag{13a}$$

$$\Omega(t) = [\omega_1^2(t) + \Delta^2(t)]^{\frac{1}{2}} \tag{13b}$$

is the precession frequency. The angle $\theta(t)$ between $\pm \vec{\Omega}(t)$ and $\hat{e}_3$ is given by

$$\sin \theta(t) \equiv \mp \ \omega_1(t)/\Omega(t) \quad , \quad \cos \theta(t) \equiv \pm \ \Delta(t)/\Omega(t) \ , \tag{14}$$

where the upper sign is to be chosen if $\Delta(-\infty) > 0$, and the lower sign if $\Delta(-\infty) < 0$. (This convention ensures that $\theta(-\infty) = 0$.)

In the ordinary adiabatic following approximation, $\vec{R}(t)$ remains nearly parallel or antiparallel to $\vec{\Omega}(t)$; i.e.,

$$X(t) \simeq Z_o \sin \theta = \mp \ Z_o \, \omega_1(t)/\Omega(t) \ , \tag{15a}$$

$$Z(t) \simeq Z_o \cos \theta(t) = \pm \ Z_o \, \Delta(t)/\Omega(t) \ , \tag{15b}$$

where $Z_o \equiv Z(-\infty)$. The small quadiature component $Y(t)$, which can be obtained from either (7a) or (7c) with $\Gamma_1 = \Gamma_2 = 0$, can be written as

$$Y(t) = \mp \ Z_o \ \dot{\theta}(t)/\Omega(t), \tag{16}$$

A81

where

$$\dot{\theta}(t) = [\dot{\Delta}(t) \, \omega_1(t) - \Delta(t) \, \dot{\omega}_1(t)]/\Omega^2(t) \quad . \tag{17}$$

Sufficient conditions for adiabatic following behavior are[16]

$$\omega_1(-\infty) = X(-\infty) = Y(-\infty) = 0 \quad , \tag{18a}$$

$$\omega_{max} \ll \Omega(t) \quad , \tag{18b}$$

$$\Gamma_1, \, \Gamma_2 \ll 1/t_p \quad , \tag{18c}$$

where t_p is the effective interaction time between the atom and driving pulse, and ω_{max} is the largest significant Fourrier component in the time dependence of $\vec{\Omega}(t)$. It should be noted that t_p can be significantly shorter than the width of the envelope $\mathcal{E}(t)$ if the pulse is chirped.

Condition (18b) is often taken to mean simply that $\vec{\Omega}(t)$ can change direction only a negligible amount in one precession period. This may be stated as $|\dot{\theta}(t)| \ll \Omega(t)$, or as $\Omega(t) \, t_p \gg 2\pi$. Such criteria, which ensure that $|Y(t)| \ll |\vec{R}|$, are adequate if the pulse is smooth and unmodulated; however, if either $\Delta(t)$ or $\omega_1(t)$ contains a small coherent modulation component at a frequency around $\Omega(t)$, it can result in a serious departure from adiabatic following behavior. A small but rapid change in $\omega_1(t)$ can also cause a deviation from adiabatic following, although the result is less drastic if the perturbation is localized. This question will be examined in more detail in Secs. IV and V.

In his recent derivation of Eqs. (15) and (16), Crisp[13] restricted the analysis to the case where $\Gamma_1 = \Gamma_2 = \dot{\Delta} = 0$. In the following section, we will generalize these equations to include both atomic relaxation effects and time dependence of Δ that even allows $\Delta = 0$ during a portion of the pulse.

III. GENERALIZED ADIABATIC FOLLOWING APPROXIMATION

In this section, we will generalize Eqs (15) and (16) to include the effects of atomic relaxation. We will then examine these results, both in the regime of small damping where an adiabatic following type of behavior is obtained, and in the regime of larger damping where the behavior is adequately described by rate equations. In obtaining our results, we shall use a second rotating coordinate system $\hat{e}_1{}'$, $\hat{e}_2'$, $\hat{e}_3'$ in which $\hat{e}_3'$ remains oriented along $\pm \vec{\Omega}(t)$ [i.e., along $+\vec{\Omega}(t)$ if $\Delta(-\infty) > 0$ and along $-\vec{\Omega}(t)$ if $\Delta(-\infty) < 0$], as is illustrated in Fig. 1. The use of this coordinate system facilitates the analysis because the role of Δ in the unprimed coordinate system is played by $\Omega = (\Delta^2 + \omega_1^2)^{\frac{1}{2}}$ in the primed system. Consequently, assumptions that are normally used to obtain adiabatic following behavior[1,2,13] remain valid in the primed system, even when the carrier frequency is swept through the resonance, causing Δ to pass through zero for portions of the pulse.

The transformation illustrated in Fig. 1 is given by

$$X(t) \equiv X'(t) \cos \theta(t) + Z'(t) \sin \theta(t) \tag{19a}$$

$$Y(t) \equiv Y'(t) \tag{19b}$$

$$Z(t) \equiv - X'(t) \sin \theta(t) + Z'(t) \cos \theta(t) \quad , \tag{19c}$$

which according to (14) can be written as

A83

$$X = \pm X' \, \Delta/\Omega \; \overline{+} \; Z' \, \omega_1/\Omega \tag{20a}$$

$$Z = \pm X' \, \omega_1/\Omega \; \pm \; Z' \, \Delta/\Omega \; . \tag{20b}$$

Substituting this transformation into Bloch's equations (7a-c), we obtain

$$S'(t) = X'(t) + i \, Y'(t), \tag{21}$$

$$\dot{S}' = (\pm i \, \Omega - \Gamma_2 + \Gamma_d \, \omega_1^2/2\Omega^2) \, S' + (\Gamma_d \, \omega_1^2/2\Omega^2) \, S'^{\,*}$$
$$- (\dot{\theta} - \Gamma_d \, \Delta\omega_1/\Omega^2) \, Z' \; \overline{+} \; \Gamma_1 \, \omega_1/\Omega \quad , \tag{22a}$$

$$\dot{Z}' = \tfrac{1}{2} \, (\dot{\theta} + \Gamma_d \, \Delta\omega_1/\Omega^2)(S' + S'^{*})$$
$$- (\Gamma_1 + \Gamma_d \, \omega_1^2/\Omega^2) \, Z' \; \overline{+} \; \Gamma_1 \, \Delta/\Omega \quad , \tag{22b}$$

where $\Gamma_d \equiv \Gamma_2 - \Gamma_1$, and $\dot{\theta}$ is given by Eq. (17).

The generalized adiabatic following approximation postulates that

$$|\dot{S}'(t)| \ll \Omega(t)|S'(t)| \tag{23}$$

at all times during the pulse. In the absence of relaxation, this inequality leads directly to the ordinary adiabatic following results. Indeed, an examination of Eqs (22) reveals that conditions (18a-c) are sufficient to ensure the validity of inequality (23). However, it is also apparent that (18c) could be replaced by the condition

$$\Gamma_1, \; \Gamma_2 \, \omega_1^2(t)/\Omega^2(t) \ll \Omega(t) \quad , \tag{24}$$

which allows the damping rates Γ_1 and Γ_2 to be of the same order as the inverse pulse duration $1/t_p$.

The formal GAF equations, defined by setting $\dot{S}' = 0$ in (22a), are

$$X' = \pm (\Gamma_2/\Omega) Y', \tag{25a}$$

$$Y' = \mp [(\dot{\theta} \, \Omega/f^2) - \Gamma_d \, \Delta \, \omega_1/\Omega f^2] \, z' - \Gamma_1 \, \omega_1/f^2 , \tag{25b}$$

where

$$f^2(t) \equiv \Omega^2(t) + \Gamma_2^2 - \Gamma_d \, \Gamma_2 \, \omega_1^2(t)/\Omega^2(t) \tag{26}$$

The equation

$$\dot{z}' = - (1/f^2) \{[(\omega_1^2 + \dot{\theta}^2) \, \Gamma_2 + (\Delta^2 + \Gamma_2^2)\Gamma_1] \, z'$$
$$\pm [(\dot{\theta} \, \Gamma_2 \, \omega_1/\Omega) + (\Omega^2 + \Gamma_2^2) \, \Delta/\Omega] \, \Gamma_1\} , \tag{27a}$$

where

$$z' (-\infty) = Z (-\infty) \tag{27b}$$

then follows by substituting (25) and (26) into (22b). These results are consistent with conditions (18a, b) and (24).[17]

For smoothly varying pulses, condition (18b) is equivalent to $\Omega t_p \gg 2\pi$. This allows a simplification of many of our results, because it implies that $|\dot{\theta}| \ll \omega_1$. To see this, we note that $|\dot{\Delta}| \approx |\Delta|/t_p$ and $|\dot{\omega}_1| \approx \omega_1/t_p$; hence, according to (17),

$$|\dot{\theta}| \approx 2 |\Delta| \, \omega_1/\Omega^2 \, t_p < 2 \, \omega_1/\Omega \, t_p \ll \omega_1. \tag{28}$$

The $\dot{\theta}$ term must be retained in (25b) because Γ_2 can be $\ll \Omega$, but it can be dropped from (27a) to a good approximation. Thus

$$\dot{z}' \simeq - (\Gamma_1 + \Gamma_d \, \omega_1^2/f^2) \, z' \mp \Gamma_1 \, \Delta/\Omega , \tag{29}$$

where we have also used (13b), (26) and (24).

The components of $\vec{R}(t)$ in the original rotating frame may be found by substituting the solutions for $X'(t)$, $Y'(t)$, $Z'(t)$ from equations (25) and (29) back into Eqs (19) or (20). They are explicitely related to Z' by the expressions

$$X = (1/f^2) \{ \mp [(\Omega^2 + \Gamma_1 \Gamma_2)(\omega_1/\Omega) + \Gamma_2 \dot{\theta} \Delta/\Omega] Z'$$
$$- \Gamma_1 \Gamma_2 \Delta\omega_1/\Omega^2 \}, \tag{30a}$$

$$Z = (1/f^2) \{ \pm [(\Omega^2 + \Gamma_2^2)(\Delta/\Omega) - \Gamma_2 \dot{\theta} \omega_1/\Omega] Z'$$
$$- \Gamma_1 \Gamma_2 \omega_1^2/\Omega^2 \}, \tag{30b}$$

with $Y = Y'$ given by Eq. (25b). Using conditions (24) and (28), one can simplify these expressions to

$$X \simeq \mp Z' \Omega \omega_1/f^2 , \quad Z \simeq \pm Z' \Delta/\Omega \tag{31a,b}$$

to a good approximation under the conditions of interest. The neglect of Γ_1 and $\dot{\theta}$ terms in (30a) is not accurate if $\Gamma_2 \gg \Omega$; however, in that case, condition (24) requires that $\omega_1 \ll \Omega$. One is then dealing with a linear system near resonance, and $|X| \ll |Y|, |Z|$.

There are two cases of particular interest in which (24) is satisfied. The first one allows $\omega_1^2/\Omega^2 \le 1$, but restricts Γ_2 so that $\Gamma_2 \ll \Omega$. (This still allows Γ_1, $\Gamma_2 \approx 1/t_p$.) The second case allows Γ_2 comparable to Ω, but imposes the restriction $\omega_1^2 \ll \Omega^2$.

Case A, $\Gamma_2 \ll \Omega$

To a good approximation, we need retain only first order terms in Γ_1/Ω or Γ_2/Ω. Equations (25) and (29) then reduce to

$$X' \simeq 0 \ , \tag{32a}$$

$$Y' \simeq \mp \ [(\dot{\theta}/\Omega) - \Gamma_d \ \Delta \ \omega_1/\Omega^3] \ Z' - \Gamma_1 \ \omega_1/\Omega^2 \tag{32b}$$

$$= \mp \ [(\dot{\theta}/\Omega) - (\Gamma_d/\Omega) \ \sin \theta \ \cos \theta] \ Z' \pm (\Gamma_1/\Omega) \ \sin \theta, \tag{32c}$$

$$\dot{Z}' \simeq - \ (\Gamma_1 + \Gamma_d \ \omega_1^2/\Omega^2) \ Z' \mp \ \Gamma_1 \ \Delta/\Omega \tag{32d}$$

$$= - \ (\Gamma_1 + \Gamma_d \ \sin^2 \theta) \ Z' - \Gamma_1 \ \cos \theta, \tag{32e}$$

giving the following expressions for the unprimed components of $\vec{R}$ from
Eqs (19):

$$X \simeq \mp \ Z' \ \omega_1/\Omega = Z' \sin \theta \ , \quad Y = Y', \tag{33a}$$

$$Z \simeq \pm \ Z' \ \Delta/\Omega = Z' \cos \theta \ . \tag{33b}$$

In the important case where $\Gamma_1 \ll 1/t_p$,

$$Y' \simeq \mp \ [(\dot{\theta}/\Omega) - \Gamma_2 \ \Delta \ \omega_1/\Omega^3] \ Z' \ , \tag{34a}$$

$$Z'(t) = Z_o \exp \left[- \Gamma_2 \int_{-\infty}^{t} \frac{\omega_1^2(t')}{\Omega^2(t')} \ dt' \right] = Z_o \ e^{-Q(t)} \ , \tag{34b}$$

and Eqs.(33a, b) become

$$X(t) = \mp \ [\omega_1(t)/\Omega(t)] \ Z_o \ e^{-Q(t)} \ , \quad Z(t) = \pm \ [\Delta(t)/\Omega(t)] \ Z_o \ e^{-Q(t)} \tag{35a,b}$$

Equations (34) and (35) describe the effects of a small amount of atomic damping
on the ordinary adiabatic following results (15). The inequality (18b) and
the condition $\Gamma_2 \ll \Omega$ imply that $|Y'(t)| \ll |Z'(t)|$; hence, Eqs. (34) and
(35) describes a Bloch vector $\vec{R}(t)$ that remain nearly parallel or antiparallel
to $\vec{\Omega}(t)$, but decays in length $R(t) \equiv |\vec{R}(t)| \simeq |Z'(t)|$ during the pulse. It

is instructive to note that this decay law can be easily obtained directly from Eqs (7). Multiplying (7a) by X, (7b) by Y, and (7c) by Z, then setting $\Gamma_1 = 0$ and using $R = (X^2 + Y^2 + Z^2)^{\frac{1}{2}} = (X'^2 + Y'^2 + Z'^2)^{\frac{1}{2}}$, we find

$$dR^2/dt = -2 \Gamma_2 (X^2 + Y^2).$$

If $\vec{R}$ lies along $\pm \vec{\Omega}$, then $X^2 + Y^2 = R^2 \sin^2 \theta$,

and

$$\dot{R} = -\Gamma_2 R \sin^2 \theta = -\Gamma_2 R \omega_1^2/\Omega^2 , \tag{36}$$

which agrees with (34b) for $R(-\infty) = |Z_o|$. The decay of $R(t)$ has two important consequences. In experiments such as Grischkowsky performed,[1,2] where Δ remains constant, it results in a net absorption of pulse energy by the atom; whereas, in an adiabatic passage experiment, it results in an incomplete inversion. In the limit where $\Gamma_2 \ll 1/t_p$, Eqs (33) and (34) reduce immediately to the ordinary adiabatic following results (15), (16), so these effects disappear.

Case B, $\omega_1^2 \ll \Omega^2 \simeq \Delta^2$

If $\Gamma_2 \gg \Gamma_1$, $1/t_p$, then Eqs (25b), (29) and (31) reduce to conventional rate equations. One can show this by combining them, and taking $\omega_1^2 \ll \Delta^2$ to get

$$X \simeq -(\Delta \omega_1/\gamma^2) Z \tag{37a}$$

$$Y \simeq -(1/\gamma^2) (\Gamma_2 \omega_1 - \dot{\theta} \Delta) Z - (\Gamma_1 \omega_1/\gamma^2) (Z + 1) \tag{37b}$$

$$\dot{Z} \simeq -[(\Gamma_2 \omega_1^2/\gamma^2) - \dot{\theta} \omega_1/\Delta] Z - \Gamma_1 (Z + 1) , \tag{37c}$$

A88

where $\gamma \equiv \Delta^2 + \Gamma_2^2$. Since $|\dot{\theta}| \approx 2\omega_1/\Omega t_p$, the condition $\Gamma_2 \gg \Gamma_1$, $1/t_p$ leads to the rate equations

$$X \simeq - (\Delta\,\omega_1/\gamma^2)\, Z \quad , \quad Y \simeq (\Gamma_2\,\omega_1/\gamma^2)\, Z, \tag{38a,b}$$

$$\dot{Z} \simeq -(\Gamma_2\,\omega_1^2/\gamma^2)\, Z - \Gamma_1\,(Z+1) \quad . \tag{38c}$$

Eqs (38) are normally obtained by setting $\dot{X}$, $\dot{Y} \to 0$ in the original rotating frame [i.e., in Eqs (7a,b)]. It is therefore not surprising that our results reduce to (38) only under the condition where $\theta^2 \simeq \omega_1^2/\Omega^2 \ll 1$.

One can derive a simple expression for the lowest order nonlinear refractive index in the case where Γ_1, Γ_2 can be comparable to $1/t_p$, and the atom remains near its ground state $Z \approx -1$. Combining Eqs (8), (10), (11) and (31a), we obtain

$$n(t) - 1 \simeq - (2\pi\, Np^2\Omega/\hbar\, f^2)\, Z' \tag{39a}$$

$$\simeq - (2\pi Np^2\, \Delta/\hbar\, \gamma^2)\, [1 - (1 - \Gamma_2^2/\Delta^2)\, \omega_1^2/2\gamma^2]\, Z', \tag{39b}$$

where we have used $\omega_1^2 \ll \Delta^2$ and $\Delta = \pm\,|\Delta|$ in deriving (39b). Taking (29) to lowest order in ω_1^2, and assuming $\omega_1^2\, Z' \simeq -\omega_1^2$, we have

$$\dot{Z}' \simeq [2\,\Gamma_2 - (1 - \Gamma_2^2/\Delta^2)\,\Gamma_1]\,(\omega_1^2/2\gamma^2) - \Gamma_1(Z' + 1), \tag{40}$$

which has the formal solution

$$Z'(t) \simeq -1 + \frac{2\Gamma_2 - \Gamma_1\,(1 - \Gamma_2^2/\Delta^2)}{2\,\gamma^2} \int_{-\infty}^{t} dt'\, e^{-\Gamma_1(t-t')}\omega_1^2(t') \tag{41}$$

for a constant Δ. Eq. (39b) then becomes

A89

$$n(t) - 1 = (2\pi N p^2 \Delta / \hbar \gamma^2) + \delta \, n^{NL}(t) \qquad (42a)$$

where $\delta n^{NL}(t)$ is the lowest order nonlinear contribution

$$\delta n^{NL}(t) \simeq - \frac{\pi N p^4 \Delta}{\hbar^3 \gamma^4} \left(1 - \frac{\Gamma_2^2}{\Delta^2} \right) \mathcal{E}^2(t)$$

$$- \left[2\Gamma_2 - \Gamma_1 \left(1 - \frac{\Gamma_2^2}{\Delta^2} \right) \right] \frac{\pi N p^4 \Delta}{\hbar^3 \gamma^4} \int_{-\infty}^{t} dt' e^{-\Gamma_1(t-t')} \mathcal{E}^2(t'). \qquad (42b)$$

If $|\Delta| \gg \Gamma_2$, then

$$\delta N^{NL}(t) \simeq \tfrac{1}{2} n_2 \left[\mathcal{E}^2(t) + (2\Gamma_2 - \Gamma_1) \int_{-\infty}^{t} dt' \, e^{-\Gamma_1(t-t')} \mathcal{E}^2(t') \right], \qquad (43a)$$

where

$$n_2 = - 2\pi N p^4 / \hbar^3 \Delta^3 . \qquad (43b)$$

Equations (43) are in agreement with results recently derived by using perturbation theory.[14]

The $\mathcal{E}^2(t)$ term has been observed in the self focusing and defocusing experiments of Grischkowsky,[1,2] in which Γ_1, $\Gamma_2 \ll 1/t_p$. When Γ_1 or Γ_2 are comparable to $1/t_p$, the integral term will generally be an important contribution. For example, it is probably responsible for the asymmetry in the spectral broadening observed by Arutyunyan, et. al.[6] However, in the case where the relaxation is due entirely to spontaneous emission, we have $\Gamma_1 = 2\Gamma_2$, and the integral contribution vanishes. This is, indeed, the case

in most of Grischkowsky's experiments,[1,2] and his lowest order results should also be valid for longer pulses, provided that t_p remains shorter than the collision time of the atoms.[18] The cancellation between Γ_1 and $2\Gamma_2$ does not occur in the higher order nonlinear contributions to the refractive index.

IV. STABILITY CONSIDERATIONS

Equations (25) and (29) remain good approximations if condition (18b) [along with (18a) and (24)] applies throughout the pulse. On the other hand, there exist pulses that remain slowly varying in comparison to $\Omega(t)$ everywhere excepting for one localized portion. An example of this would be a pulse with a small but abrupt step on its leading edge, followed by an otherwise smooth, well-behaved time dependence. The question that must be answered under these circumstances is whether the GAF approximation has any validity during the subsequent well-behaved portions; i.e., does the approximation remain stable after a small perturbation? The answer is that the perturbation causes the subsequent values of R to precess around some average value $\langle \vec{R}(t) \rangle$ with a bounded amplitude $|\delta \vec{R}(t)|$ and frequency on the order of $\Omega(t)$. If the perturbation is small, then $|\delta \vec{R}(t)| \ll 1$, and $\langle \vec{R}(t) \rangle$ satisfies Eqs (25) and (29) to a good approximation. If Γ_1, $\Gamma_2 \ll 1/t_p$, then $|\delta \vec{R}(t)|$ remains nearly constant; however, if Γ_1 or $\Gamma_2 \approx 1/t_p$, then it decays at a rate given approximately by $\Gamma_2 - \Gamma_d \, \omega_1^2/2\Omega^2$.

To examine the behavior of $\vec{R}(t)$ in greater detail, we assume the perturbation to have occurred prior to time t_o, and obtain the approximate solutions of (22a,b) for times $t \geq t_o$. We will simplify the calculations by restricting them to the case where $\Gamma_2 \ll \Omega(t)$. [In the case where $\Gamma_2 \approx \Omega(t)$, the system loses its memory of the perturbation, and relaxes to its rate equation solutions in a time on the order of $1/\Gamma_2$.]

A91

We choose the ansatz for $t \geq t_o$

$$S'(t) = \langle S'(t) \rangle + \sigma_1(t) \, e^{\pm i\alpha(t)} + \sigma_2(t) \, e^{\mp i\alpha(t)} \tag{44a}$$

$$Z'(t) = \langle Z'(t) \rangle + \zeta(t) \, e^{\pm i\alpha(t)} + \zeta^*(t) \, e^{\mp i\alpha(t)} , \tag{44b}$$

where

$$\alpha(t) \equiv \int_{t_o}^{t} \Omega(t') \, dt' , \tag{45}$$

and $|\sigma_1(t_o)|$, $|\sigma_2(t_o)|$, $|\zeta(t_o)| \ll 1$, corresponding to a small perturbation.
If $\langle S' \rangle$, σ_1, σ_2, $\langle Z' \rangle$ and ζ are assumed to be slowly varying in comparison
to $\exp(\pm i\alpha)$, one may substitute (44a,b) into (22a,b) and independently
equate the coefficients of $\exp(\pm i\alpha)$. The result is

$$d\langle S' \rangle/dt = (\pm i\,\Omega - \Gamma_p) \langle S' \rangle + (\Gamma_d \, \omega_1^2/2\Omega^2) \langle S' \rangle^*$$
$$- (\dot{\theta} - \Gamma_d \, \Delta \, \omega_1/\Omega^2) \langle Z' \rangle \mp \Gamma_1 \, \omega_1/\Omega \tag{46a}$$

$$\dot{\sigma}_1 = - \Gamma_p \sigma_1 + (\Gamma_d \, \omega_1^2/2\Omega^2) \sigma_2^* - (\dot{\theta} - \Gamma_d \, \Delta \, \omega_1/\Omega^2) \zeta \tag{46b}$$

$$\dot{\sigma}_2 = (\pm i\,2\Omega - \Gamma_p) \sigma_2 + (\Gamma_d \, \omega_1^2/2\Omega^2) \sigma_1^* - (\dot{\theta} - \Gamma_d \, \Delta\omega_1/\Omega^2) \zeta^* \tag{46c}$$

$$d\langle Z' \rangle/dt = \tfrac{1}{2} (\dot{\theta} + \Gamma_d \, \Delta \, \omega_1/\Omega^2) (\langle S' \rangle + \langle S' \rangle^*)$$
$$- (\Gamma_1 + \Gamma_d \, \omega_1^2/\Omega^2) \langle Z' \rangle \mp \Gamma_1 \, \Delta/\Omega \tag{46d}$$

$$\dot{\zeta} = (\mp i\,\Omega - \Gamma_1 - \Gamma_2 \, \omega_1^2/\Omega^2) \zeta + \tfrac{1}{2} (\dot{\theta} + \Gamma_d \, \Delta \, \omega_1/\Omega^2)(\sigma_1 + \sigma_2^*), \tag{46e}$$

A92

where

$$\Gamma_p = \Gamma_p(t) \equiv \Gamma_2 - \Gamma_d \, w_1^2/2\Omega^2 \ll \Omega(t) \ . \tag{47}$$

Since all of these quantities are assumed to be slowly varying, one may obtain approximate solutions of (46a, c, e) by setting their left-hand sides equal to zero. For $\Omega \gg \Gamma_p$, eqs (46a,d) give

$$\langle s' \rangle \simeq \mp \, i \, [(\dot{\theta}/\Omega) - \Gamma_d \, \Delta \, w_1/\Omega^3] \, \langle z' \rangle - i \, \Gamma_1 \, w_1/\Omega^2 \tag{48a}$$

$$d \, \langle z' \rangle/dt \simeq - \, (\Gamma_1 + \Gamma_d \, w_1^2/\Omega^2) \, \langle z' \rangle \mp \Gamma_1 \, \Delta/\Omega, \tag{48b}$$

which are identical to Eqs (32), and (46c,e) give

$$\sigma_2 \simeq \mp \tfrac{1}{2} \, i \, [(\dot{\theta}/\Omega) - \Gamma_d \, \Delta \, w_1/\Omega^3] \, \zeta^* \pm \tfrac{1}{2} \, i \, (\Gamma_d \, w_1^2/2\Omega^3) \, \sigma_1^*, \tag{49a}$$

$$\zeta \simeq \mp \tfrac{1}{2} \, i \, [(\dot{\theta}/\Omega) + \Gamma_d \, \Delta \, w_1/\Omega^3] \, (\sigma_1 + \sigma_2^*) \ . \tag{49b}$$

It is apparent from (49a,b) that $|\sigma_2|$, $|\zeta| \ll |\sigma_1|$; hence (46b) is approximately

$$\dot{\sigma}_1 \simeq - \, \Gamma_p \sigma_1 \ , \tag{50a}$$

and

$$\sigma_1(t) \simeq \sigma_1(t_o) \exp \left[- \int_{t_o}^{t} \Gamma_p(t') \, dt' \right] \ . \tag{50b}$$

According to Eq. (47), $\Gamma_p \geq 0$. The precession amplitude $\sigma_1(t_o)$ introduced by the perturbation will therefore either remain constant or decay for times $t > t_o$. It cannot grow.

A93

V. COMPARISON TO EXACT THEORY

To assess the accuracy of the GAF approximation and gain additional insight into its behavior, we compare it to the numerical solutions of Bloch's equations (7a-c). We choose a linearly chirped Gaussian pulse of width t_p (FWHM intensity)

$$\mathcal{E}(t) = \mathcal{E}_o \exp\left[-(2\ell n2)(t/t_p)^2\right], \tag{51a}$$

$$\omega(t) = \dot{\psi}(t) = \omega_o + \omega_c \, t/t_p \quad, \quad \omega_c \ll \omega_o ; \tag{51b}$$

hence, according to expressions (5) and (8), and definition $\omega_{10} \equiv p\,\mathcal{E}_o/\hbar$,

$$\omega_1(t) = \omega_{10} \exp\left[-(2\ell n2)(t/t_p)^2\right], \tag{52a}$$

$$\Delta(t) = -\omega_c \, t/t_p \quad. \tag{52b}$$

Since $\omega(t)$ sweeps through the atomic resonance, this pulse is capable of inverting the atom, and it should therefore provide a good test of the GAF approximation.

The numerical solutions to Bloch's equations and to the GAF approximation were carried out with the aid of predictor-corrector algorithms.[19] All of the GAF results shown here were obtained from Eqs (29), (25) and (20); however, the results obtained by using (27) instead of (29) were nearly identical. In Fig. 2, we have plotted $\omega_1(t)$ and the relevant quantities $\Omega(t) = [\omega_1^2(t) + \Delta^2(t)]^{\frac{1}{2}}$ and

$$\dot{\theta}(t) = [1 + (4\ell n2)(t/t_p)^2] \; \omega_c \; \omega_1(t)/\Omega^2(t) \; t_p \qquad (53)$$

[obtained from (17)] for the case where $\omega_{10} = \omega_c$. It should be noted here that $|\dot{\theta}(t)| \ll \omega_1(t)$.

Figures 3-6 show the comparisons for the case where $\omega_{10} = \omega_c = 25/t_p$. This corresponds to approximately four precession cycles in an interval t_p centered at $t=0$, and therefore satisfies condition (18b).

Figure 3 shows the excellent agreement and the complete inversion that one expects in the pure adiabatic following case where $\Gamma_1 = \Gamma_2 = 0$. In the primed reference frame, our solutions correspond to $X' = 0$ and $Z' = -1$. The slight discrepency in the values of Y around $t \simeq \pm 0.6 \; t_p$ results from a small precession amplitude that occurs when $\Omega(t)$ decreases to about $21/t_p$ at $t = \pm 0.6 \; t_p$. It is of interest to note here that the total bandwidth of the chirped pulse is $\omega_p = [\omega_c^2 + (4\ell n2/t_p)^2]^{\frac{1}{2}} \simeq \omega_c$, which is comparable to $\Omega(t)$. The criterion $\omega_p \ll \Omega$ that is often given for adiabatic following behavior is therefore necessary only for unchirped pulses.

Figures 4 and 5 show the effects of relaxation. In Fig. 4 where $\Gamma_1 = 0$ and $\Gamma_2 = 1/t_p$ the agreement is again excellent. Figure 4a shows the partial inversion resulting from the decay of $|\vec{R}(t)|$, as described in Sec. III. In the primed reference frame (Fig. 4b), $X'(t) \simeq 0$ and $|Y'(t)| \ll |Z'(t)| \simeq |\vec{R}(t)|$; i.e., we see that $\vec{R}(t)$ remains nearly parallel to $\hat{e}_3'(t) = \pm \hat{\Omega}(t)$, and its decay is therefore shown in the decay of $|Z'(t)|$. In Fig. 5, where $\Gamma_1 = 1/t_p$ and $\Gamma_2 = 5/t_p$, the agreement remains good, in spite of the fact that the inequality $\Gamma_2 \ll \Omega(t)$ is only marginally satisfied in this case. Around the peak of the pulse, the atom appears to be approaching steady state saturation, but it

A95

decays back to its ground state under the influence of Γ_1 as the pulse subsides. In the primed coordinate system, this behavior requires that Z' change sign, and thus, pass through zero. One can therefore no longer regard $\vec{R}$ as remaining parallel to $\vec{\Omega}(t)$, at least in the region around $Z' \approx 0$.

Figures 6-8 show the effects of localized perturbations of the type discussed in Sec. IV. Figure 6 again shows the behavior of the system (as seen in the primed reference frame) for $\Gamma_1 = 0$ and $\Gamma_2 = 1/t_p$; however, in this case, a perturbation was deliberately introduced by abruptly turning on the pulse at $t = -1.5\ t_p$, where $\omega_1 \simeq .044\ \omega_{10}$. As indicated in Sec. IV, the precession $\delta\vec{R}(t)$ is to a good approximation superimposed on the GAF solutions, and damps out a rate given by (47). If $\Gamma_2 = 0$, then it would persist at constant amplitude throughout the pulse.

In Figs. 7 and 8, we have chosen $\omega_{10} = \omega_c = 15/t_p$, corresponding to only 2.4 precession cycles in an interval t_p centered at $t = 0$. Condition (18b) is now only marginally satisfied. In Fig. 7 ($\Gamma_1 = \Gamma_2 = 0$), the resulting precession amplitude builds up near $t \simeq -.6\ t_p$ and remains superimposed on the GAF solutions throughout the remainder of the pulse. The precession prevents the atom from being completely inverted, because of the constraint $X^2 + Y^2 + Z^2 = 1$; however, it is evident from this condition (and Fig. 7) that the precession amplitude would have to become an appreciable fraction of one before it would significantly affect the inversion. These considerations are in qualitative agreement with results derived by Horwitz.[11] In Fig. 8 ($\Gamma_1 = 0$, $\Gamma_2 = 1/t_p$) the precession again builds up around $t \simeq -.6\ t_p$, but damps out on account of Γ_2.

A96

In the final comparison, shown in Fig. 9, we have fixed the detuning at $\Delta = 25/t_p$ and chosen $\omega_1 = 5/t_p$, $\Gamma_1 = 1/t_p$ and $\Gamma_2 = 25/t_p$. The Bloch equation results are essentially identical to those that would be obtained from the rate equations (38). The small discrepancy in $Y(t)$ between these solutions and the GAF approximation arises primarily from the $\dot{\theta} \Delta$ term in Eq. (37b).

REFERENCES

1. D. Grischkowsky, Phys. Rev. Lett. 24, 866 (1970); "Adiabatic Following",
    Lectures presented at the 1973 session of Physic of Quantum Electronics,
    Crystal Mountain, Washington (Sponsored by the University of Arizona).

2. D. Grischkowsky and J. A. Armstrong, Phys. Rev. A6, 1566 (1972).

3. S. A. Akhmanov, A. I. Kovrigin, S. A. Maksimov, and V. E. Ogluzdin,
    ZhETF Pis. Red. 15, 186 (1972) [JETP Lett. 15, 129 (1972)].

4. A. Javan and P. L. Kelly, IEEE J. Quant. Electron. 2, 470 (1966).

5. J. E. Bjorkholm and A. Ashkin, Phys. Rev. Lett. 32, 129 (1974).

6. V. M. Arutyunyan, N. N. Badalyan, V. A. Iradyan, and M. E. Movsesyan,
    Zh. Eksp. Teor. Fiz. 58, 37 (1970) [JETP 31, 22 (1970)].

7. D. Grischkowsky, E. Courtens, and J. A. Armstrong, Phys. Rev. Lett.
    31, 422 (1973).

8. E. B. Treacy, Phys. Lett. 27A, 421 (1968); E. B. Treacy and A. J. DeMaria,
    Phys. Lett. 29A, 369 (1969).

9. M. M. T. Loy, Phys. Rev. Lett. 32, 814 (1974).

10. I. Nebenzahl and A. Szöke, Appl. Phys. Lett. 25, 327 (1974).

11. P. Horwitz, Appl Phys. Lett. 26, 306 (1975).

12. A. Abragam, The Principles of Nuclear Magnetism (Oxford Univ. Press,
    London, 1961).

13. M. D. Crisp, Phys. Rev. A 8, 2128 (1973).

14. R. H. Lehmberg, J. Reintjes, and R. C. Eckardt; IEDM Technical Digest
    (IEEE, December 1974); Naval Research Laboratory Memorandum Report 2932
    (November 1974).

15. M. D. Crisp, Phys. Rev. Lett. **22**, 820 (1969).

16. These conditions are discussed in Refs. 1, 2, 12, and 13. If the resonance line is broadened by dipole-dipole type interactions among stationary atoms (e.g., magnetic resonance in solids), the condition $\Gamma_2 \ll 1/t_p$ can be relaxed (Ref. 12, Ch. XII); however, Blochs equations are no longer applicable in this case. For the types of broadening mechanisms ordinarily encountered in coherent optical experiments, condition (18c) must be retained.

17. Eq. (27a) appears to suggest that (24) could be replaced by the weaker condition Γ_1, $\Gamma_2 \, \omega_1^2/f^2 \ll \Omega$. In effect, the $X' = \frac{1}{2}(S' + S'^*)$ term of (22b) would cancel the rapid variation due to $(\Gamma_d \, \omega_1^2/\Omega^2) \, Z'$ that could occur if $f^2 \gg \Omega^2$. However, since expressions (25) are only approximate, this would require the near cancellation of two large terms when one of them is subject to inaccuracy. Unless the system is operating near steady state, this is clearly unrealistic, and one can therefore rely only on (24).

18. This also assumes that optical pumping effect can be neglected; e.g., by the use of linearly polarized pulses. (For reference, see R. Bernheim, Optical Pumping, an Introduction (W. A. Benjamin Co. New York, N.Y., 1965).

19. A. Icsevgi and W. E. Lamb, Jr., Phys. Rev. **185**, 517 (1969).

FIGURES

Fig. 1. Usual rotating coordinate system $\hat{e}_1$, $\hat{e}_2$, $\hat{e}_3$ and second rotating system $\hat{e}'_1$, $\hat{e}_2$, $\hat{e}'_3$ shown for the case where $\Delta(-\infty) > 0$ and $R_3(-\infty) < 0$.

Fig. 2. Chirped Gaussian pulse used to derive the curves of Figs. 3-8. The quantities $\omega_1(t)$, $\dot{\theta}(t)$ and $\Omega(t)$ are given by Eqs. (52), (53), and (13b), respectively.

Fig. 3. Comparison between solutions of the GAF approximation [Eq. (29), (25) and (20)] and those of Bloch's equations [Eqs (7)], showing the Bloch vector components in the $\hat{e}_1$, $\hat{e}_2$, $\hat{e}_3$ coordinate system, for the case where $Z(-\infty) = -1$, $\omega_{10} = \omega_c = 25/t_p$ [Eqs. (52)] and $\Gamma_1 = \Gamma_2 = 0$. In this, and all subsequent figures, the dotted lines represent the GAF approximation, while the solid lines represent Bloch's equations.

Fig. 4. Same conditions as in Fig. 3, excepting that $\Gamma_2 = 1/t_p$. (a) X, Y, Z in coordinate system $\hat{e}_1$, $\hat{e}_2$, $\hat{e}_3$, (b) X', Y', Z' in coordinate system $\hat{e}_1'$ $\hat{e}_2$, $\hat{e}_3'$.

Fig. 5. Same conditions as in Fig. 3, excepting that $\Gamma_1 = 1/t_p$, $\Gamma_2 = 5/t_p$.

Fig. 6. Same conditions as in Fig. 4b, excepting that the pulse was switched on abruptly at $t = -1.5 t_p$.

Fig. 7. Comparison between the GAF approximation and Bloch equation solutions for the case where $Z(-\infty) = -1$, $\omega_{10} = \omega_c = 15/t_p$, and $\Gamma_1 = \Gamma_2 = 0$.

Fig. 8. Same conditions as in Fig. 7, excepting that $\Gamma_2 = 1/t_p$.

A100

Fig. 9. Comparison between the GAF approximation and Bloch equation solutions for the case where $Z(-\infty) = -1$, $\omega_{10} = 5/t_p$, $\Delta = 25/t_p$, $\Gamma_1 = 1/t_p$, and $\Gamma_2 = 25/t_p$.
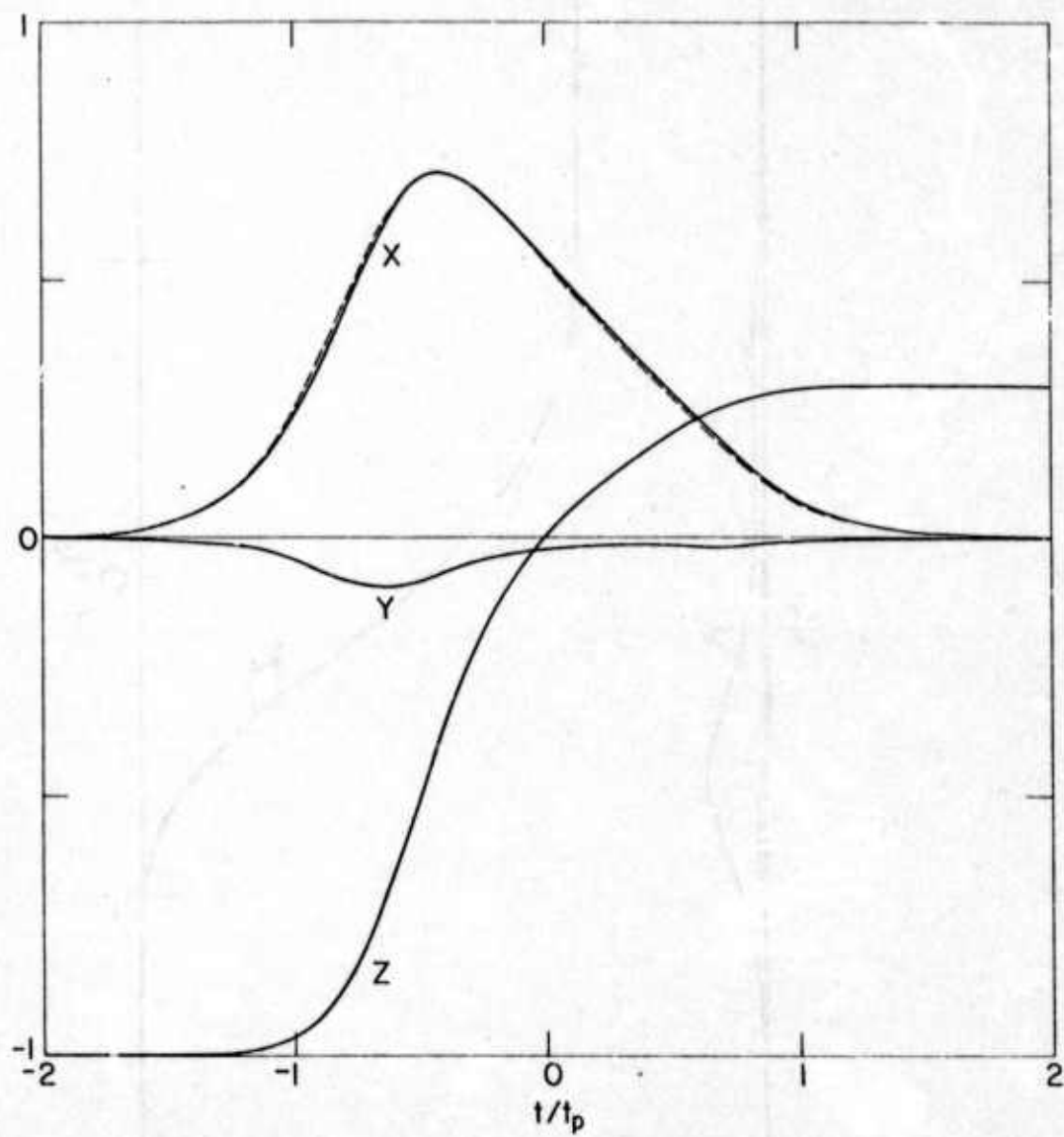
Fig. 1

A102
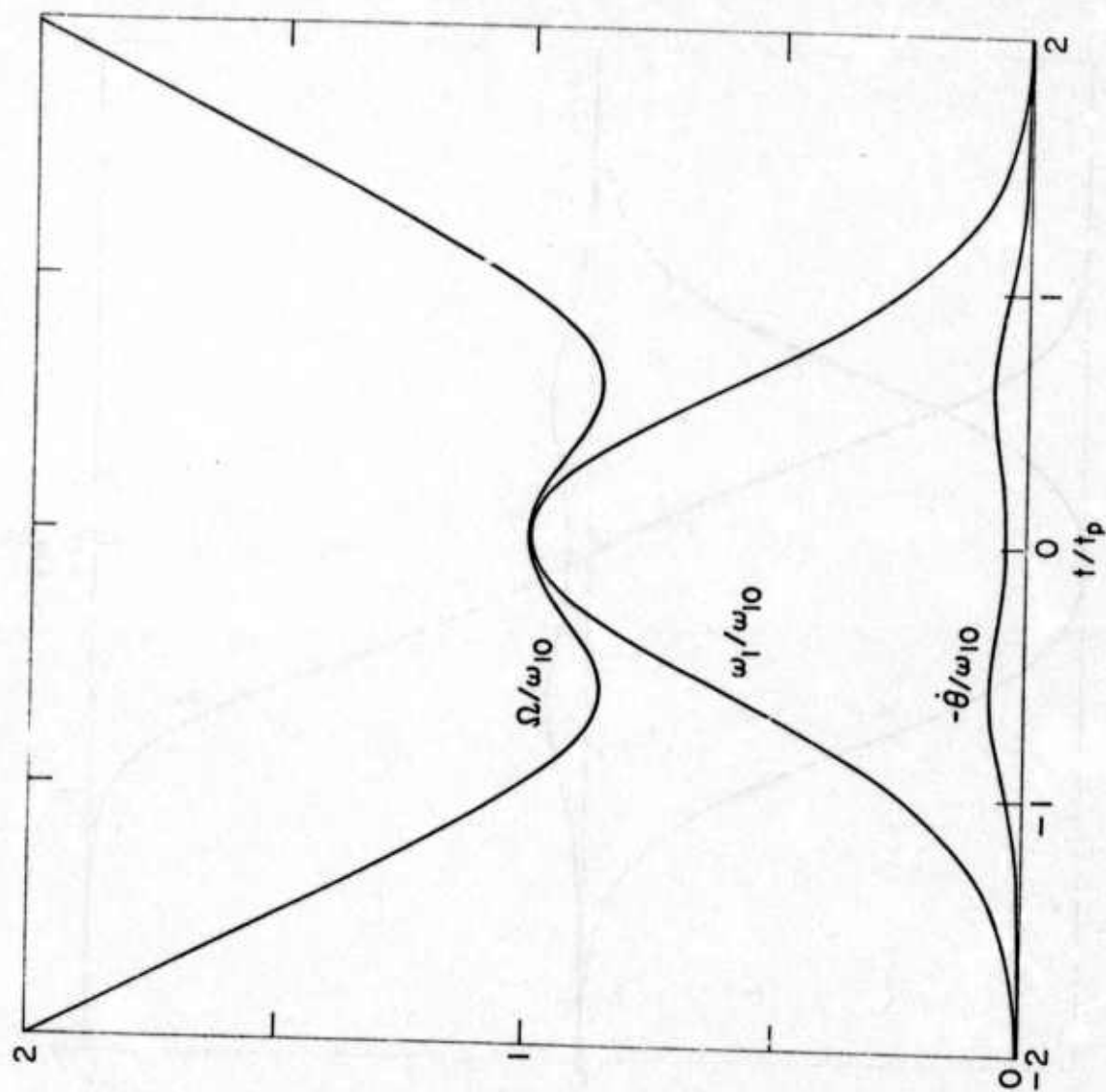
Fig. 2

A103
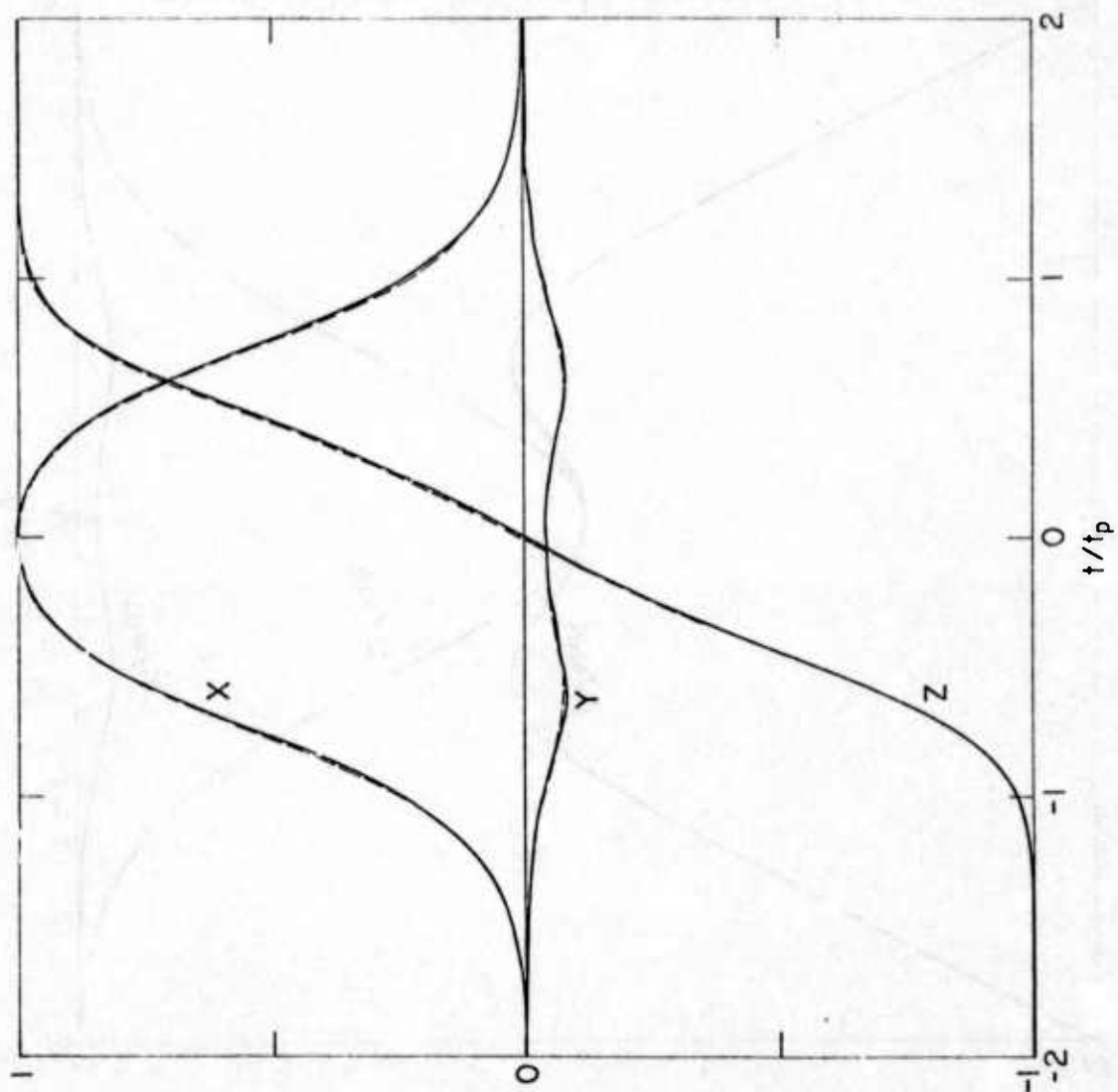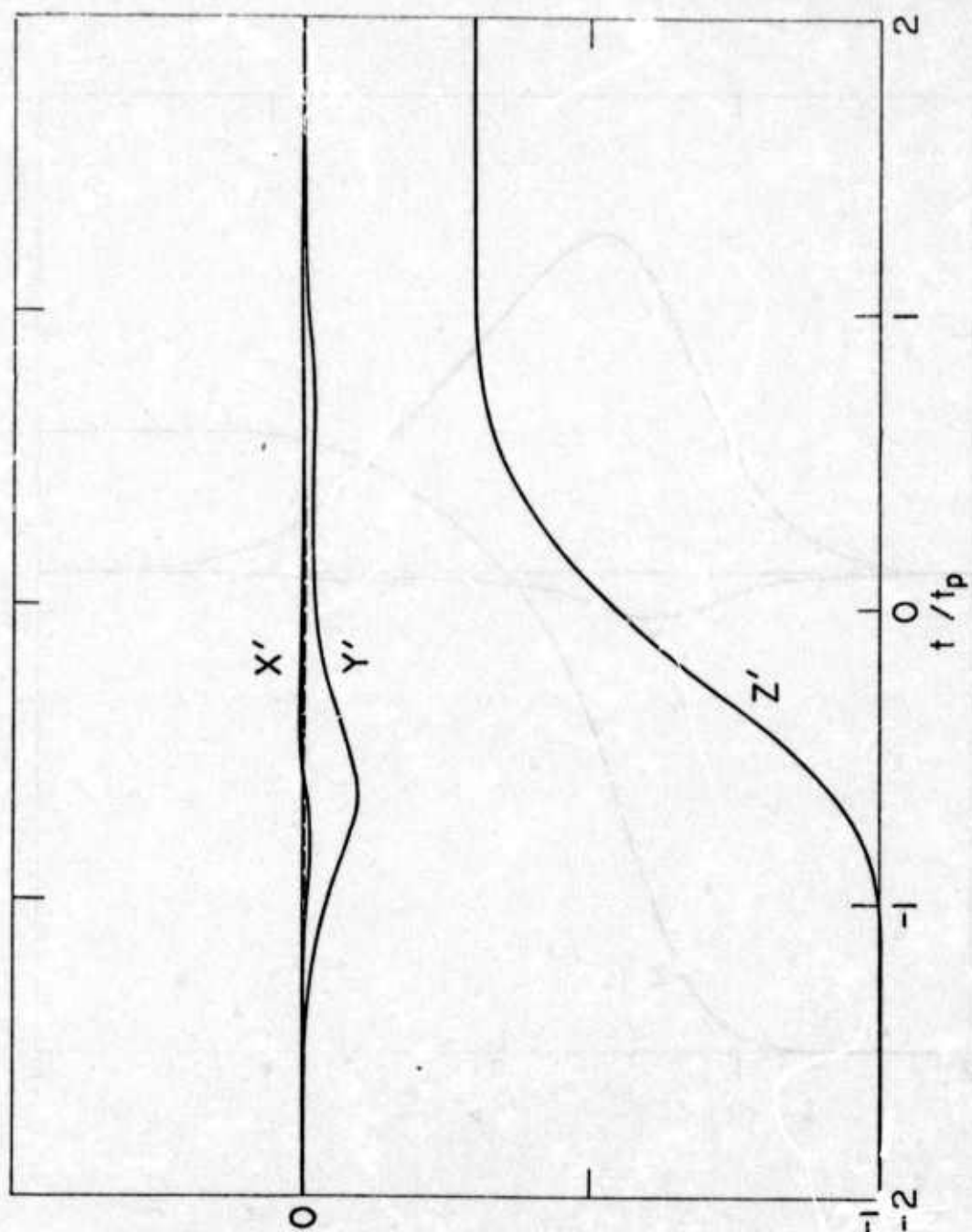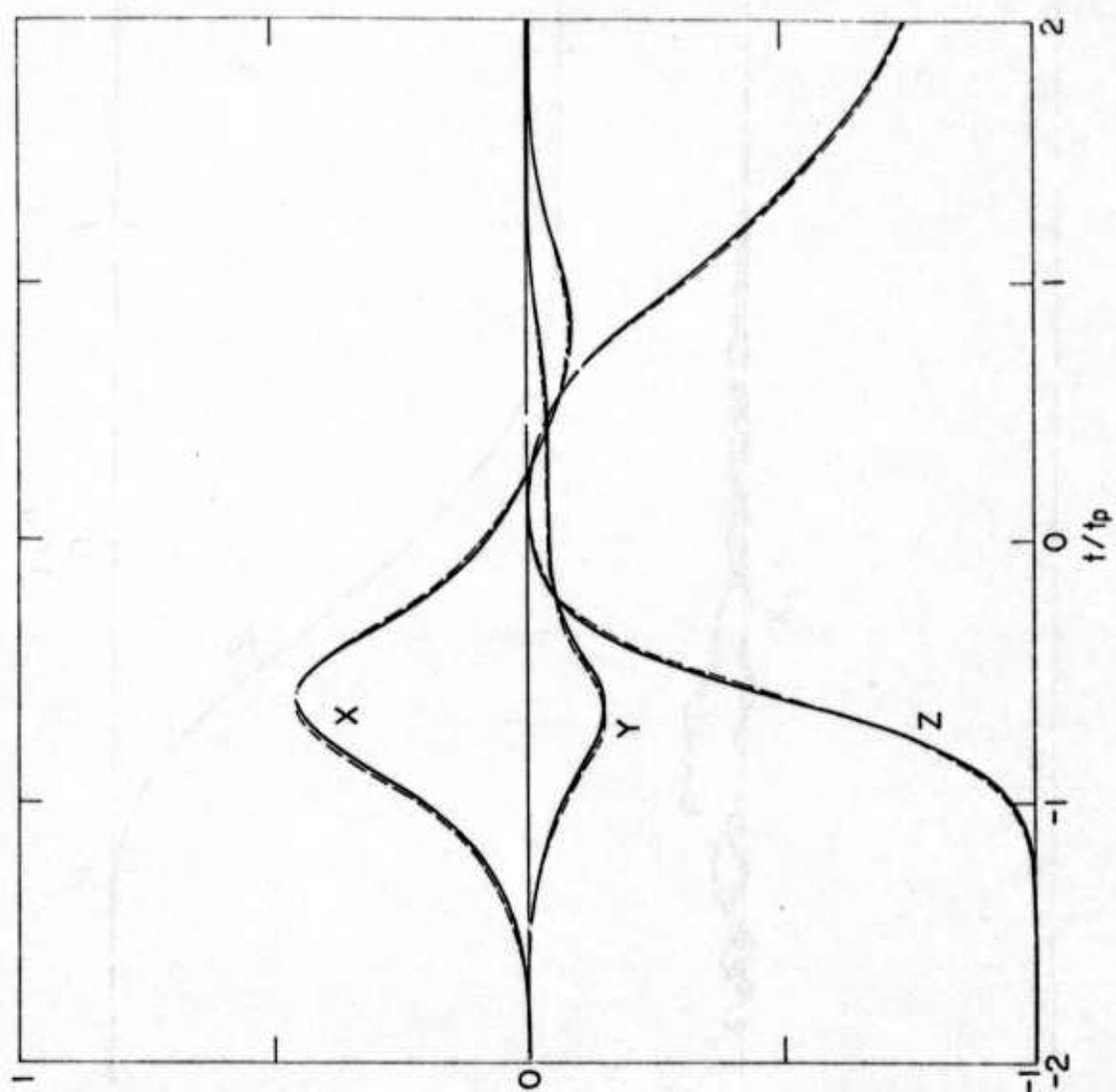
Fig. 3

A104

Fig. 4a

A105

Fig. 4b   A106

Fig. 5   A107
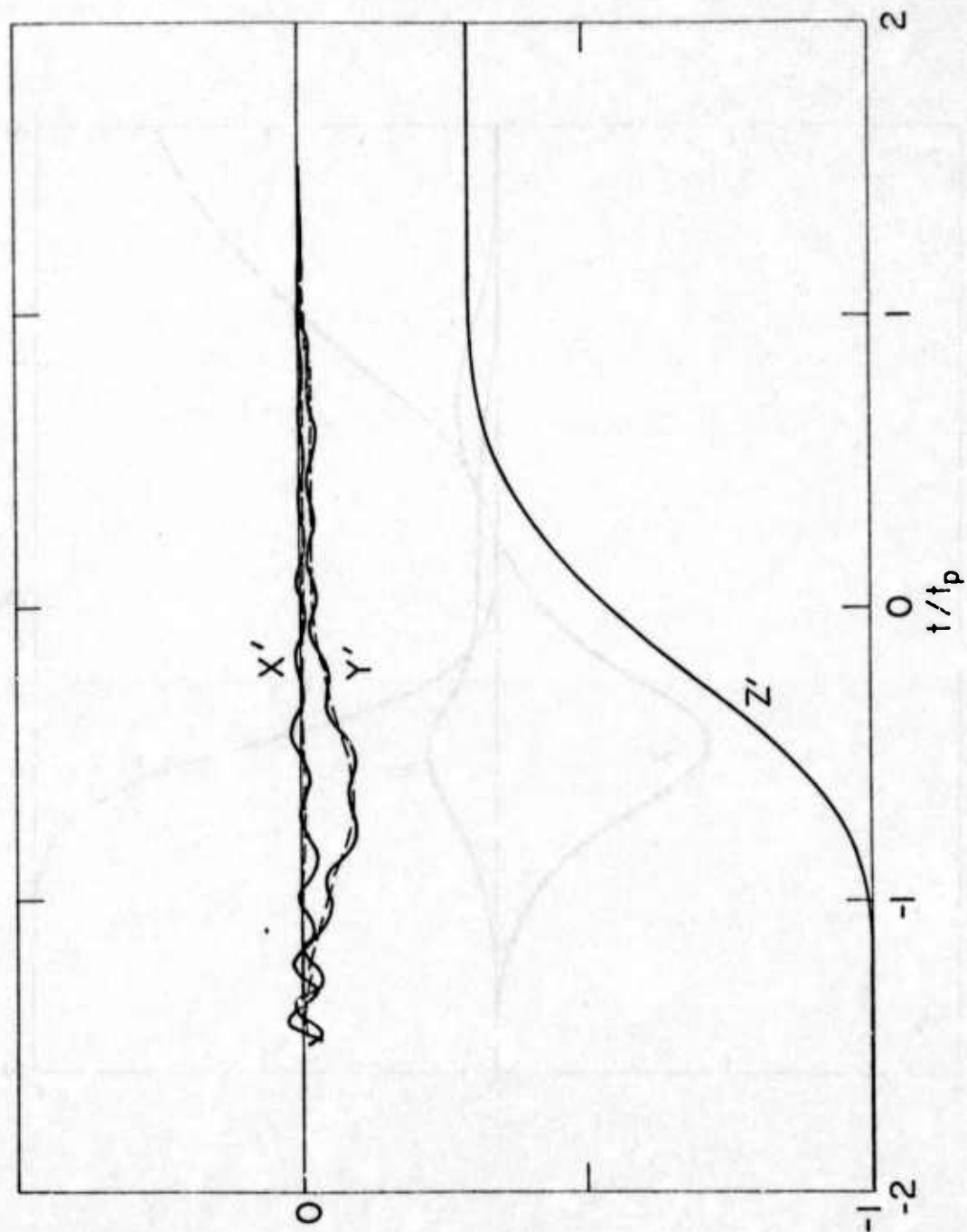
Fig. 6

A108
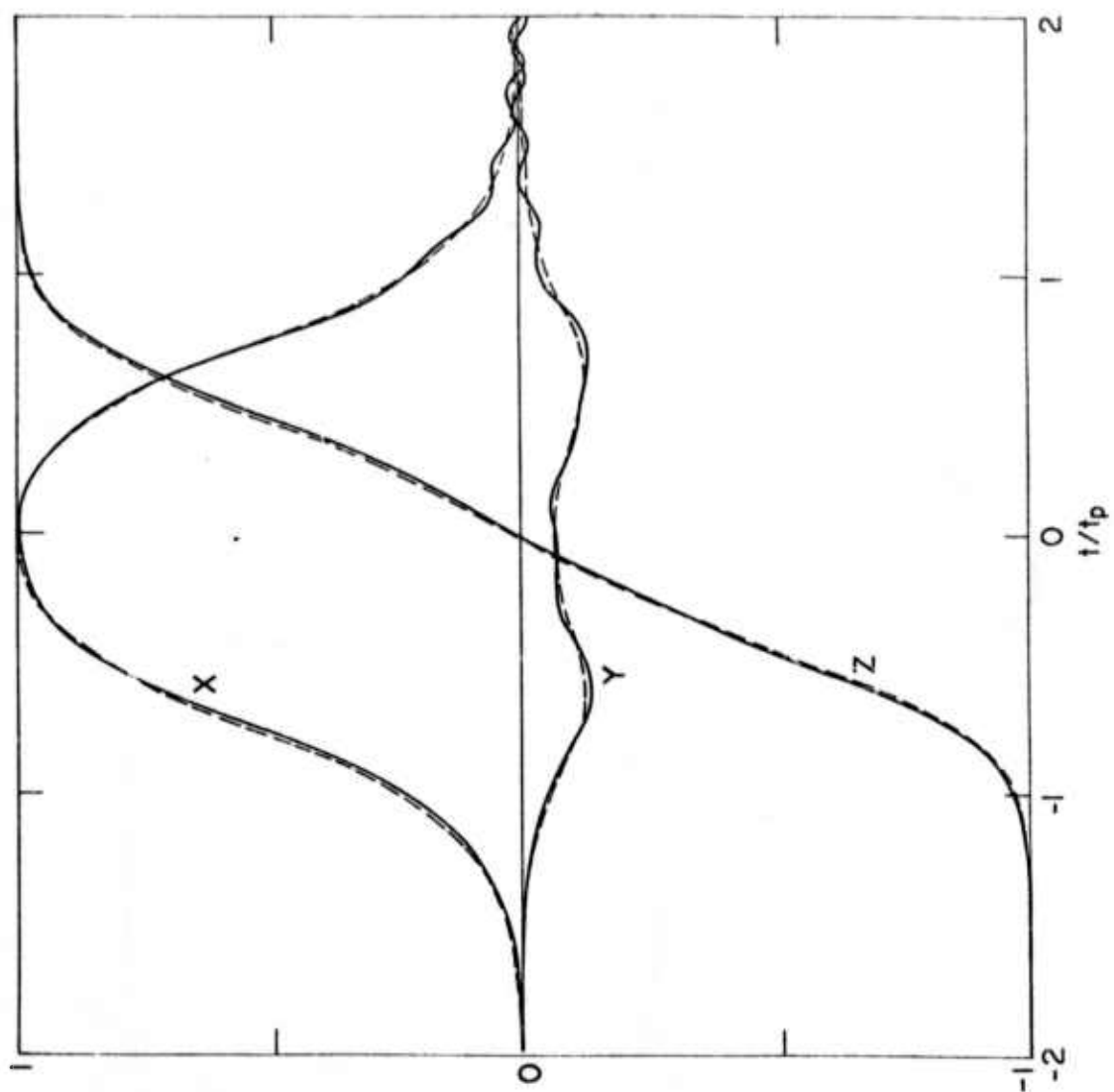
Fig. 7   A109
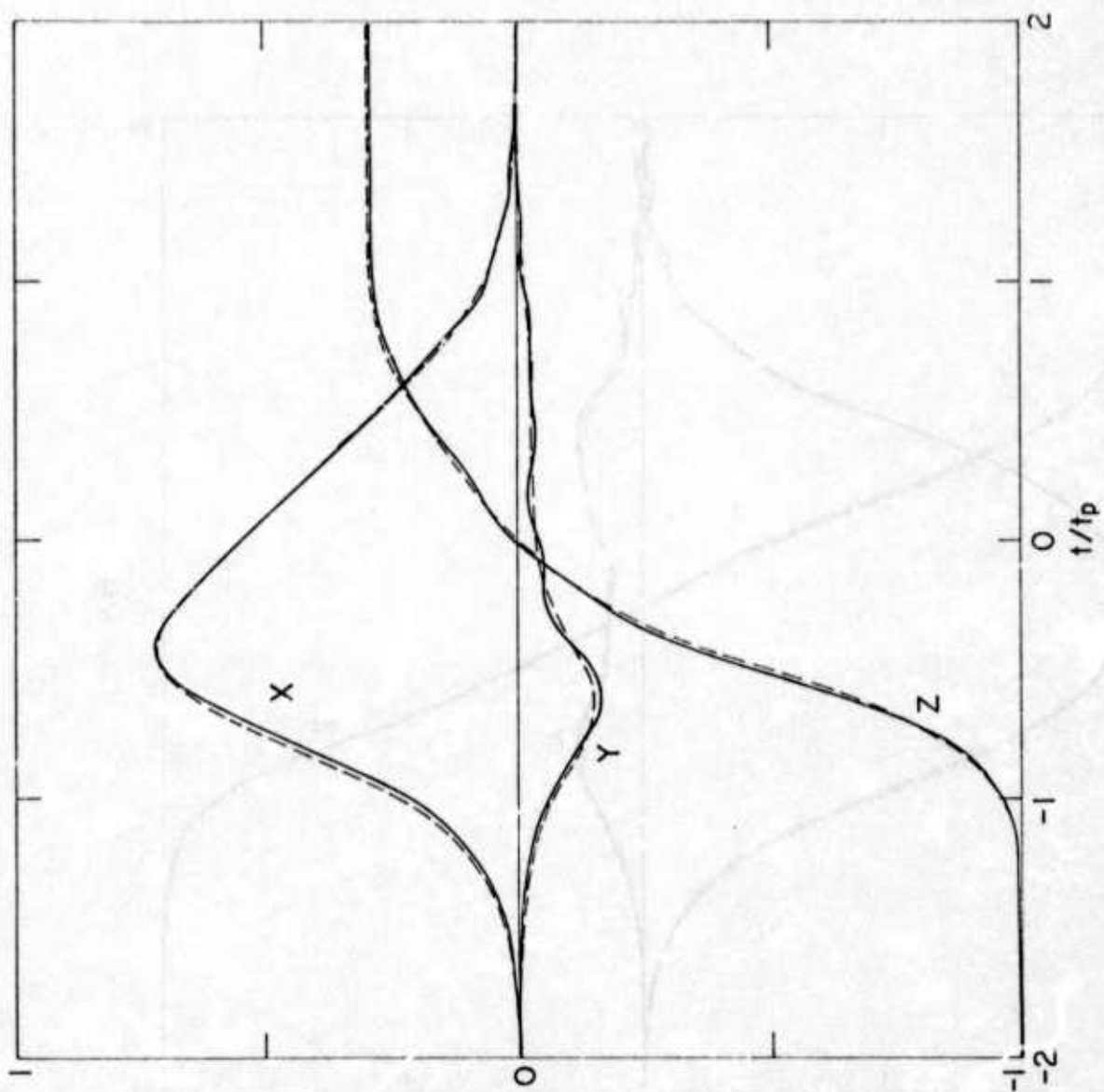
Fig. 8   A110
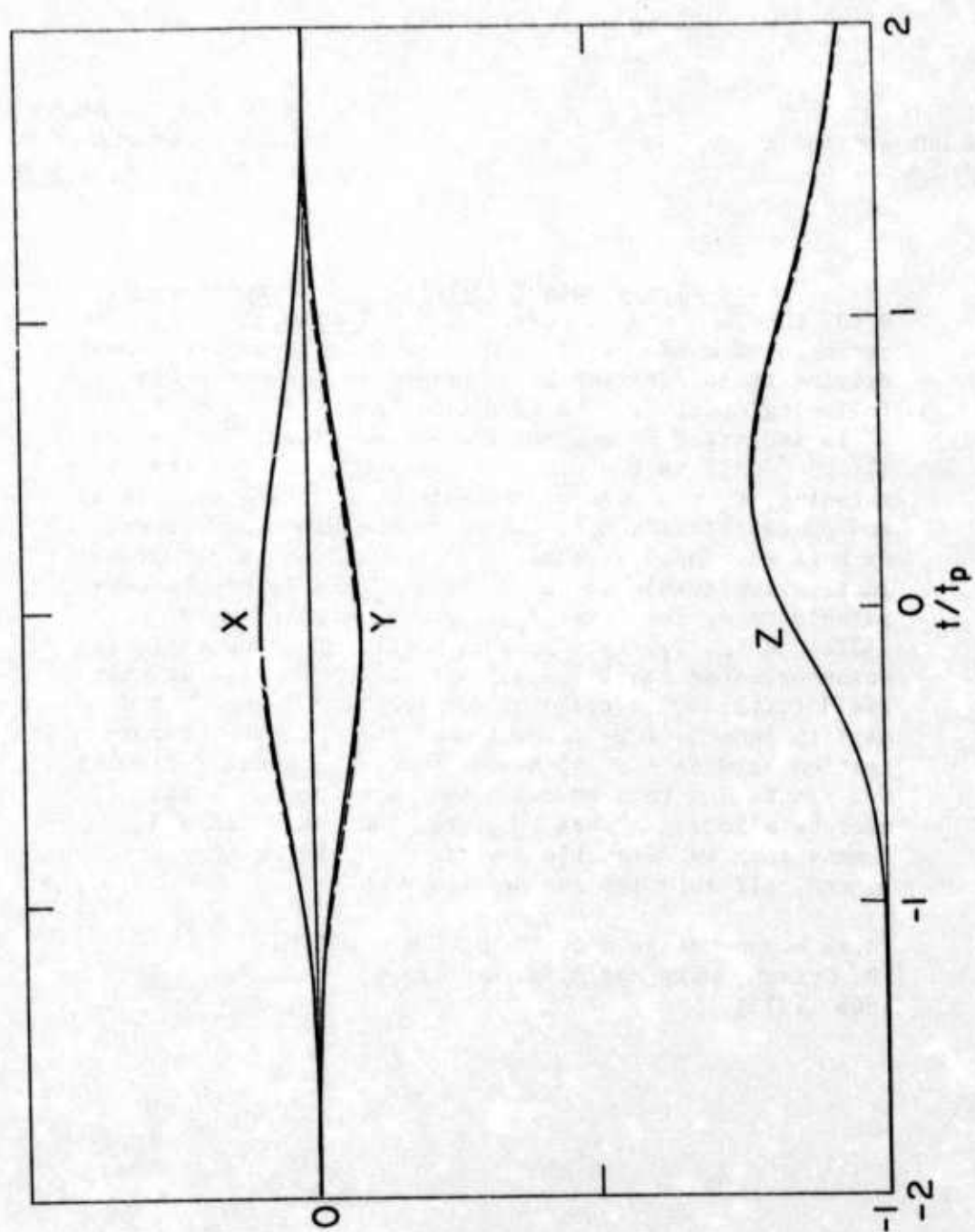
Fig. 9   A111

Generalized Adiabatic Following Approximation.*
R. H. LEHMBERG and J. REINTJES, Naval Research Lab.--The
response of a two level atom to an intense near-resonant
driving field $\varepsilon(t)$ can be described by the adiabatic
following model[1] if the condition $1/\Omega(t) \ll \tau_p \ll T_1$,
T_2 is satisfied throughout the pulse. Here, $\Omega(t) =$
$(\Delta^2 + p^2\varepsilon^2/\hbar^2)^{\frac{1}{2}}$ is the precession frequency, $\Delta(t)$ the
detuning, τ_p the pulsewidth, and T_1, T_2 the atomic level
and phase relaxation times. From the Bloch equations,
we have developed a generalized version of this approx-
imation applicable to cases where T_1 and T_2 can be com-
parable to or less than τ_p; i.e., we require only
$1/\Omega(t) \ll \tau_p$, T_1, T_2. In this model, the pseudospin re-
mains oriented nearly parallel to the effective driving
field $(\varepsilon(t), 0, \hbar\Delta(t)/\mu)$ in the rotating frame, but de-
cays in length if T_2 is comparable to τ_p. The approx-
imation bridges the gap between pure adiabatic following
for $\tau_p \ll T_2$ and rate equation behavior for $\tau_p \gg T_2$,
thereby allowing a more complete description of phe-
nomena such as adiabatic inversion and resonantly en-
hanced self focusing and defocusing.

[1] D. Grischkowsky and J. A. Armstrong, Phys. Rev. A6,
1566 (1972).

A112

Negative Nonlinear Susceptibility of Cesium
Vapor at 1.06μ.* J. REINTJES, R. H. LEHMBERG, and R. C.
ECKARDT, Naval Research Lab.--We outline a theory of the
nonlinear susceptibility of Cs at 1.06μ, and present the
first measurement of the negative nonlinear refractive
index n_2 responsible for the self defocusing recently
observed[1]. The theoretical value of n_2 is $-1.95 \times 10^{-30} N$,
in good agreement with our measured value of $-(1.5 \pm .2)$
$\times 10^{-30} N$. The main portion of n_2 comes from a two-
photon resonance between the 6s and 7s levels. An
additional negative term arises from induced population
changes between 6s and 6p. In our experiments, where
the (35 psec) pulses are shorter than the 6s-6p inverse
linewidth, the nonlinear susceptibility is proportional
to the instantaneous intensity; however, with longer
pulses, one obtains additional contributions propor-
tional to time integrals over the intensity. Since the
useful output power from large Nd laser systems is
limited by self focusing due to the laser glass, our
results suggest the possibility of increasing this
power by using Cs vapor for compensation.

X-RAY LASERS: GUIDELINES AND RECENT PROGRESS by Raymond
C. Elton, Ph.D., Naval Research Laboratory, Washington,
D. C. 20375

Based upon several general schemes currently considered
for achieving significant gain in the vacuum-ultraviolet
and x-ray spectral regions, magnitude estimates of the
plasma pumping requirements are deduced and graphed as
guidelines for future research. A high density collision
limit is also suggested as a function of wavelength.
Recent progress at NRL in numerical modeling and experi-
ments on two promising schemes will be discussed. One is
the extrapolation of existing $3p \to 3s$ cw-laser ion
transitions into the vacuum region, and optimum gain
conditions will be given. The second involves the
utilization of high probability ion-atom resonance charge
transfer reactions for pumping, for which soft x-ray
spectra of highly stripped carbon ions will be shown.

WHEN ABSTRACT IS COMPLETED DO NOT FOLD THIS SHEET.
Mail first class to the address below using card-
board backing to avoid damage. All material must
reach this office NO LATER THAN *June 2, 1975* .

Send abstract to: The Conference Director
The New York Academy of Sciences
2 East 63rd Street
New York, New York   10021

<u>Mailing address of first author</u>

..Dr. Raymond C. Elton, Code 5504...

..Naval Research Laboratory........

..Washington, D. C...20375.........

MULTIPLE MICRO-PINCH PROCESS IN VACUUM SPARK PLASMA FOCUS
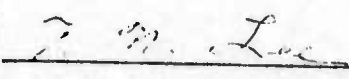
Tong-Nyong Lee

U.S. Naval Research Laboratory
Washington, D.C.   20375

ABSTRACT

Formation of a small (10-50 μm), high power density
($\sim 10^{15}$ Watts/cm^3) plasma focus[1] in a vacuum spark discharge has
been recently found to be related to a highly localized ($<$ 100 μm)
micro-pinch of the plasma column. This micro-pinch takes place at
the boundary of the moving anode plasma[2] and often occurs repetitively
within a time interval of a few nanosecond. A physical process which
is responsible for the multiple micro-pinch will be described.

[1] T. N. Lee and R. C. Elton, Phys. Rev. A $\underline{3}$ 865 (1971).

[2] T. N. Lee, Astrophys. J. $\underline{190}$ 467 (1974).

T. N. Lee
Code 5520
Naval Research Laboratory
Washington, D. C.   20375

Spectroscopy on Plasmas for Short Wavelength Lasers.
R. C. ELTON, Naval Research Laboratory, (30 min.)

The achievement of significant amplified spontaneous emission without cavities in the vacuum-ultraviolet and soft x-ray spectral regions requires either high densities or very long lengths. The former appears more promising at present for concentrating the large pumping power required, and plasma media are anticipated under such conditions. Very high density operation does rapidly deplete possible metastable states; in any case a satisfactory mechanism for population inversion on high energy transitions originating on metastable states has so far not been identified. Focused high power laser beams offer a promising source of pumping energy, with various proposed schemes for converting this concentrated energy into an inverted population. Following a general overview and projection of currently considered schemes, recent vacuum-UV and soft x-ray data from two experiments will be presented. One involves the use of resonance charge transfer reactions between hydrogenic and helium-like ions and neutral atoms, and the other rapid pumping of $3p \rightarrow 3s$ inversions in a pre-equilibrium hot-electron plasma state. Also included will be a discussion of a number of interesting features in the associated space resolved spectra obtained; this technique permits the separation of ionic species and various transitions according to distance of travel of the plasma from the target surface. Supporting numerical computations for modeling of experiments will be presented.

Submitted by

R. C. Elton

R. C. Elton
Code 5504
Naval Research Laboratory
Washington, D. C.   20375

Abstract for an Invited Paper

for the Anaheim   Meeting of the

American Physical Society

29 Jan - 2 Feb. 1975
_____
Date

Atomic Physics in Laser Produced Plasmas.
R. C. ELTON, Naval Research Laboratory, Washington, D. C.   (30 min.)

Atomic processes play a vital role in the efficient conversion of laser energy to charged par-
ticle energy in laser heated plasmas. Both classical and anomalous absorption processes must be
thoroughly understood in order to exploit their optimum heating potential. Radiation losses,
along with self-generated magnetic fields, threaten to reduce the amount of heating achieved in
laser heated plasmas; thus their presence must be minimized. Laser radiation losses due to
various scattering mechanisms are just beginning to be understood, as data become available at
increasing laser flux densities. Atomic processes also continue to play an important role in
plasma diagnostics. For the moderate particle densities encountered in gaseous target plasmas
heated by long-wavelength lasers, established diagnostic techniques such as laser scattering,
interferometry, and spectroscopy are proving satisfactory; and definitive measurements can be
expected. For the supra-solid density plasmas expected from pellet fusion experiments and also
desired for x-ray laser development, the plasma rapidly becomes opaque to visible radiation, and
x-ray diagnostics are essential for interior measurements. Here the ionic physics connected with
x-ray spectral analyses of solar observations becomes relevant, with the addition of some exotic
excitation mechanisms unique to high-density plasmas. The state-of-the-art of x-ray diagnostics
will be reviewed and problems of interpretation with existing atomic physics knowledge outlined.
Also, possible spin-off contributions to atomic physics knowledge from well diagnosed plasmas
will be made apparent. The close similarities between laser-fusion oriented experiments and x-
ray laser research will be addressed, particularly since the development of the latter may be
required for deep probing of extremely high density compressed pellet fusion plasmas.